Morphological characterization of liver fibrogenesis in animal models with genetically modulated TGF-β signal transduction

Von der Fakultät für Mathematik, Informatik und Naturwissenschaften der Rheinisch-Westfälischen Technischen Hochschule Aachen zur Erlangung des akademischen Grades eines Doktors der Naturwissenschaften genehmigte Dissertation

vorgelegt von

Diplom-Biologe
Jafar Hamzavi Sarkhaei
aus Abadan im Iran

Berichter: Universitätsprofessor Dr. rer. nat. S. Dooley

Universitätsprofessor Dr. rer. nat. F. Kreuzaler

Tag der mündlichen Prüfung: 08. Juni 2007

Diese Dissertation ist auf den Internetseiten der Hochschulbibliothek online verfügbar

Table of contents

Table of contents

Table of contents

Abbreviations

ALT	Alanine aminotransferase	Id	Inhibitor of differentiation (Inhibitor of DNA binding)
AST	Aspartate aminotransferase	IFN	Interferon
Ap	Alkaline phosphatase	IGF	Insulin-like growth factor
AMP	Adenosine-mono-phosphate	IgG	Immunglobulin G
BDL	Bile duct ligation	LAP	Latency-associated peptide
BMP	Bone morphogenic protein	MAP	Mitogen-activated protein
CBP	CREB binding protein	MFB	Myofibroblast
CCl_4	Carbon tetrachloride	MH	Mad homology domain
CMV	Cytomegalovirus	MMP	Matrix metalloproteinase
CD-1	CD-1 wild type mouse from Charles River Laboratories	Myc	Myelocytomatosis
CREB	Cyclic AMP response element binding protein	NFκB	Nuclear factor-kappaB
DMN	Dimethylnitrosamine	NASH	steatohepatitis
DTT	Dithiotreitol	PKC	Protein kinase C
ECM	Extracellular matrix	SBE	Smad binding element
ECs	Endothelial cells	siRNA	Small interfering RNA
EMT	Epithelial to mesenchymal transition	S7ΔE1	Smad7 knock out mouse with a deletion in Exon 1
ERK	Extracellular signal-related protein kinase	SMA	Smooth muscle actin
FVB	Fv-1b allele wild type strain	Smurf	Smad ubiquitination regulatory factor 1
FAST1	Forkhead activin signal transducer-1	SnoN	Ski-related novel gene
Fc	Antibody fragment c	S7tg	CRP-Smad7 transgenic mouse with FVB background
FGF	Fibroblast growth factor	SV40	Simian Virus 40
GDF	Growth and differentiation factor	ATS	Anti-thymocyte serum
HA	Hemagglutinin antigen	PanIN	Pancreatic intraepithelial neoplasia
HSC	Hepatic stellate cell		

1 Introduction

Advances in cell and cytokine biology provide insight into molecular mechanisms of tissue fibrosis. Fibrosis in liver, kidney, lung, heart, bone marrow, and skin is a major cause of suffering and death and strongly contributes to the costs of health care. Fibrosis is not a unique pathologic process but is due to an excess of the same biological events involved in normal tissue repair [28]. The release of cytokines in response to injuries is a central event in tissue repair; transforming growth factor β (TGF-β) represents a key cytokine that initiates and terminates this process [111].

1.1 Liver function

The liver regulates the level of most chemicals in the blood and excretes a fluid product, the bile, which induces fat digestion and absorption. All blood leaving the stomach and intestines passes through the liver. The liver processes the blood and breaks down nutrients and drugs into forms easier to use for the body. More than 500 vital functions of the liver are already identified, including:

- production of bile to transport waste and to digest fats in the small intestine

- production of blood plasma proteins

- production of cholesterol and proteins to transport fats

- conversion of glucose into glycogen for storage, which is later converted back to glucose for energy production

- regulation of amino acid blood levels

- processing hemoglobin (iron storage function)

- conversion ammonia to urea for excretion

- clearing the blood from drugs and other poisonous substances

- regulating blood clotting

- defending infections by producing immune factors, e.g., C-reactive protein (CRP)

1.2   Liver fibrosis

Production of fibrous scar tissue in the liver is a normal response to injuries. In fibrosis this healing process is disturbed. Liver fibrosis is defined as the accumulation this fibrous scar tissue in the liver. After hepatocyte damage due to e.g. viral infection, heavy alcohol consumption, toxins or trauma, the immune system is activated and the cell repair process of the liver is induced. Injury or death (necrosis) of hepatocytes further stimulates inflammatory immune cells to release cytokines, growth factors, and chemicals. These messengers activate hepatic stellate cells (HSCs) to produce collagen, glycoproteins (such as fibronectin) and proteoglycans. These are deposited in the liver to form the extracellular matrix (ECM). At the same time, the process of breaking down or degrading collagen is impaired. In a healthy liver, synthesis (fibrogenesis) and degradation (fibrolysis) of matrix tissue are in balance. Fibrosis occurs when scar tissue is generated in excess and faster than it is degraded and removed from the liver.

1.3   Hepatic stellate cells

Hepatic stellate cells (HSCs) are perivascular mesenchymal cells (in previous literature also named Ito cell, lipocyte, perisinusoidal, or fat storing cell) comprising about 15% of the total number of resident liver cells. In normal liver they are the principal storage site for retinoids [126]. HSCs constitute a group of cells that are functionally and anatomically similar, but different in their expression of cytoskeletal filaments, their retinoid content, and their potential for ECM production [57] (Figure 1.1.)
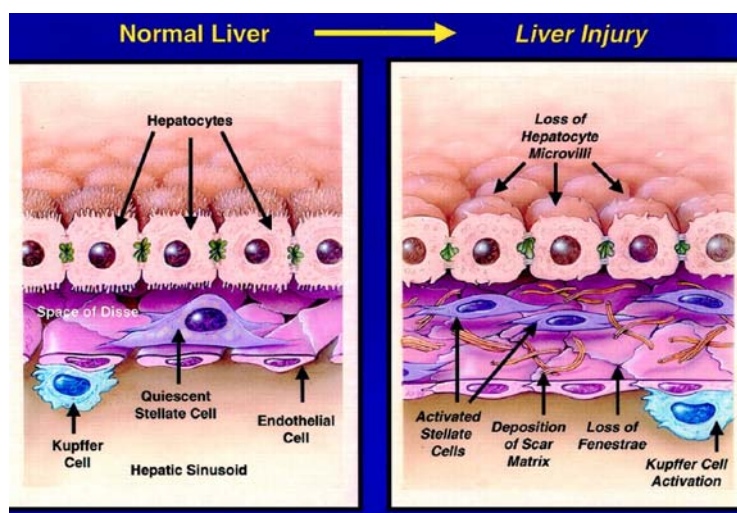
Figure 1.1: Sinusoidal events during fibrosing liver injury. Changes in the subendothelial space of Disse and sinusoid occur as fibrosis develops in response to liver injury. They include alterations in both cellular responses and extracellular matrix composition. Stellate cell activation leads to an accumulation of scar (fibril-forming) matrix. This in turn contributes to the loss of hepatocyte microvilli and sinusoidal endothelial fenestrae, which results in deterioration of the hepatic function. Kupffer cell (macrophage) activation accompanies liver injury and contributes to paracrine activation of stellate cells [40].

HSCs have an intriguing embryologic origin. Recent evidence suggests that they are neural crest-derived because they express glial fibrillary acidic protein and nestin [85]. A neural crest origin is further supported by studies with rat neural crest stem cells, which differentiate into myofibroblasts expressing α-smooth muscle actin (αSMA) [77]. αSMA in turn is a marker of activated HSCs.

1.4 Hepatic stellate cell activation

Following liver injury of any etiology, HSCs undergo a response known as "activation", which is the transition of quiescent cells into proliferative, fibrogenic, and contractile myofibroblasts.

HSC activation is a remarkably pleiotropic yet tightly programmed response occurring in a reproducible sequence (Figure 1.2). The organization of HSC activation into a defined temporal sequence provides a framework, in which cellular events can be placed into a discrete biological context. Early events have been termed *initiation* (also referred to as the "preinflammatory" stage). *Initiation* encompasses rapid changes in gene expression and phenotype that render the cells responsive to cytokines and other local stimuli. *Initiation* is associated with transcriptional events and induction of immediate early genes. It results from paracrine stimulation due to rapid, disruptive effects of liver injury on the homeostasis of neighboring cells and from early changes in ECM composition. *Perpetuation* incorporates those cellular events that amplify the activated phenotype through enhanced cytokine expression and responsiveness; this component of activation results from autocrine and paracrine stimulation, as well as from accelerated ECM remodeling.
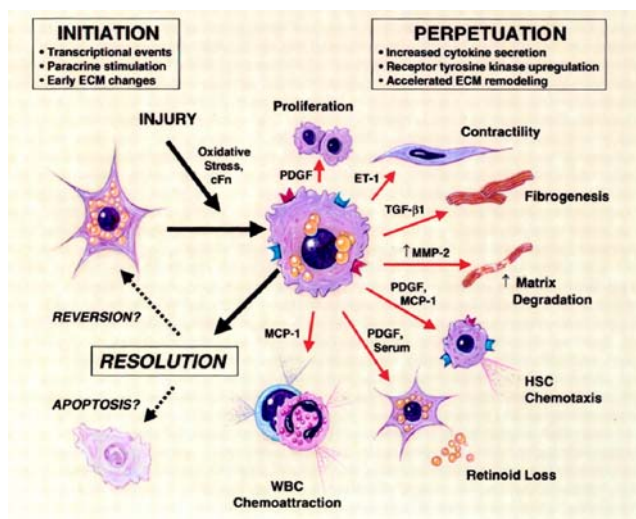
Figure 1.2: Phenotypic features of hepatic stellate cell activation during liver injury and resolution. Following liver injury, HSCs undergo "activation," which characterizes a transition from quiescent vitamin A-rich cells into proliferative, fibrogenic, and contractile myofibroblasts. The major activation dependent phenotypic changes include proliferation, contractility, fibrogenesis, matrix degradation, chemotaxis, retinoid loss, and white blood cell chemoattraction. Key mediators underlying these effects are shown. The fate of activated HSCs during resolution of liver injury is uncertain but may include reversion to a quiescent phenotype and/or selective clearance by apoptosis [40].

Changes in matrix protease activity lead to a remodeling of the hepatic ECM during liver injury, which both directly and indirectly accelerates HSC activation. HSCs express virtually all key components required for matrix degradation [6],[38]. In particular, they are a source of matrix metalloproteinase (MMP)-2 as well as stromelysin/MMP-3 [6], each of which degrades the normal subendothelial ECM. This degradation accelerates its replacement by fibril-forming collagen, which further activates stellate cell growth and MMP-2 production in a positive feedback loop [115],[8]. Through the up-regulation of tissue metalloproteinase (TIMP)-1 and -2, activated HSCs can also inhibit the activity of interstitial inhibitors like collagenases, which additionally favors the accumulation of scar [6].

1.5   TGF-β in tissue repair

Healing of a wound is composed of a coordinated sequence of biological events beginning with hemostasis induced by platelets. This is followed by an invasion of inflammatory cells and fibroblasts to the crisis area for *de novo* formation of new ECM and blood vessels and to induce proliferation of cells for restoring the tissues [28].

TGF-β1 plays an important role in each of these aforementioned events, which can be reproduced by its administration to normal tissue [97], [98]. Platelets contain high concentrations of TGF-β1 and platelet-derived growth factor (PDGF), which are released into the tissue at the site of injury. As a result of injury, inactive (latent) TGF-β1, deposited locally to the extracellular matrix (ECM), is activated. In femtomolar concentrations, TGF-β1 is strongly chemotactic for neutrophils, T-cells, monocytes, and fibroblasts [124], [93], [98]. Moving to the site of injury, these cells become activated by higher (picomolar) concentrations of TGF-β1. Monocytes begin to secret fibroblast growth factor (FGF), tumor necrosis factor (TNF), and interleukin-1 (IL-1), and fibroblasts increase the synthesis of ECM proteins [98].

TGF-β1 stimulates infiltrating cells and resident cells to produce more of it self. This autoinduction intensifies the biological effects of TGF-β1 at the site of injury and has a central role in chronic disease [55]. At normal concentrations, TGF-β1 regulates FGF (in endothelial cells), PDGF (in smooth-muscle cells and fibroblasts), TNF and IL-1 (in monocytes) by stimulating or inhibiting their production or modulating their actions to synchronize and control the repair process [7], [89]. Neonatal mice, in which the TGF-β1 gene was knocked out, live for several weeks until the maternal supply of TGF-β1 is gone, and then die of a systemic autoimmune-like disease with markedly elevated tissue concentrations of TNF and IL-1 [62],[108]. TGF-β1 also inhibits T-cell and B-cell function and their production of TNF-α and IL-1 [15]. TGF-β1 further modulates cytotoxicity of macrophages by suppressing superoxide and nitric oxide production [99; 123].

TGF-β1 can function as an agonist or antagonist of cell proliferation and inflammation and it consistently induces deposition of ECM [99]. Accumulation of matrix is the chief pathologic feature of fibrotic diseases [102]. Figure 1.3 illustrates how TGF-β1 causes the deposition of ECM by simultaneously stimulating cells to increase the synthesis of

matrix proteins several fold, decrease production of matrix-degrading proteases, increase inhibitors of these proteases, and modulate the expression of integrins for enhanced cellular adhesion to the matrix. These comprehensive effects on the ECM reflect the diverse biological properties of TGF-β and are part of a negative-feedback loop regulating the expression of TGF-β [102]. TGF-β binds to proteoglycans in the matrix or near the cell surface, and such binding may act as a signal to terminate TGF-β production after tissue repair is complete.

The regulation of TGF-β secretion and action involves complex post-transcriptional events, including among others messenger RNA (mRNA) stabilization, assembly and activation of the latent TGF-β complex, as well as the modulation of receptor expression [56].
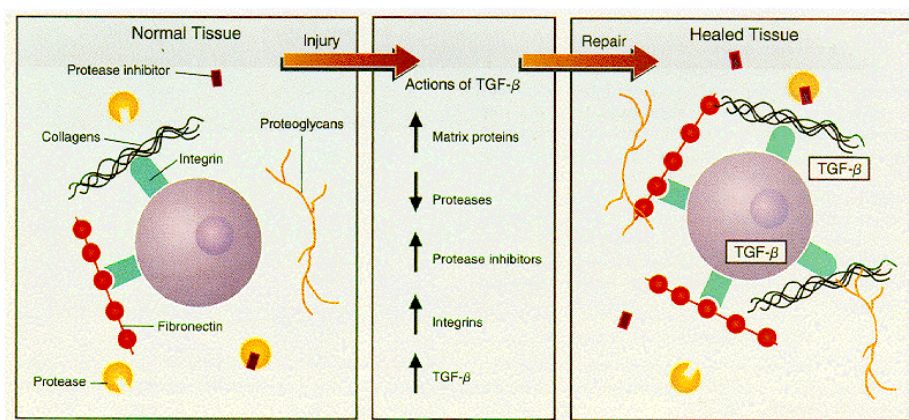
Figure 1.3: Actions of TGF-β in the healing process of injured tissue. Platelets release TGF-β at the site of tissue injury. To repair the damage, TGF-β induces the deposition of ECM by simultaneously stimulating the production of new matrix proteins (fibronectin, collagens, and proteoglycans), blocking matrix degradation by decreasing the synthesis of proteases and increasing the production of protease inhibitors, and by modulating the expression of cell-surface integrins in a manner that enhances cell-matrix interaction and matrix assembly. TGF-β also induces its own production, thus amplifying the biological effects [11].

1.6 TGF-β in fibrogenesis

The fibrogenic potential of TGF-β was established with repeated injections of higher doses into rats during two weeks, which resulted in serious systemic effects, including marked fibrosis in kidneys, liver and at the injection site [114]. Severe cachexia and generalized tissue fibrosis developed in mice given TGF-β intraperitoneally for 10 days [147]. A clinical counterpart of these results might be the rapid onset of liver and lung fibrosis in patients with advanced breast cancer, who receive high-dose chemotherapy in preparation for autologous bone marrow transplantation. The plasma TGF-β concentration, if measured after induction of the chemotherapy, strongly correlates with the development of pulmonary fibrosis or hepatic veno-occlusive disease after high-dose chemotherapy and autologous bone marrow transplantation [3]. The source of the elevated plasma TGF-β concentrations in these patients is unknown.

It is unknown how TGF-β production is normally terminated. It is suggested that repeated injury with continued autoinduction of TGF-β overrides the normal termination signals, thus creating a chronic vicious circle of TGF-β overproduction, as shown in figure 1.4 [10].
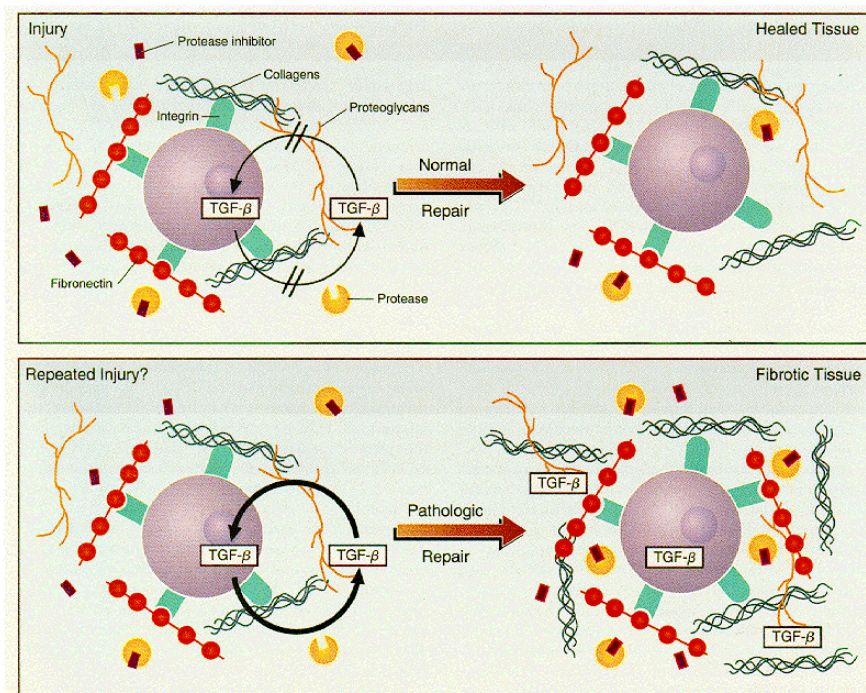
Figure 1.4: Overproduction of TGF-β in fibrogenesis. In normal tissue repair, production of TGF-β and ECM is terminated by unknown mechanisms as the damaged tissue heals. In patients with chronic diseases, repeated tissue injury, a defect in TGF-β regulation, or both lead to the continuous production of TGF-β and ECM, finally resulting in tissue fibrosis [10].

1.7   TGF-β/Smad signal transduction

TGF-β superfamily members bind to serine/threonine kinase receptors. TGF-β receptors comprise two structurally similar subfamilies, the type I and type II receptors, both with small cysteine rich extracellular regions and intracellular portions consisting mainly of their kinase domains. Type I receptors have a region rich in glycine and serine residues (GS domain) in vicinity to the receptor kinase domain [50]. To transmit a signal, type II and type I receptors act in sequence [132]. TGF-β first binds to TβRII, which resides in the cell membrane in an oligomeric form with intrinsic kinase activity; TβRI is then recruited and phosphorylated in its GS domain by TβRII, leading to activation of its kinase activity and subsequent intracellular signaling [70; 91]. Betaglycan, a transmembrane proteoglycan also known as TGF-β type III receptor (TβRIII) [66], presents TGF-β to the other receptors and allows high-affinity binding of TGF-β to TβRII. But betaglycan does not transduce a signal by itself [100], [19].

Smad proteins

Following ligand activation, signaling from TβRI to the nucleus occurs predominantly by phosphorylation of cytoplasmic mediators belonging to the Smad family [91], [71], [72]. Type I receptors specifically recognize and phosphorylate ligand-specific receptor-activated Smads (R-Smads, Fig. 1. 5).
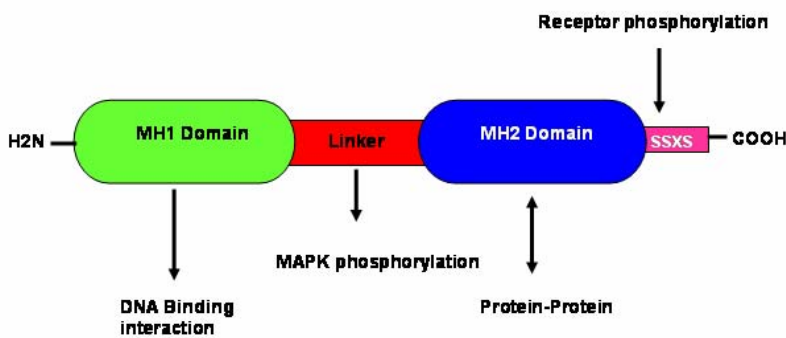
Figure 1.5: Structural domains of R-Smads**. R-Smads consist of two conserved globular domains known as MH (Mad homology) 1 and MH2 domains, connected by a linker region. In the basal state, R-Smads remain in an inactive conformation through an auto-inhibitory MH1/MH2 interaction. Phosphorylation of the C-terminal SSXS motif by activated TβRI results in R-Smad activation. Heteromerization with Smad4, and subsequent translocation into the cell nucleus follow. The MH1 domain of Smad3 recognizes the DNA sequence CAGAC; the MH2 domain is involved in protein/protein interactions with Co-Smad4, transcriptional coactivators and corepressors [122].

R-Smads are recruited to the activated TβRI by a membrane bound cytoplasmic protein called Smad anchor for receptor activation (SARA) [119]. R-Smads include Smad1, Smad5 and Smad8 downstream of the bone morphogenetic protein (BMP) cascade, and Smad2 and Smad3 downstream of TGF-β and activin signaling. R-Smads consist of two conserved Mad-homology (MH) domains that form globular structures separated by a linker region [106]. The N-terminal MH1 domain has DNA-binding activity, whereas the C-terminal MH2 domain has protein-binding properties. Phosphorylation of R-Smads by type I receptors occurs on two serine residues within a conserved SS(M/V)S-motif at the C-terminus of the Smads [72], [71]. Upon phosphorylation by TβRI, R-Smads form heteromeric complexes with a Co-Smad, Smad4. Smad4 is the product of the tumor suppressor gene "deleted in pancreatic carcinoma-4" (DPC-4) [44]. The Smad4 MH1 domain can directly interact with DNA [143] and binds to the phosphorylated C-terminus of activated R-Smads [47]. The MH2 domain is important for transcriptional activation [29], [144] and for direct protein interactions with the MH1 domain of R-Smads [107]. Smad4 lacks the COOH-terminal SSV/MS motif found in R-Smads and neither binds nor is phosphorylated by activated type I receptors [67], [81]. R-Smad/Smad4 complexes are then translocated into the nucleus by a mechanism involving the cytoplasmic protein importin [133], [63] and function as transcription factors, binding DNA either directly or in association with other DNA binding proteins [91], [71], [72]. A third group of Smad proteins, the inhibitory Smads (I-Smads), Smad6 and Smad7, prevent R-Smad phosphorylation and nuclear translocation of R-Smad/Smad4 heterocomplexes [51], [81]. Following target gene transcription, Smad complexes are released from the chromatin and undergo ubiquitination, followed by proteasomal degradation [146]. A summary of the various steps of TGF-β signaling through the Smad cascade is provided in Figure 1. 6.
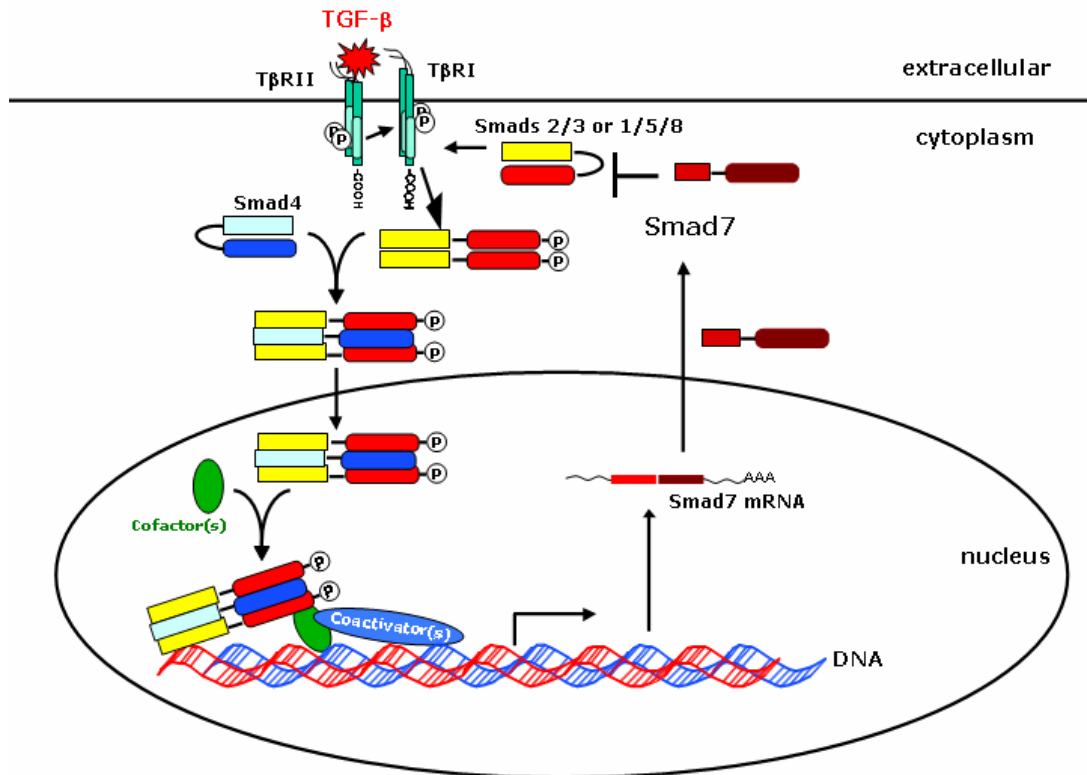
Figure 1.6: Schematic representation of the Smad signaling cascade downstream of the TGF-β receptors. Initiation of signaling occurs when TGF-β binds to the serine/threonine kinase known as TβRII. Ligand-bound TβRII interacts with and phosphorylates the transducer receptor, TβRI. Activated TβRI then recruits and phosphorylates R-Smads, which associate to Co-Smad4. The heterocomplex translocates into the nucleus where it acts as a transcriptional regulator of target genes [16]. Smad7 blocks the TGF-ß signal cascade on the level of R-Smad phosphorylation.

1.8   Animal models for liver disease

Several animal models for liver fibrosis have been established in the past and are still in use. They have contributed to the understanding how the disease develops and progresses.

Weng et al., 2001 [128] induced hepatic fibrosis successfully by subcutaneous injection of carbon tetrachloride (CCl_4) into 150 and intraperitoneal injection of dimethylnitrosamine (DMN) into 196 rats to evaluate the antifibrotic effect of recombinant human Gamma-Interferon (IFN-γ) and to observe its effect on moderate chronic hepatitis B virus fibrosis. They concluded that IFN-γ is effective in treating rat liver fibrosis induced by either CCl_4 or DMN. The higher the dose, the better the effect. IFN-γ is also effective for patients with moderate chronic hepatitis B viral fibrosis.

The antifibrotic effect of Smad7 was demonstrated by Dooley et al., 2003 [34] who subjected Sprague Dawley rats to bile duct ligature (BDL) causing cholestasis, periductular inflammation, and fibrosis. Rats were injected with AdSmad7, AdLacZ, or saline, either via the portal vein at the time of surgery or via the tail vein 1 and 2 weeks later.

1.8.1   Induction of liver damage with dimethylnitrosamine

Dimethylnitrosamine (DMN) is a hepatotoxin, mutagen and carcinogen, which is produced from the reaction of its precursors dimethylamine (DMA) or trimethylamine (TMA) and nitric acid or oxides of nitrogen in the vapor phase [69], [92]. Its hepatotoxicity was first reported by Barnes and Magee (1954) following an industrial accident. Toxicity produced by DMN is mediated by its reactive metabolites. DMN primarily targets the liver, which contains necessary enzymes for its metabolic activation, e.g., microsomal membrane-bound cytochrome P-450 II E1 (Cyp2E1) [135], [136], [141]. Activation and degradation of DMN produces formaldehyde, methanol and alkylating intermediates, which react with nucleic acids and proteins to form methylated macromolecules. In rats, DMN causes severe necrosis and deposition of ECM proteins, particularly of collagen in the liver [2], [105]. Lethal dose 50 (LD50) in rat for DMN is 26 mg/kg or 78 ppm over 4 hours [24]. A single dose of about 25 mg/kg DMN administered orally or by intravenous, intraperitoneal or subcutaneous injection produces serious destruction of liver tissue accompanied by hemorrhages into liver and lungs. Treatment is frequently accompanied by serious accumulation of fluid in the abdominal area and blood deposition in the lumen of the intestine. Death usually occurs within 2-4 days or the animal recovers completely. Rabbits, mice, guinea pigs, and dogs develop similar liver damage with this treatment [68].

1.8.2   Induction of liver fibrosis with carbon tetrachloride

Carbon tetrachloride (CCl_4) causes liver injury by damaging microsomes from the endoplasmic reticulum and ribosomes through free radical induced lipid peroxidation and direct free radical attack. Most of the adverse effect is provided by $CCl_3^\bullet$ radical production via the cytochrome P-450 system [95]. More recently, it was reported that $CCl_3^\bullet$ rapidly reacts with O_2 and forms CCl_3-$O_2^\bullet$ [87]. Today CCl_4 proves highly useful in experiments studying hepatotoxic effects [109]. It consistently induces liver injury in many species, including non-human primates, [142] and man. Investigation of the effects of CCl_4 on metabolic processes in the liver have been performed using living animals [54] as well as perfused livers [73] and cultured hepatocytes [46]. In the presented study, mice routinely obtained intraperitoneal injections of CCl_4 (25 % vol/vol in mineral oil, 50 µl/25 g body weight) two days a week for a period of 8 weeks.

1.8.3   Establishing liver damage with bile duct ligation

Venous blood from the ileum is distributed from the portal vein through the sinusoids throughout the liver. Hepatocytes extract bile acids from sinusoidal blood and only little escapes from healthy livers into the systemic circulation. Bile acids are then transported across the hepatocytes and secreted into canaliculi from where they are transported to the gallbladder. Based on this mechanism, bile duct ligation (BDL) was established as a further method to induce liver damage. It is achieved by a surgical procedure, tying a ligature tightly around the bile duct in order to interrupt the enterohepatic recirculation of bile to the gallbladder. This model for *in vivo* studies generates liver fibrogenesis very efficiently based on cholestasis [60].

1.9   Blunting fibrogenesis by blocking TGF-β

The role of TGF-β as a potent profibrotic cytokine has been demonstrated in a number of animal models [12], [59]. Overexpression of TGF-β in transgenic mice results in liver and kidney fibrosis [103]. Several lines of evidence indicate that fibrosis is caused by unbalanced expression of TGF-β in several organs e.g., liver, kidney and heart. For that reason a sensible antifibrotic therapy must be based on controlling of TGF-β expression.

1.9.1   Anti-TGF-β antibodies

TGF-β is usually secreted in a biologically inactive form as small (SLTC) or large latent complex (LLTC). The inactive ECM-bound LLTC, containing mature TGF-β, latency-associated peptide (LAP) and latent TGF-β binding protein-1 (LTBP-1) is released from the ECM by proteases, and activated at the cell surface to release mature TGF-β [41].

Several lines of evidence indicate that TGF-β beside being involved in liver fibrosis plays a role in the pathogenesis of renal disease associated with diabetes and hypertension [10], [61]. Circulating and local concentrations of TGF-β in the kidney are elevated in humans and experimental animals with glomerulonephritis, diabetic nephropathy, and hypertensive glomerular injury [10]. Moreover, transgenic animals overexpressing TGF-β, develop glomerular lesions and tubulointerstitial renal disease that resemble the types of lesions seen in patients with diabetes or hypertension [13]. It was reported, that anti-latent TGF-β binding protein-1 (anti-LTBP-1) antibodies were used to prevent progression of glomerulosclerosis [49] based on blunting LTBP-ECM interactions.

Further, a murine monoclonal antibody (1D11) that neutralizes all three isoforms of TGF-β (β1, β2, and β3) successfully abrogated the development of hypertension, glomerulosclerosis, and/or tubulointerstitial renal disease in Dahl salt-sensitive (Dahl S) rats fed a high-salt diet for 3 weeks. This indicates that chronic treatment of Dahl S rats with anti-TGF-β antibodies significantly reduces blood pressure, proteinuria and albuminuria.

1.9.2   Dominant-negative and soluble TGF-β type II receptors

A promising strategy to prevent fibrosis is eliminating TGF-β signaling by adenovirus-mediated local expression of a dominant-negative TβRII in the liver of rats treated with DMN [94]. Since transphosphorylation of the type I receptor by the type II receptor is essential for TGF-β signal propagation [132], a mutated type II receptor, e.g., truncation of its kinase domain [131] or substituted with one critical amino acid resulting in loss of transphosphorylation activity [21] can inhibit many signaling responses induced by TGF-β. Accordingly, rats receiving a single application of adenoviral vectors expressing a truncated (kinase domain) human TβRII (AdCATβ-TR) via the portal vein, displayed significantly attenuated liver fibrosis as assessed by histology and hydroxyproline content. All AdCATβ-TR treated rats remained alive, and their serum levels of hyaluronic acid and transaminases remained at low levels, whereas control animals died due to liver dysfunction [94]. Functionality of this construct was further confirmed in mink lung epithelial cells (Mv1Lu), where TGF-β-induced antiproliferative signaling was blocked by AdCATβ-TR [134]. Further, a soluble TβR-II protein was successfully used to ameliorate liver fibrosis based on scavenging exogenous TGF-β [145], [120]. The soluble receptor fusion protein acts by binding TGF-β1 (as well as TGF-β3) with high affinity, thereby preventing the

interaction of TGF-β1 with its cell surface receptors and effectively neutralizing TGF-β1 bioactivity. Two different soluble TGF-β II receptor constructs were composed either of the extracellular portion of mouse TβR-II and the Fc (fragment crystallizable) portion of mouse immunoglobulin (Ig) G [145], or of an entire ectodomain of human TβRII fused to the Fc portion of human IgG expressed by AdTbeta-ExR. [120]. Chimeric TβR-II:Fc proteins localize predominantly to sites of TGF-β1 activity and attenuated markedly liver fibrosis in rats exposed to DMN [120], reduced postangioplasty vascular intimal lesion formation in rats [110], bleomycin-induced lung fibrosis in hamsters [126], and hepatic fibrosis after bile duct ligation in rats [43].

Recently a similar strategy was used to block the actions of tumor necrosis factor (TNF) α in rheumatoid arthritis. The approach was already tested successfully in a randomized clinical trial [127], thus showing applicability, safety, and clinical potential of soluble cytokine receptors.

1.9.3   Smad7

To interfere with the TGF-β signaling pathway further downstream may lead to a more specific blunting, since not all TGF-β effects would be abrogated. Nakao and his coworkers were the first to use adenoviral overexpression of antagonistic Smad7 to inhibit TGF-β effects in a fibroproliferative disease [83]. Delivery of CMV-Smad7 adenovirus via intratracheal injection to C57BL/6 mice 8-12 hours after initiation of bleomycin-induced lung fibrosis led to inhibition of profibrogenic TGF-β signaling and subsequent responses in animal lungs. Overexpression of the BMP specific inhibitor Smad6 was also used in these studies but displayed no beneficial effect.

Accordingly, we used this approach and showed that Smad7 is equally effective in inhibiting liver fibrosis [34]. Ligation of the common bile duct (BDL) was used to induce liver fibrosis in rats. Subsequently the animals received injections of an adenovirus carrying Smad7 cDNA into the portal vein during surgery and via the tail vein at later stages. Smad7 overexpressing BDL rats displayed reduced collagen expression and hydroxyproline content in total liver lysates. In addition, α-smooth muscle actin (α-SMA) staining was strongly reduced in animals treated with the Smad7 expression cassette compared to a LacZ control, indicating a significant reduction of activated HSCs *in vivo*. Importantly, such a beneficial effect was also observed when Smad7 was expressed in animals with established fibrosis. Additionally, the effect of Smad7 on TGF-β signaling and activation of HSCs was analysed in primary cultured cells. Ectopic Smad7 expression arrested transdifferentiation and blocked TGF-β signal transduction, shown by inhibition of Smad2/3 phosphorylation, nuclear translocation of activated Smad complexes, and activation of (CAGA)$_9$-MLP-Luc. This resulted in decreased collagen I expression and destruction of the fibrillar organization of the α-SMA cytoskeleton. Our data suggest that gene transfer of Smad7 inhibits experimental liver fibrogenesis *in vivo*. The underlying mechanism

most likely involves inhibition of TGF-β signaling and HSC transdifferentiation. However, while interpreting the data and creating a mechanistic model, it has to be taken into account that Smad7 is also very efficient in abrogating the effects of other members of the TGF-β family, e.g., isotypes 2 and 3 and BMPs. In addition, Smad7 may also have other, yet unidentified functions, also contributing to the observed effects. Thus, its involvement in apoptosis was described recently [35] and its clearly documented localization within the nucleus can still not be related to any function of Smad7. Therefore, further research about details of TGF-β signaling and the impact of Smad7 in the different cell types of the liver is needed to optimize treatment strategies based on Smad7.

Smad7 was also used as antifibrotic tool in several models of kidney fibrosis. Lan and coworkers [65] transferred a doxycycline-regulated Smad7 gene into rat kidneys. Induction of Smad7 resulted in complete inhibition of Smad2/3 nuclear translocation and tubulointerstitial fibrosis, as evidenced by decreased expression of α-SMA and collagen types I and III. Similarly, decreased fibrosis could be detected if Smad7 was introduced one day after ureter ligation by injection [113].

Another possibility to block certain pathways more specifically will be to inhibit downstream targets of TGF-β, directly. Smad3, which was identified as important regulator of fibrotic responses in many different organs might be such a target [39].

1.9.4   Compound drugs to inhibit profibrogenic TGF-β signaling

Another strategy of TGF-β neutralization is targeting the activation process of latent TGF-β. Thus, the serine protease inhibitor camostat mesilate was used to attenuate hepatic fibrogenesis at least in part by inhibiting plasmin activity [86]. Plasmin treatment of cultured HSCs induces release of TGF-β from the matrix resulting in an increased TGF-β dependent gene response, e.g. upregulation of Smad7 mRNA expression [17]. This indicates that plasmin participates in the activation process of latent TGF-β. Interestingly, camostat mesilate also blunted the effect of recombinant, active TGF-β itself, suggesting an additional antagonizing mechanism of this drug or plasmin. This was confirmed by the observation that the phenotype of plasmin knock out animals is different from that of TGF-β1 knock-out mice [22], [108].

Thrombospondin-1 (TSP-1), an ECM protein involved in the regulation of cellular responses following injuries ([96] plays an important role as an activator of the small latent TGF-β complex [26], [79]. TSP-1 expression is increased in livers from patients who suffer from congenital hepatic fibrosis [36]. A peptide derived from the latency-associated peptide (LAP), i.e. Leu-Ser-Lys-Leu (LSKL), inhibits the activation of TGF-β1 by blunting the LAP-TSP-1 interaction, which is necessary for the TSP-1 mediated activation mechanism [58]. To study the effects of LSKL on hepatocyte

damage and fibrogenesis in DMN-induced liver fibrosis, rats obtained an intraperitoneal injection of DMN or saline three times per week for four weeks. In addition, the animals were treated with LSKL, a control peptide, or saline daily. LSKL peptides prevented progression of hepatic damage and fibrosis through inhibition of TGF-β1 activation and subsequent signal transduction *in vivo*. At the cellular level, neutralization of TSP-1 in activated HSCs abrogated TGF-β signaling as demonstrated with an adenoviral reporter construct, (CAGA)$_9$-MLP-Luc, containing a Smad3/Smad4 response element driving expression of luciferase [18], [32]. While these data strengthen the potential importance of TSP-1 in TGF-β mediated hepatic fibrosis *in vivo*, the mechanism leading to activation of latent TGF-β1 and subsequent initiation of intracellular signaling in liver cells needs further examination.

A promising method to disrupt the TGF-β/Smad pathway is to block the serine/threonine kinase activity of TβRI, also known as activin receptor-like kinase (ALK) 5. The identification of GW6604 (2-phenyl-4-(3-pyridin-2-yl-1H-pyrazol-4-yl) pyridine), an ALK5 inhibitor, allowed de Gouville et al. [30] to evaluate the therapeutic potential of inhibiting the TGF-β pathway in different models of liver disease. The ALK5 inhibitor was tested in TGF-β overexpressing transgenic mice exhibiting liver hepatectomy, in an acute model of liver disease and in a chronic model of dimethylnitrosamine (DMN)-induced liver fibrosis. *In vitro* GW6604 inhibited autophosphorylation of ALK5 and in a cellular assay it inhibited TGF-β-induced transcription of PAI-1. *In vivo* GW6604 increased liver regeneration in TGF-β overexpressing mice, which had undergone partial hepatectomy. In an acute model of liver disease, GW6604 reduced the expression of collagen Iα1 by 80%. In a chronic model of DMN-induced fibrosis, mortality was prevented and DMN induced elevations of mRNA encoding collagen Iα1, Iα2, III, TIMP-1 and TGF-β were reduced by 50–75 % by the administration of GW6604. Inhibition of matrix genes overexpression was accompanied by reduced matrix deposition and reduction in liver function deterioration.

1.10   C-reactive protein in liver damage

C-reactive protein (CRP) is a phylogenetically highly conserved plasma protein with homologs in vertebrates and invertebrates that participates in the systemic response to inflammation. Its plasma concentration increases during inflammatory stages, which is useful for clinical purposes. CRP is a pattern recognition molecule, which binds to specific molecular configurations typically exposed during cell death or found on the surfaces of pathogens like lipopolysacharide (LPS). Its rapid increase in synthesis within hours after tissue injury or infection suggests that it contributes to host defense and is part of the innate immune response.

CRP is a β-globulin and as a hallmark for inflammation it is primarily synthesized in hepatocytes [78]. Preliminary evidence suggests that CRP is also expressed in vascular cells and atherosclerotic lesions [138], [20]. An inducer of CRP synthesis is Interleukin-6 (IL-6), produced and secreted from macrophages activated as a reaction to pathogenic agents like LPS and bacterial infection. The IL-6 effect can be enhanced by interleukin-1β (IL-Iβ) [64]. CRP is a component of the acute phase protein and the congenital immune system in humans. It imitates an antibody by binding phosphorylcholine on the bacterial cell membrane in the presence of Ca^{++} and triggers the complement cascade. CRP is taken into the cells by Toll-like receptors (TLR). This allows an immediate response to microbial invasions before the development of active immunity. TLRs are conserved throughout evolution, are the primary sensors of this innate (natural) immunity and thus play a crucial role in the primary defense against infections [112]. Inflammatory effects of CRP as responses to chronic bacterial infections lead to serious organ damage by triggering a primary defense mechanism including migration of immune cells to the crisis regions.

Even though serum amyloid proteins rather than CRP are the major acute phase proteins in mice [90] and [130], the expression of the human CRP gene is regulated in transgenic mice as it is regulated in humans [25]. Thus the human CRP promoter offers a useful tool to express transgenically derived proteins under tight induction control specifically in hepatocytes of mice.

Structure of C-reactive protein
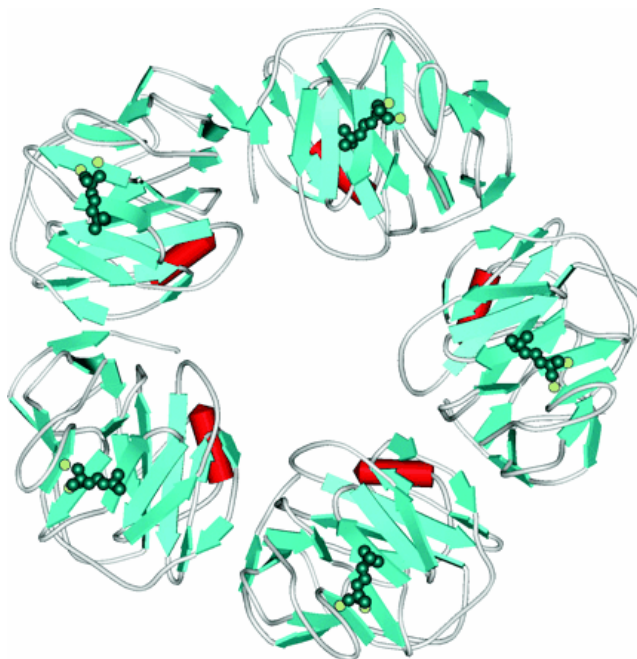
Figure 1.7: Crystal structure of C-reactive protein complexed with phosphocholine [116]   ViewerPro 4.2 software (Accelrys, San Diego, CA) was used to generate the ribbon diagram of the x-ray crystal structure of CRP-phosphocholine complex obtained from Brookhaven Protein Data Bank (PDB entry 1B09 [PDB]). Calcium ions in yellow, phosphocholine in green.

1.11   Aim of the study

The study presented here is based on previous work [34], where we succeeded in ameliorating fibrogenesis in BDL rats by injection of AdSmad7 via the portal/tail vein. Smad7 overexpression in rats with BDL displayed reduced collagen and α-SMA expression as well as decresed hydroxyproline content in the liver compared to animals treated with AdLacZ. A beneficial effect was even observed when Smad7 was expressed in animals with established fibrosis. In this model Smad7 was expressed in all liver cell types. In the present study, we were interested to investigate the effects of Smad7 overexpression specifically in hepatocytes. Therefore CRP-Smad7 transgenic mice expressing Smad7 under the control of the hepatocyte specific CRP promoter were generated for this purpose. Ectopic Samd7 expression can be induced by LPS. As reference strains FVB and CD-1 wild type as well as mice with a disrupted Smad7 gene (S7ΔE1) were examined. Animals were treated with CCl_4 to induce fibrosis and with LPS to stimulate transgenic Smad7 overexpression. After 8 weeks, tissues were analysed for the expression of fibrotic marker proteins. Sirius red staining was performed to assay collagen deposition and immunostaining was used to quantify the expression of α-SMA. Further, Western blot analysis of whole liver protein lysates was done and liver enzyme activities in the serum were measured.

The results show that Smad7 overexpression in hepatocytes attenuates production of fibrotic marker proteins, e.g., α-SMA, collagen, hyaluronic acid, hydroxyproline and serum enzymes by up to 70% compared to controls.

In summary, this investigation indicates that Smad7 can inhibit or at least attenuate the development of liver fibrosis by reducing TGF-β signaling in hepatocytes.

2   Materials and Methods

2.1   Materials

2.1.1   General chemicals

Table 2.1: General chemicals

Reagent	Company	Cat. No.
Agarose DNA	Qbiogene,Heidelberg,Germany	AGAH0250
Agarose / DNA	Biozym, Hess. Oldendorf, Germany	97342
Citric acid, monohydrate	Calbiochem, Darmstadt, Germany	231211
Diaminobenzidine	Sigma, Munich, Germany	D-5905
Dithiothreitol (DTT)	Sigma, Munich, Germany	D-9779
Sodium chloride	Sigma, Munich, Germany	S-9625
NaOH, 2 mol/l	Merck, Darmstadt, Germany	1.091361.000
Tris (hydroxymethyl) aminomethane	Merck, Darmstadt, Germany	1.08382.1000
Tween 20	Merck, Darmstadt, Germany	8.22184.0500
Titriplex III	Merck, Darmstadt, Germany	1.08418.0250
Picric acid solution	drugstore of medical clinical Aachen, Germany	
Phosphate buffered saline, pH 7,4 (10 x)	Gibco, Karlsruhe, Germany	70011-036
Potassium chloride	Merck, Darmstadt, Germany	1.04936.0500
TAE Buffer 50 x pH 8.3	Promega, Mannheim, Germany	H5231
Ethidiumbromide solution 10 mg/ml	BIO-RAD,Hemel Hempstead, UK	161-0433
Gene RulerTM 100 bp DNA Ladder Plus	Fermentas, St. Leon-Rot, Germany	SM0321
Gene rulerTM 1Kb DNA ladder Plus	Fermentas, St. Leon-Rot, Germany	SM0311
Loading dye solution x 6	Fermentas, St. Leon-Rot, Germany	R0611

2.1.2   Antibodies

First antibodies for histochemical immunostaining and Western blotting

Table 2.2: First antibodies used for histochemical immunostaining. The antibodies were diluted according to instructions recommended by companies.

First antibodies against:	Company	Cat. No.
Flag	Sigma, Munich, Germany	F3165
MADH7	Abcam, Cambridge, UK	ab5825
β-Actin	Sigma, Munich, Germany	A 5441
Phopho-Smad1 (Ser463/465)	Cell Signaling, Danvers, MA, USA	9511
Phopho-Smad2 (Ser465/467)	Cell Signaling, Danvers, MA, USA	3101
Phopho-Smad3 (ser423/425)	Cell Signaling, Danvers, MA, USA	9514
α-Smooth muscle actin	Sigma, Munich, Germany	A 2547
Smad3	Zymed, Karlsruhe, Germany	51-1500
Smad2	Zymed, Karlsruhe, Germany	51-1300
CD43	BD Pharmingen, California, USA	552366
Proliferating cell nuclear antigen (PCNA)	Sigma, Munich, Germany	P 8825
Cleaved caspase-3 (Asp175)	Cell Signaling, Danvers, MA, USA	9664
Collagen type I (M-19)	Santa Cruz Biotechnology, California, USA	sc-8788

Second antibodies for histochemical immunostaining

Table 2.3: Horseradish peroxidase (HRP)-conjugated antibodies used for immunostaining. Dilutions of the antibodies were used according to instructions recommended by cpmpanies.

Second antibodies	Company	Cat. No.
Goat anti-mouse	DAKO, Glostrup, Denmark A/S	P 0447
Rabbit anti-goat	DAKO, Glostrup, Denmark A/S	P0449
Swine anti-rabbit	DAKO, Glostrup, Denmark A/S	P0217

Second antibodies for Western blot analysis

Table 2.4: Horseradish peroxidase (HRP)-conjugated antibodies used for Western blot analysis. Dilutions of antibodies were used according to instructions recommended by companies.

Secondary antibodies	Company	Cat. No
Goat anti-mouse	Santa Cruz Biotechnology, California, USA	2005
Swine anti-rabbit	Santa Cruz Biotechnology, California, USA	2004
Rabbit anti-goat	Santa Cruz Biotechnology, California, USA	2768
Goat anti-rabbit	Santa Cruz Biotechnology, California, USA	2301
Bovine anti-mouse IgG AP	Santa Cruz Biotechnology, California, USA	2389

2.1.3 Reagents and material for animal experiments

Table 2.7: Reagents and material for animal experiments

Reagent and material	Company	Cat. No.
Lipopolysaccharide (LPS)	Sigma, Munich, Germany	L-8274
Carbon tetrachloride (CCl_4)	Fluka, Seelze, Germany	87032
Mineral oil	Sigma, Munich, Germany	M-8410
Syringe	BD Plastipak, Dilsberg, Germany	REF 300013
Cannula (27 G x ¾ -Nr.20) 0.4mm x 19 mm	BD Microlance TM 3, Planegg-München, Germany	REF 302200
Glas capillaries	Hilgenberg GmbH, Malsfeld, Germany	1410213
Multi Ultra Tubes 0,2 ml	Roth, Karlsruhe, Germany	H561.1
Nunc CryoTube Vilas 1,8 ml	Nunc, London, UK	340711

2.1.4   Reagents for immunhistochemistry

Table 2.8: Reagents for immunohistochemistry

Reagent	Company	Cat. No
3-(Triethoxysilyl)-propylamin (Silane)	Merck, Darmstadt, Germany	821619.0100
Mayers Hämalaun	Merck, Darmstadt, Germany	1.09249.2500
Malinol	Waldeck GmbH, Münster, Germany	3C 242
3,3'-diaminobenzidine tetrahydrochloride (DAB)	DAKO, Hamburg, Germany	S 3000
Sirius red F3BA, 1A 280	Chroma	35780
Saturated picric acid solution	Fluka	80456
PBS Dublecco	Biochrom AG, Berlin, Germany	L182-50
Tris (hydroxymethyl) aminomethane	Merck, Darmstadt, Germany	1.08382.1000
Gelatin type A	Sigma, Munich, Germany	G-7041
Tri-Sodium citrat dihydrate	Merck, Darmstadt, Germany	A570148442
Xylene	J.T.Baker, Deventer Holland	108681
Absolute ethanol	House drugstore, medical clinical Mannheim, Germany	
Hydrogen peroxide	Merck, Darmstadt, Germany	K31856110335

2.1.5   Reagents for preparation of protein lysates

Table 2.9: Reagents for preparation of protein lysates

Reagent and material	Company	Cat. No.
Tris (hydroxymethyl) aminomethane	Merck, Darmstadt, Germany	1.08382.1000
Sodium chloride	Sigma, Munich, Germany	S-9625
Deoxycholic acid.Na-salt	Serva, Heidelberg, Germany	18330
Sodium dedocyl sulfate (SDS)	Roche, Penzberg, Germany	23262
Nonidet P-40	Roche, Penzberg, Germany	1754599
Complete (Protease inhibitor cocktail)	Roche, Penzberg, Germany	1697498
Phosphatase inhibitor cocktail II	Sigma, Munich, Germany	P-5726
liquid nitrogen		

2.1.6   Protocol for RIPA buffer preparation

Table 2.10: Components of RIPA buffer for 1000 ml

Reagent	Molarity	For 1000 ml	
Tris (hydroxymethyl) aminomethane	20 mM	2.42	g
Sodium chloride	150 mM	8.76	g
Sodium dedocyl sulfate (SDS)	0,1 % (w/v)	1	g
Deoxycholic acid. Na-salt (DOC)	0,5 % (w/v)	5	g
Nonidet P-40	2 % (v/v)	20	ml

pH 7.2, concentrated HCl

Notice: Mix all salts together and adjust to pH 7.2. Finally add Nonidet P-40 and adjust again to pH 7.2.

2.2   Animals

All protocols for experiments with animals were carried out in full compliance with the guidelines for animal care and were approved by the Animal Care Committee from the German government.

2.2.1   Origin of the FVB/N strain

The inbred strain FVB/NJ is available from the Jackson Laboratory. This strain is preferred for production of transgenic mice due to several unique characteristics. The pronuclei of the zygotes are large and easily visible making microinjection much easier. The strain has large litters with an average litter size of 9.5 pups/litter. It is favored to use inbred strains over hybrid F1 or F2 mice. Because after successful insertion of DNA into hybrid mice, extensive backcrossing is required to establish the mutation on an inbred background. Thus, using an inbred strain simplifies genetic manipulation and analysis. The Jackson Laboratory obtained FVB/N mice from the NIH in 1987 at F38.
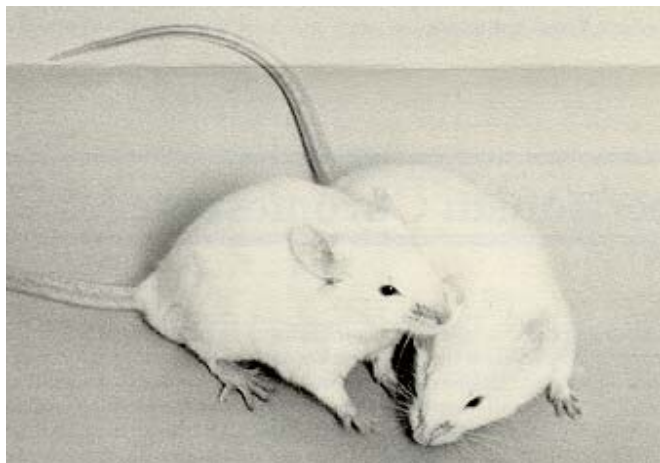
Figure 2.3: The FVB/N strain. This strain was developed from an outbred strain of a Swiss stock selected for histamine sensitivity. The line was later identified to carry the Fv-1b allele (therefore its name) for sensitivity to the B strain of Friend leukemia virus. (Source: Jackson Laboratory)

2.2.2   Origin of the CD-1 strain

The CD-1 mouse was provided from the Charles River Laboratory and is officially designated Crl:CD-1 (ICR)BR. It is an albino animal that carries a black agouti coat color behind its albino gene and represents an outbred strain. Its origin is a group of progenitors consisting of two male and seven female albino mice from a noninbred strain (origin unknown) in the laboratory of de Coulon, at the Centre Anticancereux Romand, Lausanne, Switzerland. These animals were imported into the United States by Clara Lynch from the Rockefeller Institute in 1926, outbred and passed over to other institutions and commercial breeders from 1928 to the early 1950s. The CD-1 mouse represents a useful model for toxicological studies supporting drug development and product registration.

2.3   Bacteria

The competent *Escherichia coli* stem DH5α purchased from Invitrogen, Karlsruhe, Germany was cultured for reproduction and transformation with plasmids.

Cat. No. 18265-017

Bacteria were cultured in liquid LB medium or on LB-agar plates containing suitable antibiotics for colony selection.

LB-Medium

Material

LB Medium (Luria/Miller), Roth, Karlsruhe, Germany, Cat. No. X968.1

Ampicillin 100 mg/ml, Mannheim, Germany, Cat. No. 10835269001

Protocol

1. Add 12.5 g LB Medium to 1000 ml dH$_2$O.
2. Autoclave at 121°C for 20 minutes.
3. Cool the LB-medium to 60°C.
4. Add 1 ml ampicillin (100 mg/ml) to reach an end concentration of 100 µg/ml.

For agar plates add 20g agar (Gibco-BRL, USA, Cat. No. 30391/023) to the medium before autoclaving. After adding ampicillin pour thin layers (5mm) of LB-agar into each culture plate.

2.4   Plasmids

A: Plasmid pcDNA3.1-Flag-Smad7

Table 2.5: Characteristics of pcDNA3.1-Flag-Smad7

Plasmid name	pcDNA3.1-Flag-Smad7
Plasmid size	6.689 kb
Fragment of interest	Flag-Smad7
Restriction sites used	BamHI-XhoI
Smad7 insert size	1.3 kb
Kindly provided by P. ten Dijke	Division of cellular biochemistry, the Netherlands cancer institute, Amsterdam, the Netherlands
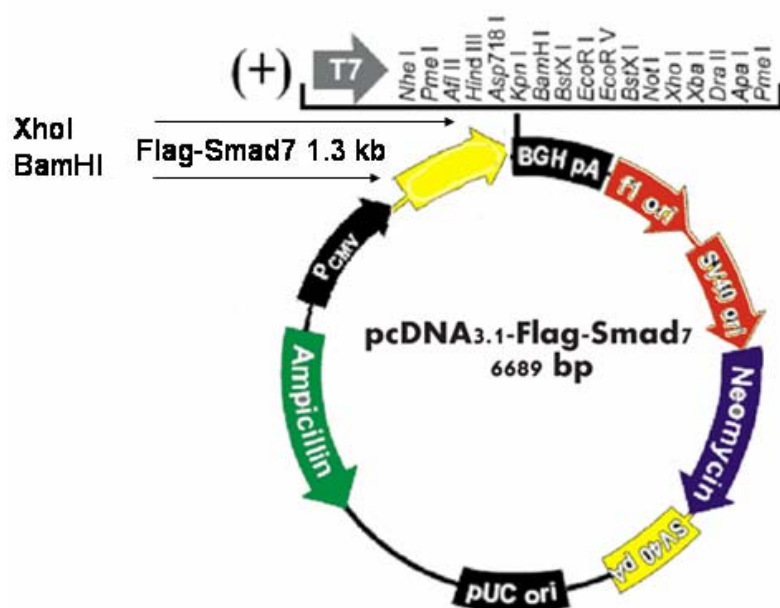
Figure 2.1: Gene map of the plasmid pcDNA3.1-Flag-Smad7 containing mouse Smad7 cDNA. Analytic restriction sites are indicated. CMV promoter: bases 232-819; T7 promoter/priming site: bases 863-882; Multiple cloning site: bases 895-1010; pcFNA3.1/BGH reverse priming site: bases 1022-1039 ; BGH polyadenylation sequence: bases 1028-1252; f1 origin: bases 1298- 1726; SV40 early promoter and origin: bases 1731-2047; Neomycin resistance gene (ORF): bases 2136-2930; SV40 early polyadenylation signal: bases 3104-3234; pUC origin: bases 3617-4287 (complementary strand); Ampicillin resistance gene: bases 4432-5428 (complementary strand); (Source: Modified from Invitrogen life technologies)

B: Plasmid U2

Table 2.6: Characteristics of Plasmid U2

Plasmid name	U2
Fragment of interest	CRP promoter from human
Plasmid size	8.2 kb
Restriction site used	SmaI
Kindly provided by	S. Kanzler (Department of Medicine I, University of Mainz)
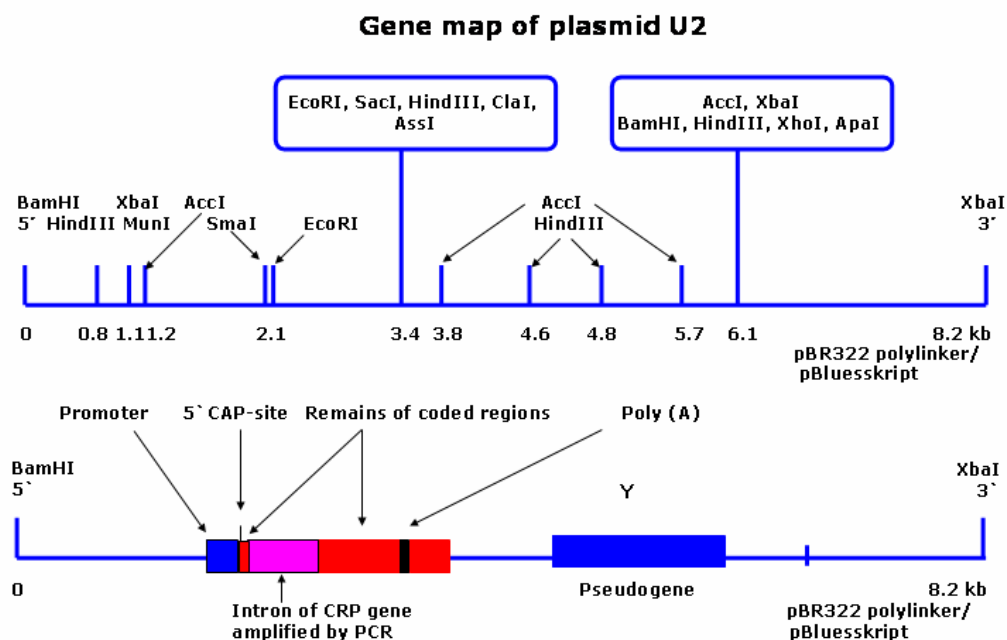
Figure 2.2: Gene map of the 8.2 kb plasmid U2 containing the human C reactive protein (CRP)-promoter. (Source: S. Kanzler, Department of Medicine I, University of Mainz).

2.5   Cloning strategy to create CRP-Smad7

In order to create CRP-Smad7 the plasmids U2 and pcDNA3.1-Flag-Smad7 harboring the human CRP-promoter and mouse Smad7, respectively were amplified. After cutting the plasmids at suitable sites using restriction enzymes, the fragments of interest were ligated as follows.

2.5.1   Amplification of plasmids pcDNA3.1-Flag-Smad7 and U2

Plasmid amplification was done in competent *Escherichia coli* DH5α cells.

Material and reagents

LB Medium
Agar, Gibco-BRL
Ampicillin 100 mg/ml
1.5 ml microfuge tubes
42° C water bath
Ice
37° C shaker

Protocol

1. Thaw competent cells (DH5α) on ice. 20–50 µl per tube.
2. Add max. 1-2 µl of a ligation reaction (10 ng/µl plasmid pcDNA3.1).
3. Mix very gently!
4. Incubate the tubes on ice for 30 minutes.
5. Heat shock the cells for 45 sec at 42° C.
6. Place the tubes immediately on ice for at least 2 minutes.
7. Add 950 µl of 2.5% LB-medium (100 µg/ml ampicillin) to each tube.
8. Incubate for 1 hour at 37° C and shake vigorously.
9. Spin down briefly and remove most supernatant (steps 9 and 10 are optional).
10. Resuspend thecell pellet with the remaining LB medium in the tube by pipetting.

11. Plate out 50-100 µl of the suspension on a LB agar plate (1.25% LB-Medium, 2% agar) containing the appropriate antibiotic (100 µg/ml ampicillin).

12. Incubate the plates at 37° C overnight.

2.5.2   Preparation of bacterial preparatory cultures

Protocol

1. Add 10 ml of sterile LB-Medium to a 50 ml falcon tube.

2. Pick one bacterial colony with an inoculation loop from the LB-Agar plate and transfer the bacteria to the liquid medium.

3. Incubate the flask with shaking at 37° C overnight.

2.5.3   Growth of bacteria

Protocol

1. Add 400 ml of LB medium to a sterile Erlenmeyer flask.

2. Transfer 0.8 ml of a preparatory culture into the Erlenmeyer flask

3. Incubate with shaking at 37° C overnight.

2.5.4   DNA plasmid maxi preparation

Plasmid-DNA preparation was carried out according to the "EndoFree Plasmid Maxi Protocol" (QIAGEN, Cat. No.12362).

2.5.5   Measuring plasmid DNA concentration

The concentration of plasmid DNA was measured at 260 and 280 nm using the RNA/DNA Calculator (Gene Quannt II, Pharmacia Biotech).

2.5.6 Plasmid restriction digestion analysis

Restriction enzyme digestions were performed by incubating double-stranded DNA molecules with a suitable amount of restriction enzyme, in its respective buffer as recommended by the supplier, and at the optimal temperature for that specific enzyme. All restriction enzymes and buffers were purchased from Roche. Standard digestions included one unit of enzyme per 200 ng of DNA.

2.5.7 Digestion of plasmid pcDNA3.1-Flag-Smad7

To isolate the fragment Flag-Smad7 from the plasmid pcDNA3.1-Flag-Smad7, the plasmid was treated with XhoI and BamHI as follows:

Protocol

1. Plasmid-DNA   50-100 ng
2. Restriction buffer B (10 x)   1.5   µl
3. Restriction enzyme XhoI (10 U/µl)   1   µl
4. Restriction enzyme BamHI (10 U/µl)   1   µl
5. dH$_2$O   15   µl
6. Incubation at 37° C   2   h

2.5.8   Digestion of plasmid U2

In order to ligate the fragment Flag-Smad7 into the plasmid U2 a SmaI (Roche, Mannheim, Cat. No. 656348)) restriction digestion of the vector was required:

Protocol

1. DNA   50-100 ng
2. Restriction buffer A (10 x)   2   µl
3. Restriction enzyme SmaI (10 U/µl) 1   µl
4. Add dH_2O 20   µl
5. Incubation at 25° C   2   h

2.5.9   DNA agarose gel electrophoresis

For DNA agarose gel electrophoresis gel concentrations were chosen according to expected fragment sizes.

Protocol

1. Agarose gels of different concentrations are prepared by mixing agarose with an appropriate volume of 1 x TAE buffer and dissolving the agarose by heating the mixture in a microwave for 2-4 minutes.
2. When the temperature reaches about 60° C, pour the gel onto a taped plate with casting combs in place. Allow the gel to polymerize for 1 hour.
3. Remove the tape and the gel casting combs carefully and lay the gel in a horizontal electrophoresis apparatus. Pour 1 x TAE buffer until the agarose gel dives 1 cm under the buffer.
4. Add DNA loading dye to each DNA sample, mix and load into the slots.
5. Electrophorese the gel at 90 V for 30-60 minutes until the required separation is achieved.
6. Place the gel for staining into ethidiumbromide solution (0,5µg/ml TAE buffer) for about 30 minutes.
7. Wash the gel with water and visualize DNA fragments in a UV light box (MWG Biotech, Germany).

2.5.10   Dephosphorylation of DNA fragments

Cleavage of the phosphate group

To avoid religation of digested vector DNA, 5´-phosphate groups of restriction fragments are treated with alkaline phosphatase (Roche Mannheim, Cat. No. 1758250, 1000 U) according to the following protocol:

Protocol

1. 100 ng digested plasmid e.g. U2   10 µl
2. 10 x dephosphorylation buffer   2 µl
3. Alkaline phosphatase (1 U/µl)   2 µl
4. dH$_2$O   6 µl
5. Incubation at 37°C   15 min

2.5.11   Purification of plasmid U2

Purification of plasmid U2 was performed with a QIAquick PCR purification kit (Cat. No. 28104). This protocol is designed to purify single- or double-stranded DNA fragments from enzymatic reactions. Fragments ranging from 100 bp to 10 kb are purified from primers, nucleotides, polymerases, and salts using QIAquick spin columns in a microcentrifuge.

2.5.12   Treatment of the fragment Flag-Smad7 with Klenow fragment

Klenow fragment was purchased from Roche, Cat. No. 008 412 001, 500 U (2 U/ µl)

The Klenow fragment (Mr 75000) of DNA polymerase I is used for partial or complete filling of 3´recessed ends (e.g. after restriction enzyme digestion). It carries a 5´→3´polymerase and a 3´→5´exonuclease activity of intact DNA polymerase I, but lacks the 5´→3´exonuclease activity of the native enzyme. The enzyme catalyzes the addition of mononucleotides from deoxynucleoside-5´-triphosphates to the 3´-hydroxyterminus of a primer/template DNA. This property can be used to synthesize DNA complementary to single-stranded DNA templates.

Protocol

1. Template DNA   1 μg
2. Nucleotides*, final concentration   1 mM of each dNTP* needed
3. 10 x Filling buffer   2 μl
4. Klenow fragment   1 U
5. Add dH_2O up to   20 μl
6. Incubation at 37° C   15 min

* Add dNTP`s as needed according to the sequence only. Filling buffer (10 x): 500 mM Tris (pH 7.5), 100 mM $MgCl_2$, 10 mM DTT, 500 μg/ml BSA. Inactivation of the enzyme is carried out by adding 2 μl 0.2 M EDTA (pH 8.0) and/or heat to 65°C for 10 minutes

2.5.13 Elution of DNA fragments from agarose gel slices

DNA fragments were eluted from Seakem agarose gels using the "freeze squeeze" method according to Thuring et al., 1975 [117] .

2.5.14 Test ligations and transformations (FERAY)

To test whether dephosphorylation has worked, religation of the vector was checked. For this, the "LigaFast TM Rapid DNA Ligation System", from Promega (Cat. No M8225, 500 Weiss units) was used.

Protocol

1. Digested and dephosphorylated plasmid e.g. U2   1 μl = 100 ng
2. T4 DNA ligase   1 μl = 3 U
3. 2 x rapid ligase buffer   5 μl
4. H_2O (nuclease-free)   3 μl

Incubate the reaction at room temperature for 15 minutes or over night at 16° C.

Size-fractionate the digestion mix on a 0.8% agarose gel along with the phosphorylated digested vector and compare the patterns. If you see linearized plasmid DNA dephosphorylation has worked.

Transformation of religated vector could be used as an alternative to assess success of dephosphorylation.

Protocol

1. Digested and dephosphorylated plasmid U2   1 µl = 100 ng
2. T4 DNA ligase   1 µl = 3 U
3. 2 x rapid ligase buffer   5 µl
4. H_2O (nuclease-free)   3 µl
5. Incubation for15 minutes at room temperature

For transformations, 1 µl of the ligation mix is added to 50 µl DH5α competent *E. coli* cells. These were plated on LB-Agar plates containing the appropriate antibiotics (see transformation of competent cells). After incubation at 37° C overnight, the number of colonies on each plate is counted. Dephosphorylation should reduce transformation efficiency of a linear plasmid by a factor of at least 50.

2.5.15   Ligation of the DNA fragment Flag-Smad7 into plasmid U2

The ligation was carried out by using "LigaFast TM Rapid DNA Ligation System" (Promega, Cat. No. M8225, 500 Weiss units).

Protocol

1. Assemble the following reaction in a sterile microcentrifuge tube:

Vector DNA (plasmid U2)	100 ng (1 µl)
Insert DNA (Flag-Smad7)	33 ng (1 µl)
2 x Rapid Ligation Buffer	5 µl
T4 DNA Ligase (Weiss units)	3 U
Nuclease-free water to final volume of	10 µl

2. Incubate the reaction at room temperature for 15 minute for blunt-end ligations.

Different concentrations (100, 20, 10 and 5 ng) of the plasmid U2 were used. Ligations were transformed into competent *E. coli* DH5α separately (see 2.7.1). Selected clones were picked up sterilely from LB-Agar plates and amplified in 10 ml LB-medium culture under shaking at 37°C overnight. For clone screening 3 ml culture were used for plasmid isolation using QIAGEN Plasmid Mini preparation Kit (Cat. No 12123).

Afterwards an analytical restriction analysis was performed. In order to obtain up to 500 µg endotoxin-free plasmid DNA for enzymatic reactions, EndoFree Plasmid Maxi Kit was used (QIAGEN-tip 500, Cat. No.12263).

The resulting plasmid was named CRP-Smad7.

2.6   DNA sequencing

Generated plasmids were checked by sequencing. An ABI310 sequencer and "ABI PRISM BigDye Terminator Cycler Sequencing Ready Reaction kit" with AmpliTaq® DNA polymerase, FS (PE-Applied Biosystems, Weiterstadt, Germany) was used for sequencing reactions.

1000 ng double stranded plasmid DNA/PCR product served as templates. The following primers were obtained from MWG-Biotech AG (Ebersberg) to sequence CRP-Smad7.

Table 2.11: Primers for CRP-Smad7 DNA sequencing

Designation	Region	Sequences
SmaI-sense	50 bases distance from SmaI restriction site of plasmid U2	5`- GTG AGG GGA TAG ATC TGT GTG-3`
StyI-sense	195 bases distance from 3`end of plasmid Flag-Smad7	5`-GCC TAC AGC CTG CAG CGG CCC-3`

The sequencing reaction was performed as follows.

Protocol

1. Big Dye Terminator premix   8   µl
2. Primer   40   ng
3. DNA template   1,000   ng
4. Add H_2O 20   µl

Cycling conditions for 25 cycles:

Denaturation	96° C	1 min
Denaturation	96° C	10 sec
Annealing	50° C	5 sec
Elongation	60° C	4 min
Cool down	4° C	∞

To remove excess of dye terminators, the product was purified with a Centri Sep Spin Column (PE-Applied Biosystems, Weiterstadt, Germany) and subsequently dried in a speed vacuum system.

Centri-Sep spin columns from Princeton Separations (P/N CS-901), are recommended. See manufacturer's instructions and User Bulletin Number 20 for more details.

Then each sample was resuspended in 25 µl of TSR (template suppression reagent, PE-Applied Biosystems, Weiterstadt, Germany) and denatured at 95° C for 2 min. Finally the sample was loaded into the capillary with a 30 second injection time at 2,000 V.

After purification of the DNA, sequence data were analysed by ABI Prism Sequencing Analysis version 3.0.1b3 software

2.7   Transfection and stimulation of CRP-Smad7 in vitro

Material

FuGENE-6 (Roche, Cat.No 1814443)

Lipopolysaccaride (LPS; L-8274; SigmaChemicals, Heidelberg, Germany)

Interleukin-1β (recombinant human IL-1β; Chemicon; IL038)

Interleukin-6 (recombinant IL-6; Chemicon; IL006)

HepG2 cells (human liver carcinoma)

DMEM (Dulbecco's Modified Eagle Medium)

Streptomycin

Penestrep

L-Glutamine

Protocol

Transfection using the FuGENE 6 reagent was performed as described by the manufacturer.

Stimulation of CRP-Smad7 was carried out by exposing the cells to either 100 ng/ml LPS, or 10 ng (100 U) /ml IL-6 plus 20 ng (200 U) /ml IL-1β, for 24 h. Control cells were left untreated.

2.8 RT-PCR

2.8.1 Isolation of total RNA from animal tissue

Total RNA from mouse liver tissue was isolated using the RNeasy Protect Mini Kit (QIAGEN, Cat. No. 74124). The kit provided an RNAlater RNA stabilization reagent to protect the RNA from degradation.

Material

RNeasy Protect Mini Kit (QIAGEN, Cat. No. 74124)
Mortar and pestle
20-gauge needle and syringe
Nunc CryoTubeTM Vilas 1.8 ml (Nunc, London, UK, 340711).

2.8.2 Omniscript® reverse transcription

Material

Omniscript RT Kit (50) (QIAGEN, Cat. No. 205111)
RNase inhibitor
Perkins Elmer 9700 Thermal Cycler

Protocol

For reverse transcription of total RNA follow the protocol recommended by Omniscript RT Kit (50) (QIAGEN, Cat. No. 205111

2.8.3   Polymerase chain reaction (PCR) to genotype transgenic mice:

To genotype CRP-Smad7 transgenic offsprings an automated cycler (PE 9700 Thermal Cycler) was used.

As templates 120 ng of the following double stranded DNAs were used:

- Plasmid U2 after reception of Flag-Smad7 fragment (CRP/Smad7)
- Mouse genomic DNA

Primers used were designed to flank a region of the sequence of Smad7. After a PCR reaction a specific 550 bp product was expected. Primers as indicated were synthesized by MWG Biotech, Ebersberg, Germany.

Designation	Region	Sequences
CRP-sense C	Correspond to the region beginning with nucleotide number 18181 on human CRP gene bank data	5`- AGA CTG TAT GAA CAG AAC AGT GG-3`
Smad7 –antisense C	Correspond to the region beginning with Nucleotide number 1770 on mouse Smad7 gene bank	5`-GGA CTC CAC GGC CTG AAG-3`

A mixture of dATP, dCTP, dGTP and dTTP with a final concentration of 10 mM of each triphosphate was used as working solution for all PCR reactions. Deoxynucleotides were purchased from Roche, Mannheim, Germany.

Taq DNA polymerase was provided from Amersham Pharmacia Biotech, Freiburg, Germany.

The following protocol was used for PCR reactions:

1. Let the frozen components thaw on ice and work on ice throughout.
2. Prepare a master mix
3. Vortex briefly the mix and distribute it in 0.2 ml PCR reaction tubes.
4. Add DNA template to each PCR tube.
5. Add the enzyme Taq DNA polymerase as the last component to each reaction.

Pipetting plan

Table 2.14: Pipetting plan

Component	Amount
Mg^{2+} containing 10 x buffer 10 mM	2.5 µl
DNA Template	120 ng
Downstream primer	5 pmol
Upstream primer	5 pmol
Deoxynucleotide mix (10 mM)	0.5 µl
Taq DNA polymerase	0.5 µl
H_2O up to	25 µl

A thermal Cycler PE 9700 (Perkin/Elmer USA) was programmed as below program for 35 cycles.

PCR step	Reaction time	Temperature
Preheat	5 minutes	95° C
Denaturation	1 minute	95° C
Annealing	30 seconds	56° C
Extension	1 minute	72° C
Extension of supposedly loop	7 minutes	72° C
Cool down	∞	4° C

2.9   Histopathology analysis

2.9.1   Immunohistochemistry

The basic principle of any immunochemical technique is that a specific antibody will combine with its specific antigen to give an exclusive antibody-antigen complex.

A specific antibody derived from an immunized animal recognizes and binds to specific amino acid sequences (epitopes) of its antigen. With the help of an e.g. horseradish peroxidase (HRP)-conjugated second antibody it is possible to detect specific antigen-antibody complexes.

2.9.2   Fixation and blocking of tissue in paraffin

Protocol

1. Incubation of tissue samples in 4% formaldehyde (10% formalin) for 12-24 h.
2. Remove the formalin and incubate in distilled water.
3. Ethanol 70% 2 x 4 h.
4. Ethanol 96% 2 x 4 h.
5. Ethanol absolute 2 x 4 h.
6. Xylene 3 x 2.5 h.
7. Liquid paraffin at 60° C 2 x 4 h.
8. Blocking of the tissue in a cassette.

2.9.3   Preparing and coating of slides with silane

Protocol

1. Incubate the slides 5 minutes in acetone.
2. Dry the slides at 60° C in a drying chamber.
3. Incubate the slides in a mix of 3-(Triethoxysilyl)-propylamin and acetone in a relation of 1:10.
4. Immerse the slides in acetone 2 x 3 minutes.
5. Immerse the slides in distilled water 1 x 3 minutes.
6. Dry the slides at 60° C in a drying chamber overnight.

Cutting of section

Cut the tissue section 4 μm thick and incubate at 37° C overnight.

2.9.4   Picro Sirius red staining

Sirius red staining is a method to detect collagen fibers. As a result of unbalanced tissue repair, fibrotic tissues synthesize increasing amounts of collagen fibrils. The difference to healthy can be visualized by Sirius red staining.

Material

1N HCl
NaOH
Xylene
Ethanol 100%, 95% and 70%
Distilled water
Formalin fixed and Paraffin embedded tissue section 5 μm thick

Reagents for 0.1% Picro-sirius red solution:

1. Sirius red F3B   0.5 g
2. Add Saturated aqueous picric acid 500 ml
3. Adjust pH 2 with NaOH
4. Keep the solution for 6 months at 4° C

Protocol

Deparaffinization:	Incubate the sections 40min at 60° C. Deparaffinize with xylene 3 x 5 minutes.
Dehydration through descending ethanol:	100% 1 x 2 minutes. 95% 1 x 2 minutes. 70% 1 x 2 minutes.
Hydration:	Running water for 1 minute.
Staining:	Dip the sections into 0.1% Picro Sirius red solution for 1 h.
Differentiation:	0.01 N HCl for 2 minutes.
Wash:	Running water 1 x 5 minutes.
Dehydration through ascending ethanol:	95% 2 x 10 seconds 100% 2 x 10 seconds
Saving the tissues by conservation:	xylene 2 x 10 sec. and cover the section with malin oil and cover glass.
Microscopy:	Use a bright field microscope.

2.9.5   Immunohistochemical staining

This protocol is based on immunostaining protocol recommended by "Cell Signaling" with modifications as indicated below:

Antigen unmasking using microwave:

1. Heat sections up to 95° C in 10 mM sodium citrate buffer pH 6.0 or EDTA pH 8 (depends on the antibody in use), then maintain the temperature at a sub-boiling temperature for 9 minutes (2 min 200 watt and 7 min. 150 watt).
2. Cool sections on the bench top for 35-40 minutes to reach a temperature of 37° C.
3. Wash sections in dH$_2$O three times for 5 minutes each.

Removing of endogenous peroxidase

Note: At this step work in a moist atmosphere by using a moist box.

4. Cover the tissues with some drops of "Peroxidase Blocking Reagenz" (DAKO, Cat. No. S2001) for 30 minutes.

Preparation and application of peroxidase substrate 3,3'-diaminobenzidine tetrahydrochloride (DAB)

5. Prepare substrate by dissolving 1 tablet of DAB in 16.6 ml 0.05 M Tris (hydroxymethyl) aminomethane, pH 7.6 (keep in dark).
6. Filter with filter paper.
7. Add 12 μl H$_2$O$_2$ to filtrate.
8. Cover sections by pipetting 200 μl of the substrate to each sample.
9. As soon as the color turns weakly brown, stop the reaction by immersing sections in running water for 5 minutes.

Counterstaining

10. Immerse the sections in Mayers Hämalaun solution for 30 seconds
11. Wash the sections in running water for 10 minutes.

2.10   Western blot

Western blot was used to analyse protein expression.

2.10.1   Production of protein lysate from tissues by homogenization

Material

mortar

liquid nitrogen

syringe with 0.75 mm needle

Protocol

1. Chill the mortar with liquid nitrogen.
2. Grind the tissue with mortal while adding nitrogen.
3. Mix a little grinded tissue (a spatula tip) with 500 µl RIPA (containing complete protease inhibitor) + (phosphatase inhibitor cocktail II).
4. Homogenize the tissue mix using a 0.75 mm needle.
5. Centrifuge at 14000 rpm for 10 minutes.
6. Remove the supernatant.
7. Measure the protein concentration with program CD Assay Biorad at 690 nm by means of Wallac Victor-1420 a multilabel, multitask plate r

2.10.2   Measurement of protein concentration

Protein concentrations were determined using the Dc Protein Assay (Bio-Rad Laboratories) based on the Lowry assay. Each sample was pipetted threefold into a microtiterplate and measured. The absorbance was read at 690 nm using a spectrophotometer (Wallac 1420 Victor, Wallac, Turku, Finland). Protein concentrations were calculated as an average value of three counts and related to the protein standard curve and blank value of RIPA.

2.10.3   SDS gel electrophoresis

Material

NuPAGE MOPS SDS running buffer (20 x) 500 ml (Invitrogen, NP0001)

NuPage LDS sample buffer (4 x), 10 ml (Invitrogen , NP0007)

SeeBlue (Invitrogen. LC5925)

Dithiothreitol (DTT, reducing agent, Sigma, D-9779,)

NuPAGE 4-12 % Bis-Tris Gel 1.5 mm x 10 well (Invitrogen, NP0335BOX)

NuPAGE transfer buffer (20 x) 1 L (Invitrogen, NP0006-1)

Nitrocellulose membrane sheet, 0.5 micron, 33 cm x 3 m roll (Pierce, Pierce, Woburn, MA, U.S.A.Prod # 88018)

Super Signal west dura stable peroxidase buffer (Pierce, Prod # 1856146)

Super Signal west dura luminol/enhancer solution (Pierce, Prod # 1856145)

Nitrocellulose membrane (Schleicher & Schuell, Dassel, Germany,10401180)

Whatman 3 MM (Schleicher & Schuell, 10426693)

Top-Block (Aluminum replacement, Fluka, Biochemika, 37766)

Protocol

Preparing samples for denaturing NuPAGE® gel electrophoresis

1. Preheat the NuPage Lsample buffer (4 x) to 37 °C
2. Pipet 30 µg of each protein in a 1.5 ml Eppendorf tube
3. Ad up to 27.5 µl dH$_2$O
4. Ad 2.5 µl 1 M DDT
5. Add 10 µl preheated NuPage SDS sample buffer (4x)
6. Vortex and centrifuge shortly
7. Heat to 70° C on a heat plate for 10 minutes while shaking
8. Centrifuge shortly
9. Put 40 µl of each sample per well on a NuPAGE 4-12% Bis-Tris Gel
10. Use 6 µl of SeeBlue as protein marker

11. Separate the proteins in the XCell SureLock™ Novex Mini-Cell (Invitrogen) at 100-150 V for 90 minutes.

For NuPAGE® Gel Electrophoresis and transfer of the proteins on a nitrocellulose membrane see "Instruction Manual NuPAGE® Technical Guide General Information" and protocols for using the NuPAGE® electrophoresis system. Transfer the proteins from a gel on a NC-membrane at 50-65 V and 300 mA for 2 h.
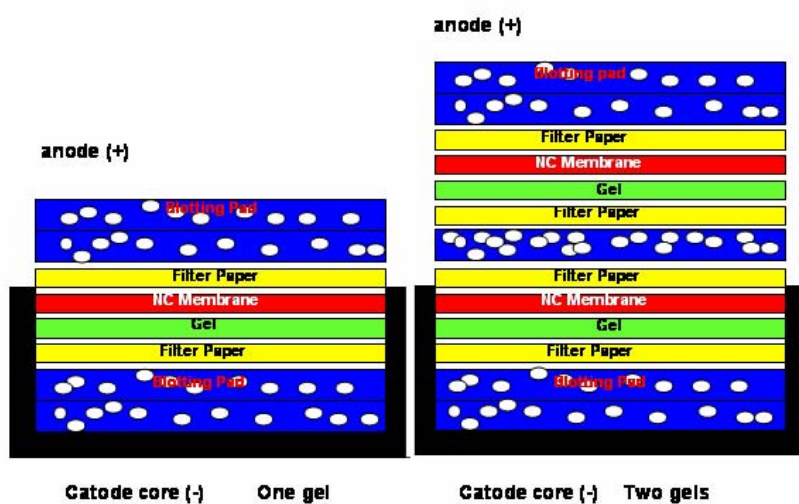

Figure 2.4: Diagrammatic construction of one gel and two gels Western Blot arrangements.

2.10.4   Detection of antigens

1. Wash the NC-membrane with 25 ml TBS for 5 minutes

2. Incubate the transfer membrane with 15 ml of 5% Bio-Skim Milk in TBST for later treatment with monoclonal antibodies (or 5% Top-Block in TBST for later treatment with polyclonal antibodies, albumin replacement, Fluka) while shaking for 1 hour

3. Incubate the transfer membrane overnight in 5% Bio-Skim Milk in TBST with a first antibody at 4° C while shaking

4. Wash three times with TPST, 5 minutes each

5. Incubate the transfer membrane in 5% Bio-Skim Milk in TBST with second HRP-conjugated antibodies

6. Wash three times with TBST, 5 minutes each

7. Mix 350 µl peroxide buffer with 350 µl luminol/enhancer solution

8. Distribute the mix equally on the transfer membrane

9. Incubate for 5 minutes

10. Develop the transfer membrane using the Lymi-Analyser as soon as you see a colour change.

2.11   Analysis of hydroxyproline

Hydroxyproline and proline are main components of collagen. The prime structure of collagen consists of glycine-X-Y, where proline substitutes X and hydroxyproline Y. Hydroxyproline is built of proline in the presence of vitamin C. Hydroxyproline gives strength to the collagen molecule and its level increases during fibrosis. For this reason it is a useful marker of fibrosis.

2.11.1   Hydroxyproline assay

Material

Nitrogen and nitrogen container

Special glass tube (Schott Duran 12 x 100, 26 135 11 55, Roth, K248.1)

1.9 ml reaction tube (Roth, 7550.1)

Microtube Tough-Tags, sticker (Roth, 1.5-2 ml Tubes)

Analysis balance

Incubator 110° C

Water bath 50-56° C

Spatula

Filter paper

50 ml Erlenmeyer flask

Spectrophotometer, Pharmacia Biotech, Ultraspec 2000

Filter papers, Folded MN 615, ¼ 9 diameter (Machery Nagel, 531009)

Glas funnel

Reagents

37% concentrated HCl (Merck, 1.00317.1000)

4-(Dimethyl-amino) benzaldehyde, Ehrliche`s Reagenz (Sigma, D2004-100G).

Chloramine-T-hydrate (Sigma, C9887-250G)

Isopropanol (Merck, 1.09634.2500)

Perchloric acid 70% (Fluka, 77230)

Natriumacetat

Citric acid

Protocol

Refer to Jamall et al. 1981, Boigk et al. 1997 [9].

Note: Spatula and special glass tubes (Schott Duran) are prechilled in nitrogen. Do not let the pulverized tissues be thawed before mixing it with 6N HCl. To make 6N HCl mix 49.7 ml (12N, 37% concentrated HCl) with 53.3 ml H_2O

1. Put at least 50 mg of pulverized liver tissues in cold special glass tube (Schott Duran) using a chilled spatula and add 1 ml 6N HCl
2. Incubate at 110° C overnight for 16 hours in an incubator
3. Vortex for 10 seconds
4. Filtrate the homogenate with filter paper
5. Pipette 2 x 30 µl of the filtrate in 1.5 ml Eppendorf tubes for double measurements
6. Add 10-30 µl of methanol to the filtrate
7. Vortex briefly
8. Let the reagent dry for 30 minutes in a heat block at 37° C under nitogen gas access.
9. The pellet can be stored at -20° C
10. Prepare a Hydroxyproline standard sample as described below

Note: Hydroxyproline (HP) stock solution is 1 mg/ml in 50 % Isopropanol. Dilute the HP stock solution 1:100 in 50% Isopropanol to reach a concentration of 10 µg/ml.

Standard Nr.	Hydroxyproline µg	HP working solution (10µg/ml) µl	50 % Isopropanol µl
0	Blank value	0	500
1	0.1	10	490
2	0.2	20	480
3	0.3	30	470
4	0.4	40	460
5	0.5	50	450
6	0.7	70	430
7	0.8	90	410
8	1.1	110	390
9	1.3	130	370
10	1.5	150	350
11	1.7	170	330

11. Treat the hydroxproline standards from Step 13 like samples

12. Dissolve the pellet in 1 ml of 50% Isopropanol

13. Pipette 100 µl of freshly prepared 0.84% Chloramin-T solution to 0.5 ml of the sample solution

14. Vortex briefly

0.84 % Chloramin-T solution (fresh)	Reagent	Volume for 100 ml
	Chloramin T	840 mg
	Cloramin-T Puffer	60.5 ml
	Isopropanol 100%	39.5 ml

Chloramin-T buffer:	Reagent	Concentration mM
pH 6 (2 N sodium hydroxyd)	Sodium acetate	42
	Citric acid	2.6

15. Incubate for 10 minutes at room temperature

16. Add 0.5 ml of freshly prepared Ehrlich´s reagent solution.

Ehrlich´s Reagent solution (Fresh)	Reagant	Volume for 500 µl
	Ehrlich´s Reagent	124 mg
	70% perchloric acid	135 µl
	Isopropanol 100%	365 µl

17. Incubate in awater bath at 50-56 °C for 90 minutes.

18. Measure the absorbance of all HP standards and samples at 558 nm against a blank value.

19. The HP value is calculated in µg/g liver.

2.12   Hyaluronic acid assay

Serum hyaluronic acid (HA) levels can be elevated in various liver diseases, e.g. liver fibrosis and cirrhosis, due to decreased hepatic removal and/or increased hepatic production. Increased HA levels have shown a better correlation with the degree of histopathological damage than conventional liver function tests including ALT/GOT, alkaline phosphatase and bilirubin. HA levels have also been shown to be an early marker of liver damage from toxic agents such as ethanol, acetaminophen, and bacterial lipopolysaccharide. Changes of the sinusoidal endothelial cells (SEC) in response to these agents precede pathological changes of the hepatocytes.

Protocol

Hyaluronic acid assay

The concentration of hyaluronic acid in the serum of mice was determined with a Hyaluronic Acid (HA) Quantitative Test Kit (Corgenix, Colorado, USA). Absorbance at 450 nm was determined using a Victor 1420 Multilable Counter spectrometer (Wallac, Wellesley, USA).

2.13   Measurement of liver enzymes in the serum of mice

To measure the concentration of serum enzymes ca. 1 ml of blood was taken from anaesthetized mice by a needle prick into their eyes. Serum was produced by centrifuging the blood at 3000 rpm for 10 min. Aspartate aminotransferase (AST), alanine aminotransferase (ALT) and alkaline phosphatase (AP) concentrations were determined by using the VITROS Chemistry Products Calibrator Kit 3 and VITROS Chemistry Systems (Ortho-Clinical Diagnostics).

2.14   Induction of fibrosis with CCl$_4$ and stimulation of CRP-Smad7 construct with LPS

Animals were divided in four groups e.g. CCl$_4$ group, LPS group, CCl$_4$ + LPS group and control group in an experiment arranged for 8 weeks. In order to keep small mortality rate of animals in the CCl$_4$ group a pretreatment with CCl$_4$ was necessary . This was achieved by i.p. of 12.5% CCl$_4$ in mineral oil two times/week followed with one week rest period. Thereafter they were treated with 25% CCl$_4$ in mineral oil two times /week for entire 8 weeks. The LPS group were injected i.p. with 10 µg LPS in PBS/ 25 g mice three times/week.. After six weeks the LPS dose was increased up to 25 µg LPS in PBS/ 25 g mice for entire further two weeks. The control mice for CCl$_4$ group were treated with 50 µl mineral oil two times/week. for 8 weeks. To limit mortality, experimental mice determined for CCl$_4$ and LPS treatment have been injected at alternate days with both.

2.15   Statistical analysis

At least 20 animals were used for each group investigation. The data presented are representative for 3 or more similar experiments. The results were expressed as means ± standard deviation (SD), and statistical analysis was carried out using Student t-test for paired data. Differences at P< 0.01 were considered to be significant.

Notification: Graphic designation with one star (*) refers to statisticcal analyse between the FVB mice and S7tg mice in CCl$_4$ + LPS treated group. Two stars (**) refer to statisticcal analyse between the FVB mice and S7tg mice in CCl$_4$ treated group and three stars (***) refer to statistical analyse between the CD-1 mice and S7△E1 mice in CCl$_4$ treated group

3   Results

3.1   Cloning of CRP-Smad7

In order to investigate the antifibrotic effect of Smad7 on liver fibrosis, CRP-Smad7 transgenic mice were generated. For that purpose a plasmid CRP-Smad7 was created. 1.3 kb mouse Smad7 cDNA was cloned into a vector under control of the human C-reactive protein promoter. In order to simplify the detection of transgenic derived Smad7 in protein lysates a 42 bp long Flag-tag was linked to Smad7. The mouse Flag-Smad7 cDNA deriving from the 6.689 kb pcDNA3.1-Flag-Smad7 plasmid (friendly gift of P. ten Dijke) was cut using the BamHI and XhoI restriction sites. The resulting sticky ends were completed using the Klenow fragment achieving a smooth end. To subject the mouse Smad7 cDNA fragment (Flag-Smad7 insert) under control of the human C-reactive protein, a 8.2 kb plasmid, U2 (friendly gift from department of Medicine I, University of Mainz, Dr. S. Kanzler) harboring a human CRP promoter fragment, was digested at its SmaI restriction site. After that the Flag-Smad7 fragment was inserted into the promoter site as follows (figure 3.1).
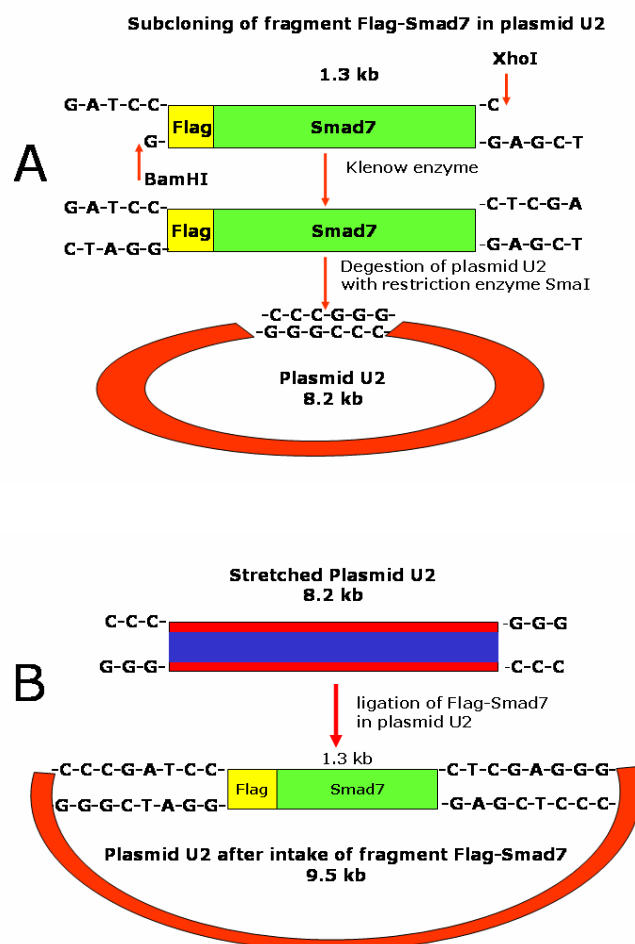
Figure 3.1: Diagram showing the cloning strategy for CRP-Smad7
 A: The Fragment Flag-Smad7 was obtained by digestion of pCNA3.1-Flag-Smad7 using BmaHI and XhoI. The digestion sites were extended using Klenow fragment; B: In order to clone the fragment Flag-Smad7 into the plasmid U2 it was digested with SmaI.

After ligation of the Flag-Smad7 fragment into the plasmid U2, the samples were transformed into competent *E. coli* DH5α cells. Colonies were picked up sterilely from the agar plate and amplified in 10 ml LB-medium. For clone screening 3 ml of transfected competent cells (DH5α) were prepared using the QIAGEN Plasmid Mini preparation Kit. The isolated DNA was restricted by XbaI and subjected to agarose gel electrophoresis (figure 3.2). The expected fragments of 6.3, 2.1 and 1.1 kb could be visualized on an agarose gel indicating the successful cloning of CRP-Smad7.
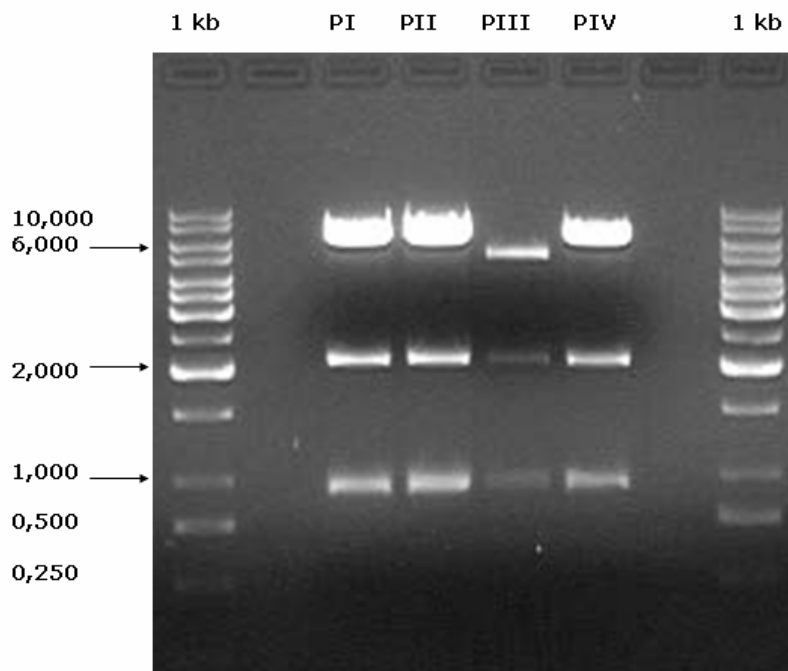
Figure 3.2: Control gel to check CRP-Smad7. Four different clones (PI to PIV) were checked. After plasmid mini preparation the DNA was digested with XbaI. Three different fragment sizes i.e. 6.3. 2.1 and 1.1 kb were expected.

Insertion of Flag-Smad7 increased the size of U2 by 1.3kb. The resulting plasmid CRP-Smad7 contained 9.5 kb. Figure 3.3 shows a gene as well as a restriction map of CRP-Smad7.
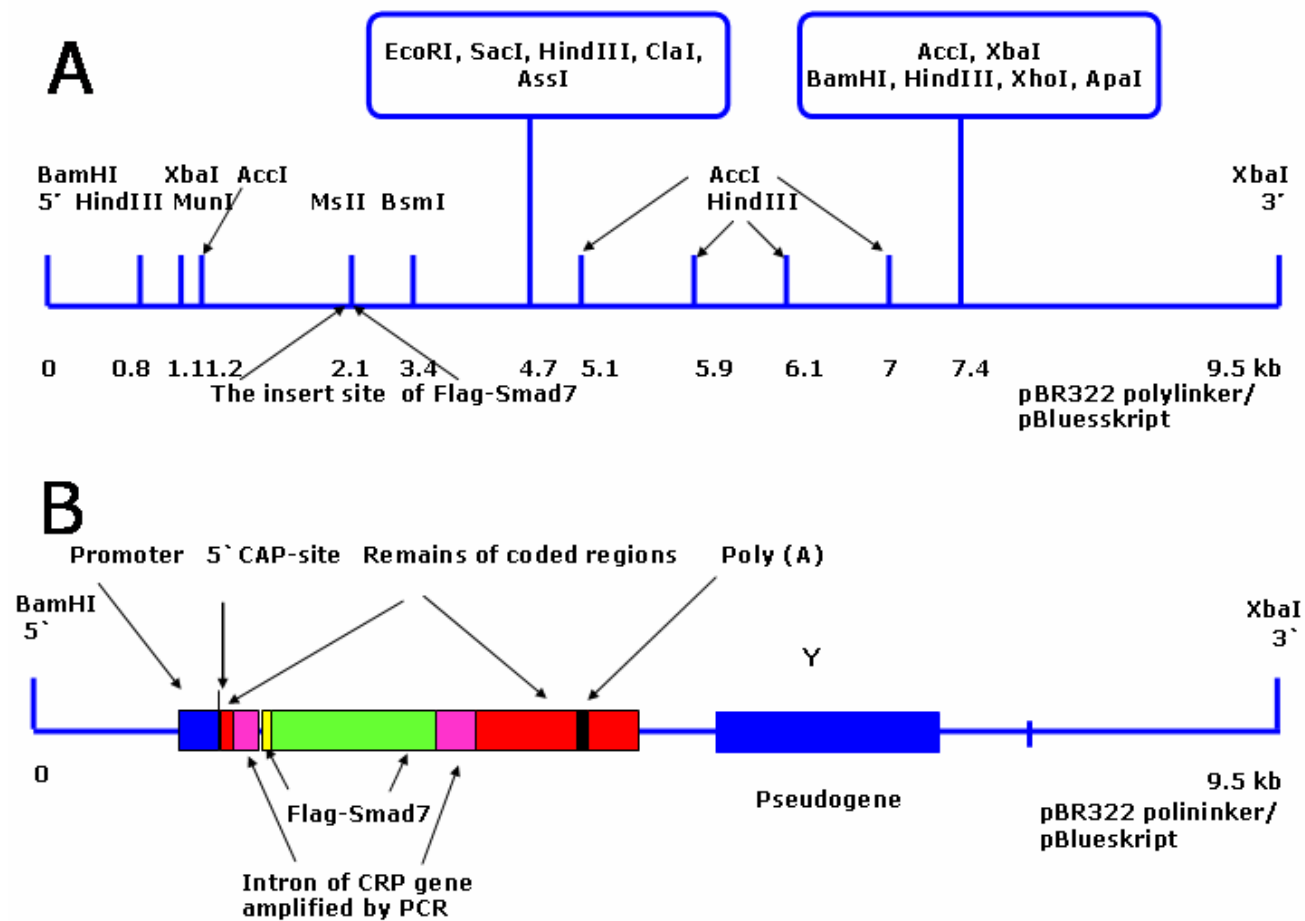
Figure 3.3: Restriction map (A) and gene map (B) of CRP-Smad7.

Sequence analysis confirmed successful insertion of the fragment Flag-Smad7 into the vector U2 (figure 3.4).
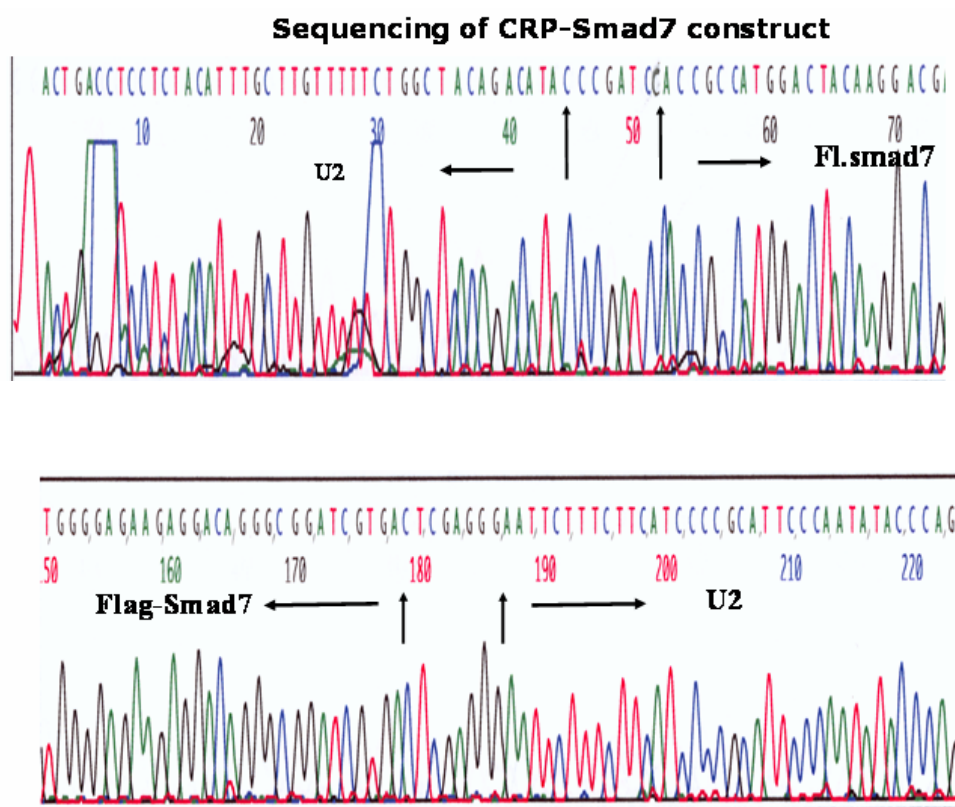
Figure 3.4: Sequencing of CRP-Smad7. The arrows indicate the ligation sites between Flag-Smad7 and the original U2 vector.

3.2   Smad7 expression in HepG2 cells

To prove the biological activity of CRP-Smad7 HepG2 cells were transfected with plasmid DNA using FuGENE. Expression of Smad7 was stimulated by treatment of the cells with IL-1 (10 ng/ml), IL-1 + IL-6 (30 ng/ml) and LPS (100 ng/well) for 24 h. Afterwards cell lysates were analysed by immunoblotting as shown in figure 3.5. Whereas IL-1 was not able to stimulate the CRP promoter, co-induction of the CRP promoter with both, IL-1 and IL-6, as well as LPS application resulted in the stimulation of the CRP promoter. Flag-Smad7 expression was determined by Western blotting and immunostaining. A lysate obtained from HSCs infected with Adenovirus-Smad7 (AdSmad7) in cell culture served as a positive control.
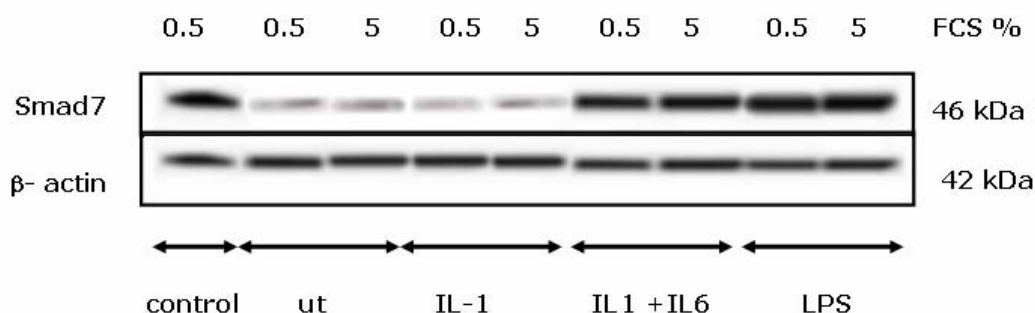
Figure 3.5: Expression of Flag-Smad7 in HepG2 cells transfected with CRP-Smad7. Expression was induced *in vitro* by treatment with either IL-1 (10 ng / ml), IL-1 (10 ng/ml) + IL-6 (30 ng / ml) or LPS, 100 ng / well, for 24 h. Smad7 expression (46,428 kDa) was visualized by Western blotting using polyclonal goat anti-Smad7 antibodies. (abcam; ab5825;2 µg/ml). A lysate of HSCs infected with AdSmad7 was used as a positive control. As a loading control, the blot was reprobed with monoclonal mouse anti-β-actin antibodies (SIGMA;A5441;1:10000). The protein load per well was 20 µg. Abbr. ut = untreated., FCS = focal calf serum.

3.3   Generation of CRP-Smad7 transgenic mice

3.3.1   Microinjection of CRP-Smad7 into fertilized eggs of FVB/N mice

Transgenic mice were generated according to standard procedures (Hogan, B. L. M., F. Costatini, and E. Lacy. Manipulating the Mouse Embryo. A Laboratory Manual. Cold Spring Harbor, New York: Cold Spring Harbor Laboratory, 1986.) by microinjection of vector-free CRP-Smad7 DNA (Figure 3.6) into fertilized eggs of FVB/N mice. By transformation 70 potentially transgenic mice were generated. By PCR 9 CRP-Smad7 transgenic mice founders could be verified. Finally, two positive transgenic founders survived and built two stable lines (2408 and 2448). Genotyping of transgenic mice was done by analysing DNA from tails of 4 weeks old offspring by PCR and subsequent gel electrophoresis analysis (figure 3.7). Positive transgenic offspring were mated to build stable transgenic lines.
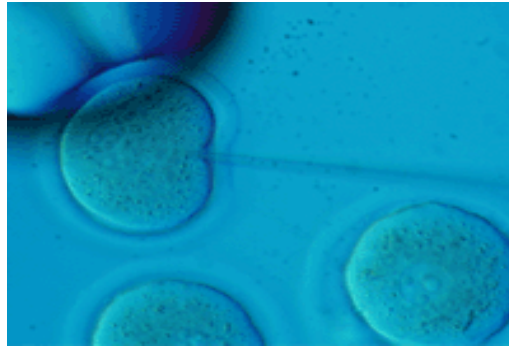
Figure 3.6: Microinjection of CRP-Smad7 into fertilized eggs of a superovulated female FVB/N mouse.
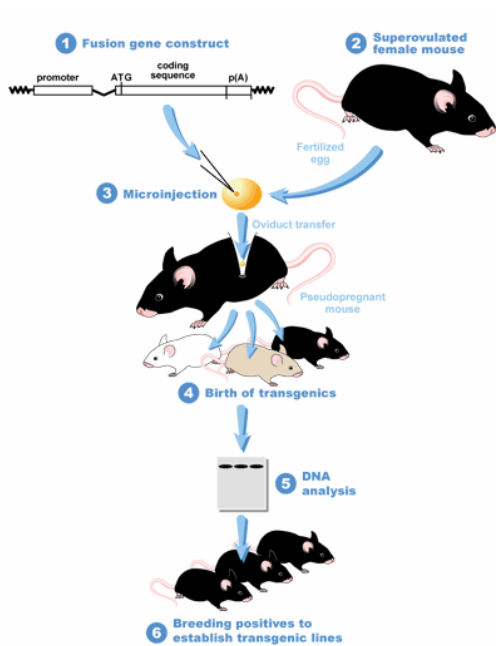

Figure 3.7: Schematic presentation to show the creation of CRP-Smad7 transgenic mice.

The transmission of CRP-Smad7 was differently between new generations of line 2408 and 2448. Whereas CRP-Smad7 construct was distributed evenly between offspring from line 2448, it was transmitted predominantly by female mice of line 2408 as shown in figures 3.8 and 3.9.
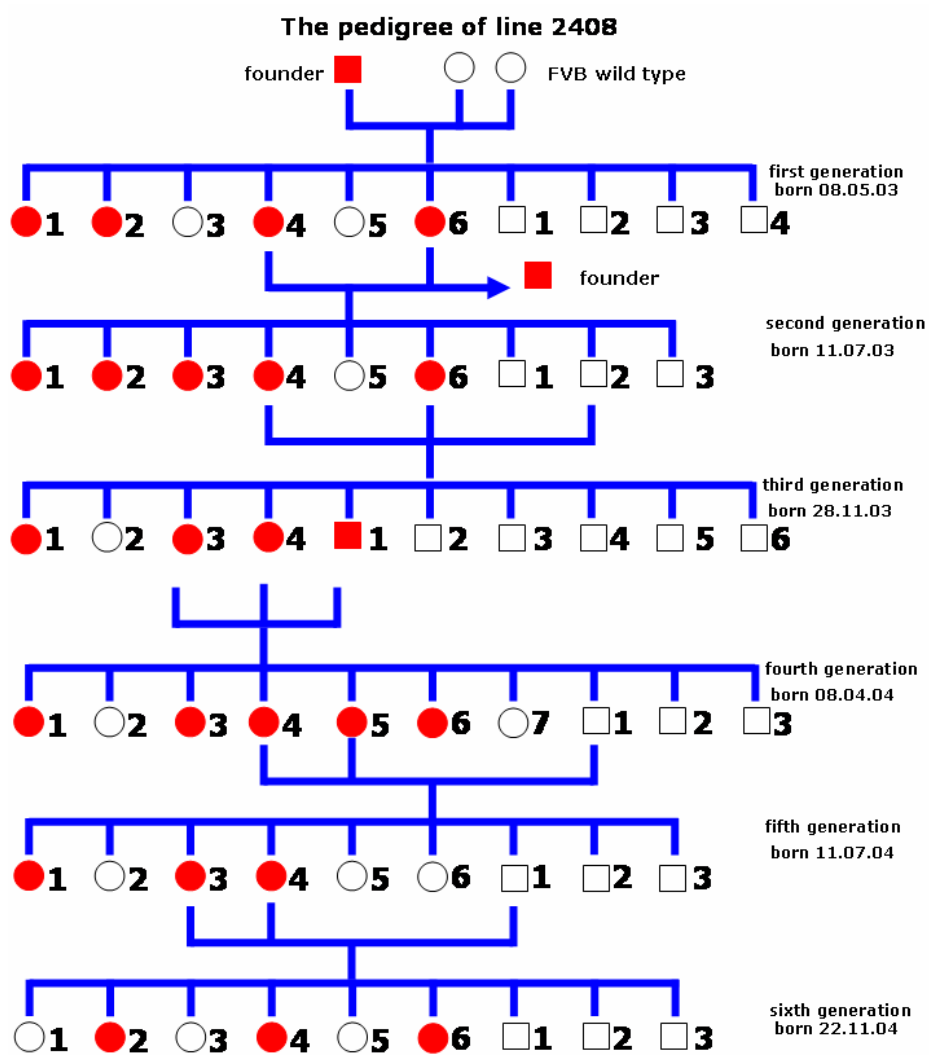
Figure 3.8: Pedigree of CRP-Smad7 transgenic mice line 2408. CRP-Smad7 was transmitted mainly by female transgenic animals.

Indications: female wild type ◯ ,   male wild type ☐ ,

female transgenic ● ,   male transgenic ■ .

Figure 3.9: Pedigree of CRP-Smad7 transgenic mice line 2448. The diagram indicates even distribution of CRP-Smad7 within different generations.

Indications: female wild type ◯ ,   male wild type ☐ ,

female transgenic ● ,   male transgenic ■ .

3.4   Genotyping of CRP-Smad7 transgenic mice

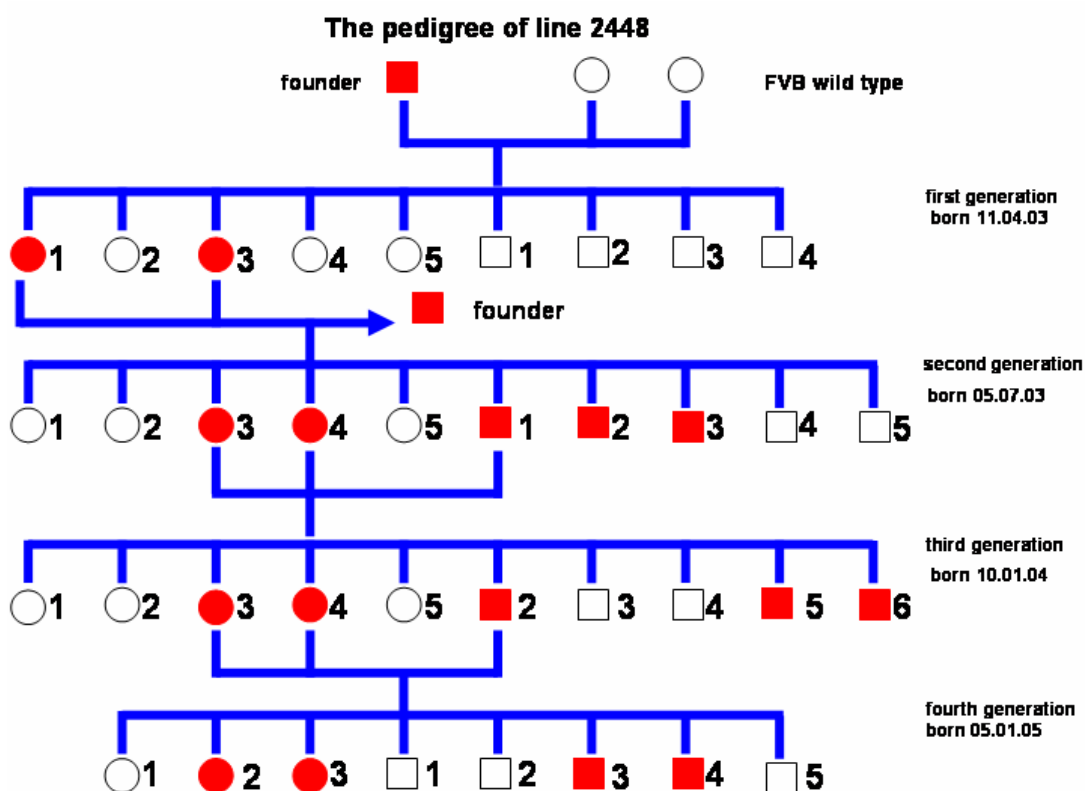In order to genotype transgenic offspring mouse tail DNA was isolated 4 weeks after birth and was analysed by PCR. Primers used are listed in Table 3.1. The expected PCR fragment using the CRP-sense C and Smad7 antisense C primers is 550 bp long. The result was checked by subsequent agarose gel electrophoresis. Figure 3.10 shows examples of the results of transgenic offspring as well as CRP-Smad7 negative animals.

Table 3.1: Primers used to genotype CRP-Smad7 transgenic mice.

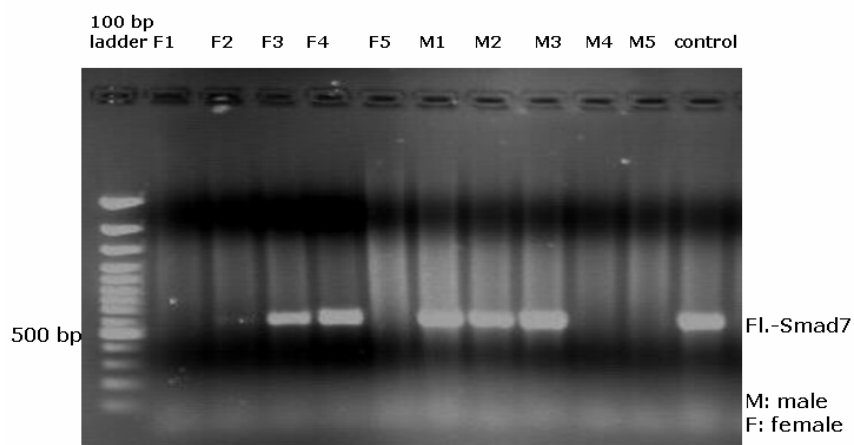| Designation	Region	Sequences
CRP-sense C	Correspond to the region beginning with nucleotide number 18181 on human CRP gene bank	5`- AGA CTG TAT GAA CAG AAC AGT GG-3`
Smad7 antisense C	Correspond to the region beginning with nucleotide number 1770 on mouse Smad7 gene bank	5`-GGA CTC CAC GGC CTG AAG-3`

Figure 3.10: Genotyping of transgenic offspring. To select CRP-Smad7 positive transgenic mice from negative ones, tail DNA from 4 weeks old offspring was analysed by PCR. Positive transgenic animals are indicated by a PCR product of 550 bp; abbreviations: F= female, M= male.

3.5 In vivo stimulation of Flag-Smad7 expression by LPS

To prove the expression of Smad7 in the created transgenic animals analysis of protein lysates, tissue sections and RNA was performed by Western blots, immunohistochemical staining and RT-PCR after stimulation of the CRP promoter by i.p. LPS injections.

3.5.1 Analysis of Flag-Smad7 expression by Western blotting

In order to investigate the expression of Smad7 in transgenic mice Western blot analysis was done. To simplify the detection of transgenic derived Smad7 in protein lysates a Flag-tag was linked to Smad7 in the CRP-Smad7 plasmid. Detection of the Flag-tag by specific monoclonal antibodies in protein lysates from CRP-Smad7 transgenic mice was used to study the expression of transgenic derived Smad7 indirectly. As figure 3.11 shows CRP-Smad7 transgenic mice stimulated with LPS expressed Flag-Smad7. In comparison FVB, CD-1 wild type and S7$\triangle$E1 (S7KO) mice do not express Flag-Smad7. Neither CCl$_4$ nor LPS treatment alone induced expression of Flag-Smad7 in these mice strains.
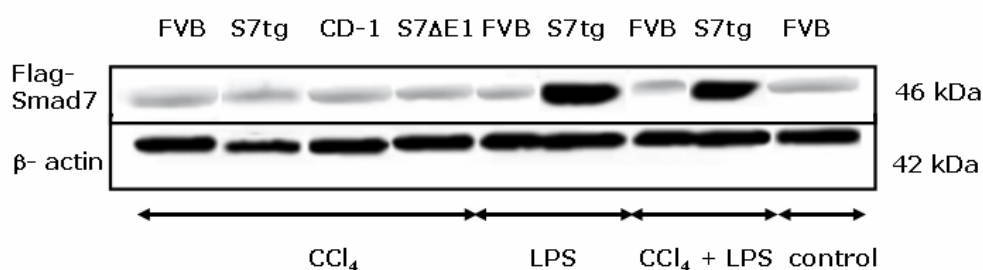
Figure 3.11: Liver protein lysates (20 µg) from different strains as indicated were examined for expression of Flag (Flag-Smad7) by Western blot analysis. Representative photomicrographs of results obtained with 10 S7tg and 10 FVB wild type mice as well as 8 S7$\triangle$E1 and 8 CD-1 wild type mice after 8 weeks of CCl$_4$, LPS and CCl$_4$ + LPS intoxication are shown. For the detection of the Flag-tag monoclonal mouse anti-Flag antibodies (SIGMA; F3165;20 µg/ml) and a Peroxidase-conjugated (HRP) polyclonal goat anti-mouse serum (Santa Cruz: sc-2005; 1:5000) were used. Blots were reprobed with monoclonal mouse anti-β-actin antibodies (SIGMA; A5441; 1:10000) to confirm equal protein loading. abbr.:S7tg = CRP-Smad7 transgenic mouse, FVB = wild type strain; S7$\triangle$E1 = Smad7 knockout mouse, CD-1 = mixed wild type strain.

3.5.2   Analysis of Flag-Smad7 expression by immunohistochemical staining

A further evidence for the expression of Flag-Smad7 in the transgenic animals created in this study provided immunohistochemical staining of tissue sections from CRP-Smad7 transgenic offspring after stimulation by i.p. injection of LPS. 4 μm thick sections from 3.5% formaldehyde (10% formalin) fixed tissues were stained with monoclonal antibodies against the Flag fragment. As expected transgenic mice stimulated by LPS or both CCl_4 + LPS expressed Flag-Smad7 (figure 3.12).
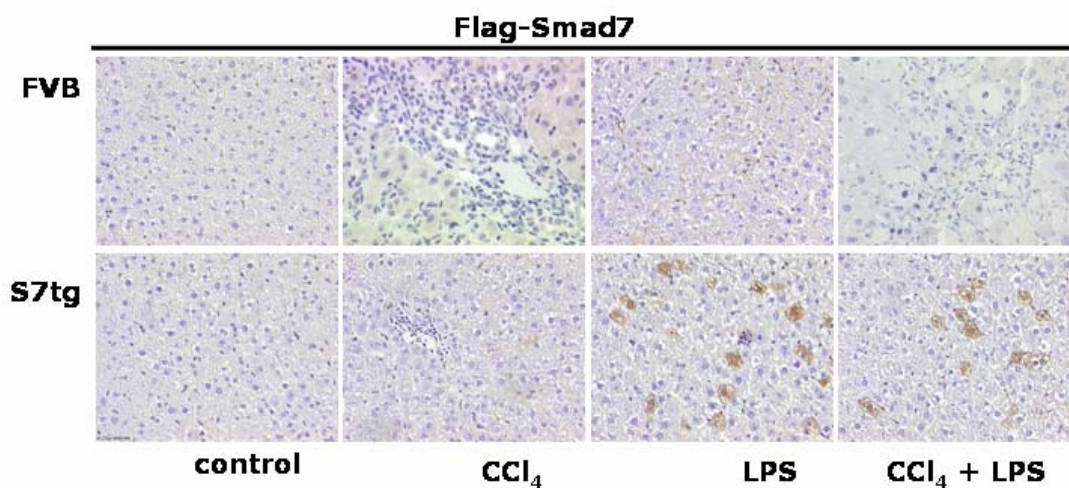
Figure 3.12: S7tg mice stimulated with both, LPS or CCl_4 + LPS express the Flag fragment. Representative photomicrographs of mice liver sections from S7tg and FVB wild type treated for 8 weeks with CCl_4 and/or LPS are shown. Untreated cells of both strains serve as controls. Brownish signals indicate Flag-Smad7 expression; Magnification x 100.

3.5.3   RT-PCR analysis to detect CRP-Smad7 RNA expression

For RT-PCR analysis, RNA was isolated from liver tissues of transgenic offspring with "RNeasy Protect Mini Kit". 2 µg of total RNA was used in order to amplify a potential Flag-Smad7-fragment of 550 bp using specific primers (see Material and Methods). To control the quality of the RNA used a CSRP2 gene fragment constitutively expressed in all the mouse genomes, was identified with two specifies primers. As figure 3.13 shows transgenic mice stimulated with LPS or both, CCl$_4$ + LPS transcribed Flag-Smad7 specific RNA in contrast to wild type animals.

Figure 3.13: Detection of Flag-Smad7-RNA. 2 µg of total RNA from mice was analysed by RT-PCR using a Omniscript RT Kit (50) (QIAGEN). Only LPS stimulated CRP-Smad7 transgenic mice expressed Flag-Smad7. The expression of CSRP2 RNA was analysed as a RNA quality control.

3.6   Induction of fibrotic liver damage in mice

In order to investigate the antagonizing effect of Smad7 overexpression in hepatocytes during liver fibrogenesis, experimental mice were subjected to CCl_4 induced fibrotic conditions.

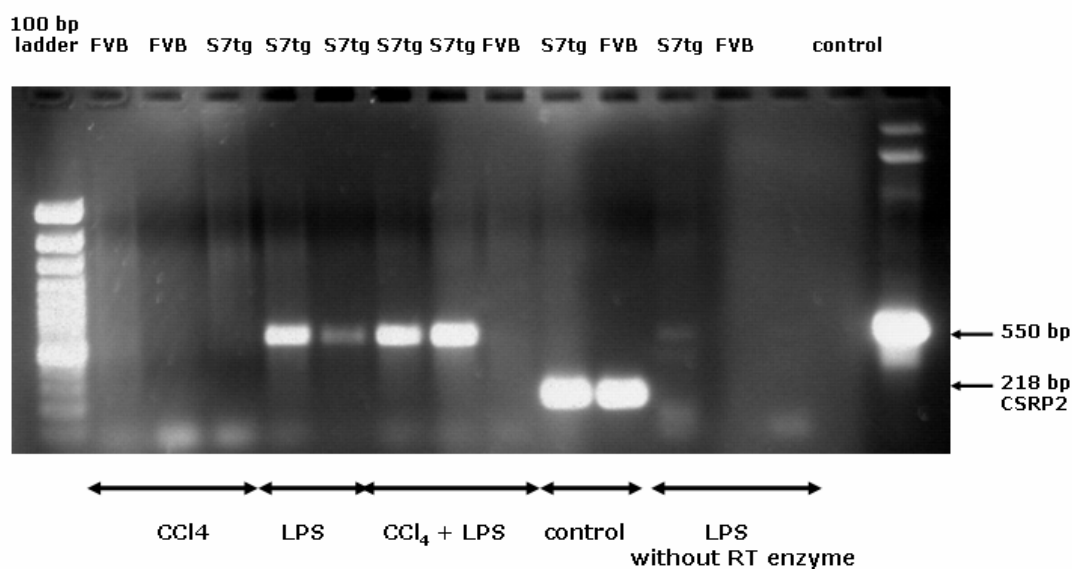For this 78 experimental mice in the age of 4-8 months were chosen. CRP-Smad7 transgenic mice (S7tg), wild type mice with FVB background, Smad7 knockout animals and the corresponding wild type mice with CD-1 background were used for this study. The Smad7 knockout mouse strain carries a targeted deletion of exon1, including the start codon and parts of intron 1, within the Smad7 gene. These mice will be referred to herein as S7$\triangle$E1 mice.

The animals were divided into four groups. For induction of fibrosis the first group was administered 25% CCl_4 in mineral oil interperitoneal (i.p.) two times per week. To induce the CRP promoter and cause Smad7 overproduction in hepatocytes of CRP-Smad7 transgenic mice the second group was treated with LPS (10 µg LPS in PBS/25 g mouse. The LPS dose was increased up to 25 µg/ mouse after six weeks.) i.p. only three times per week. In order to compare the effect of the Smad7 overproduction in hepatocytes of transgenic mice to FVB wild type animals under CCl_4 fibrotic conditions, the third group was injected i.p. with both, CCl_4 and LPS, two and three times per week, respectively. The fourth group of animals, consisting of mice with FVB and CD-1 backgrounds, was left untreated and served as a control. As an exception the control group of CCl_4-treated animals was injected with mineral oil (50 µl/25 g body).

The state of health of all experimental animals was controlled by determining their body weights every day. After 8 weeks of stimulation and induction of experimental mice with LPS and/or CCl_4 they were killed. The extent of liver damage could be determined preliminary by the observation of morphological changes of the liver (e.g. white pearls covering damaged livers of experimental mice). Further blood was taken for serum analysis; liver tissues were used for RT-PCR, Western blot and immunohistochemicla staining. Figure 3.14 gives an overview about the experimental setup.
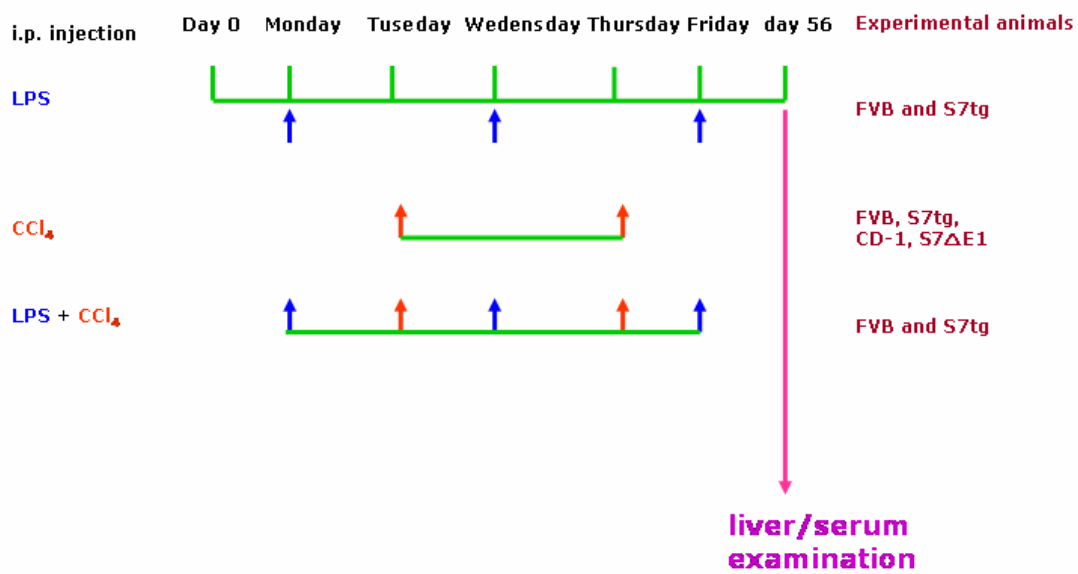
Figure 3.14: Experimental setup for *in vivo* induction of fibrosis and stimulation of Smad7 expression in mice of different strains as indicated.

3.7 Smad7 expression in hepatocytes decreases collagen deposition in CCl$_4$ treated mice

A significant feature of chronic liver fibrosis is the deposition of abnormal matrix by up-regulation of matrix components including collagen. Collagen is one of main the components of the ECM produced by activated HSC in damaged tissues. Correspondingly, an effective method to reduce fibrosis could be the inhibition of collagen synthesis. Further increased collagen synthesis can serve as a marker of fibrosis.

The collagen content measured by Picro Sirius red staining in all four animal groups (figure 3.15) proves that CCl$_4$ treatment induces liver damage. 10 FVB wild type mice (i.e. n = 10) synthesized 3.5 ± 0.4% collagen whereas S7tg mice (n = 10) produced 2.48 ± 0.2% collagen. That translates into a ratio of 1:1.4 (Table 3.2). Percentages give the size of stained areas compared to the total area investigated and are assumed to be proportional to the expression level of detected proteins. In the LPS treated group no noticeable difference between collagen expression in FVB wild type and S7tg mice can be detected. A significant difference in collagen synthesis between FVB wild type and S7tg can be observed in the CCl$_4$ + LPS treated group. S7tg mice treated like this showed a reduced collagen synthesis (1.14 ± 0.3%), whereas FVB wild type mice synthesize a relatively higher amount of collagen fibrils under the same fibrotic condition (3.84 ± 0.45%), (figure 3.15). That implies a 3.4 times higher collagen synthesis in FVB wild type than in S7tg mice. The quantitative data suggests a dramatic decrease of collagen fibrils by 70% in S7tg mice (n = 10) compared to wild type animals after induction of Smad7 expression. This finding is confirmed by Western blot analysis of protein lysates (figure 3.16). Treatment of the nitrocellulose membrane with polyclonal anti-collagen antibodies reveals a significant difference of collagen expression in S7tg mice compared to FVB wild type mice. This is visualized by different signal intensities in figure 3.16 lane 8 and 9. These results demonstrate that the decrease of collagen expression in CRP-Smad7 transgenic mice is due to Smad7 overexpression hepatocytes triggered by LPS co-administration.

Table 3.2: Quantification of collagen in the liver of different mouse strains. The percentage gives the size of stained areas compared to the total area investigated. n=number of animals investigated, n. d.: not determined. For more information see legend of figure 3.15 and 3.17.

Experimental mice	Control (%)	CCl$_4$ (%)	LPS (%)	CCl$_4$ + LPS (%)
FVB (n = 10)	0.1 ± 0.01	3.5 ± 0.4	0.2 ± 0.03	3.84 ± 0.45
S7tg (n = 10)	0.06 ± 0.02	2.48 ± 0.2	0.1 ± 0.01	1.14 ± 0.3
CD-1 (n = 8)	0.08 ± 0.03	2.019 ± 0.4	n. d.	n. d.
S7△E1 (n = 8)	0.09 ± 0.02	4.98 ± 0.2	n. d.	n. d.

(A)

(B)
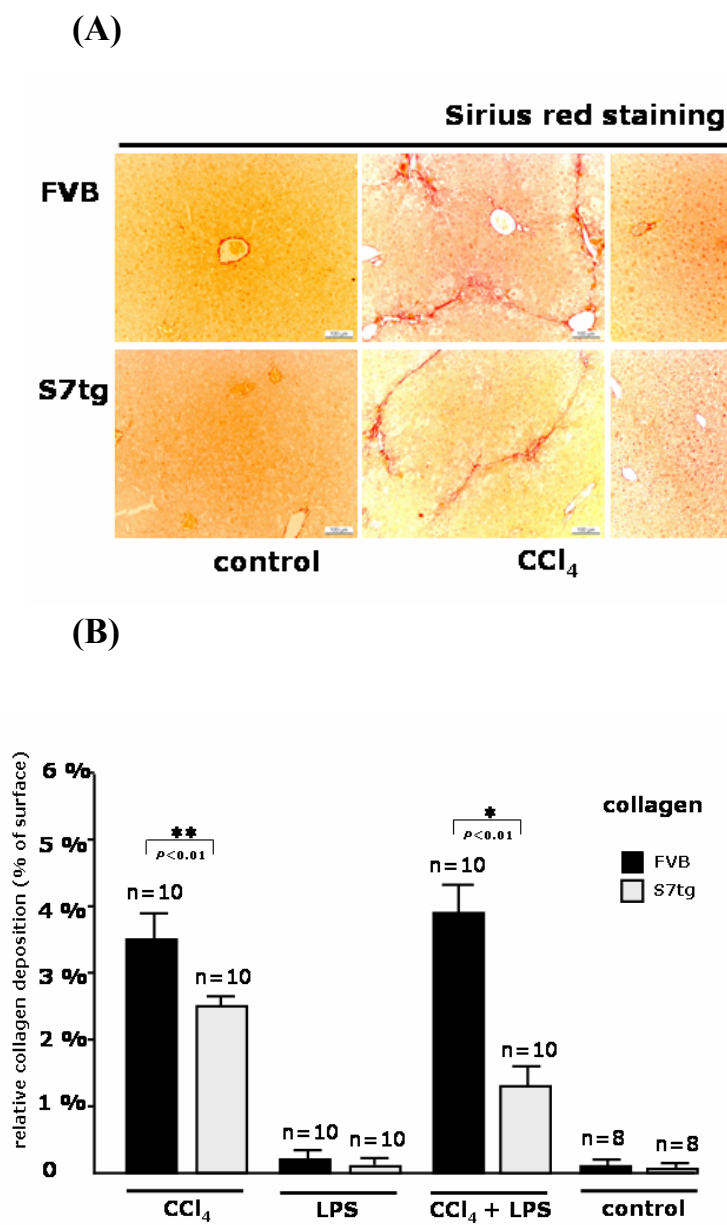
Figure 3.15: Smad7 overexpression leads to a reduction of the TGF-β signaling, displayed by a decrease of type I collagen synthesis in CCl_4 treated liver cells of mouse strains as indicated. (A) Representative photomicrographs of mice liver sections from S7tg mice and FVB wild type animals treated for 8 weeks with CCl_4 and/or LPS are shown. Untreated cells served as controls. Sirius red staining was performed to measure collagen deposition; magnification x 100. (B) Morphometric quantification of immunohistochemical staining of type I collagen was carried out by selecting ten fields randomly from each section of different groups (8-10 animals/group); LEICA QWIN software (Germany) was used. The graph shows the percentage of positive staining related to the total area investigated.
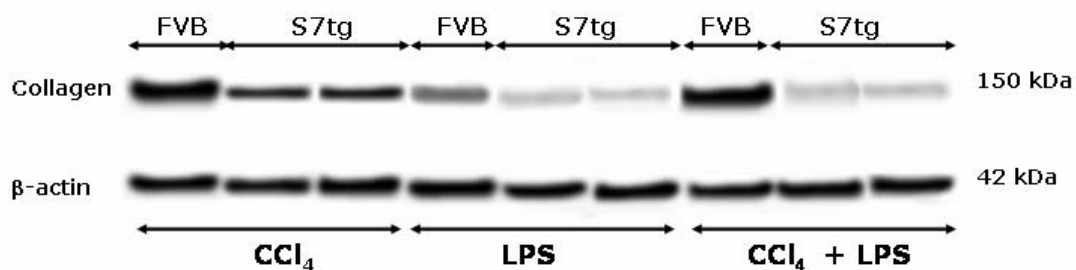
Figure 3.16: Protein lysates of different experimental mice were subjected to Western blot analysis for detection of collagen type I. Goat polyclonal anti-collagen type I antibodies (M-19, Santa Cruz Biotechnology, sc-8788, dilution 1:100) were used as first antibodies. Horseradish peroxidase linked anti–goat antibodies (Santa Cruz, sc-2033, donkey anti-goat Ig-HRP, dilution 1:2500) were used as second antibodies. Representative samples of differently treated FVB and S7tg derived liver tissues are shown as indicated. Blots were reprobed with anti-ß-actin antibodies to show equal loading.

Comparison between S7△E1 mice and their correspondent CD-1 wild type animals (table 3.2) shows that S7△E1 mice produce 2.5 times more collagen fibrils than CD-1 wild type mice (figure 3.17). This result was confirmed by Western blot analysis (figure 3.18). After CCl$_4$ treatment S7△E1 mice (n = 8) develop serious liver damage demonstrated by the synthesis of the highest amount of collagen (4.98 ± 0.2%) compared to all other strains tested. In sharp contrast S7tg mice (n = 10) synthesized 4.4 times less collagen when LPS was administered additionally. From these results it can be repeatedly concluded that Smad7 overexpression in hepatocytes of S7tg mice plays a pivotal role in the attenuation of collagen deposition in this mice strain.

(A)

(B)
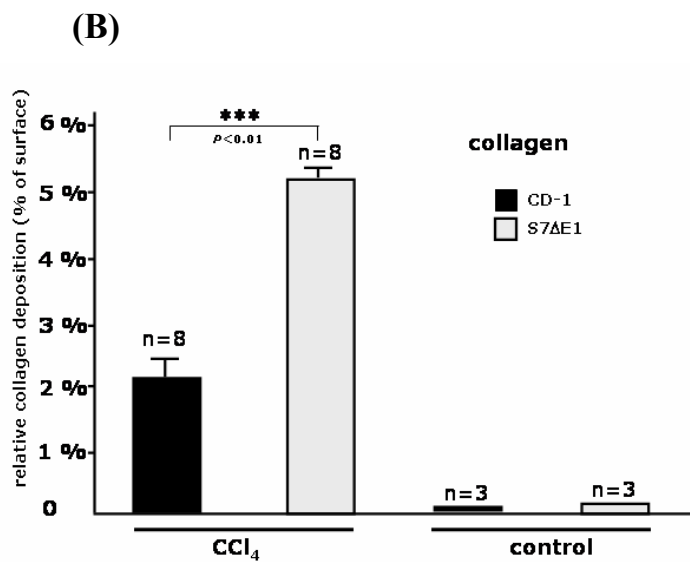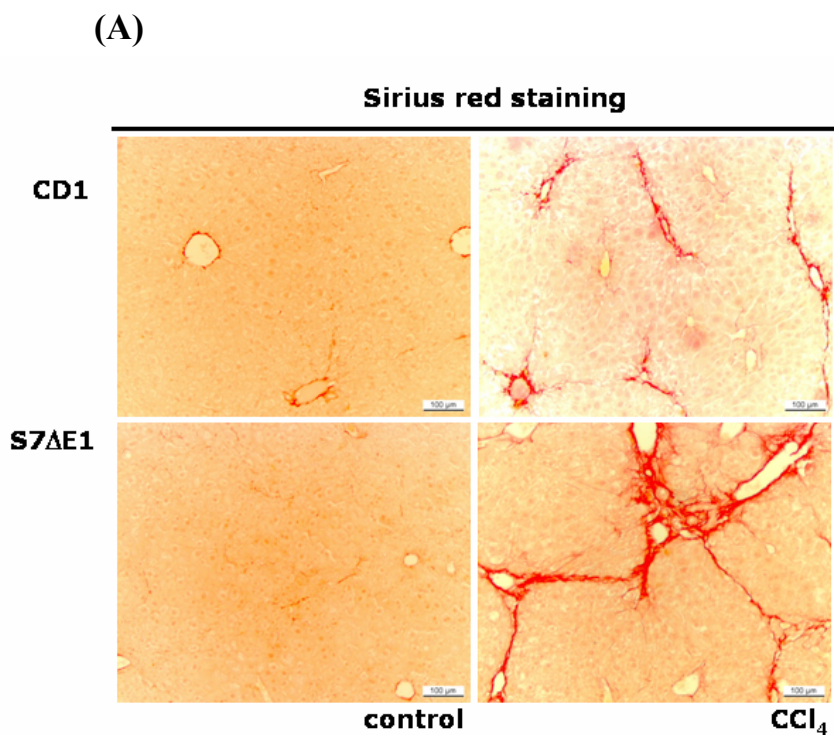
Figure 3.17: Loss of Smad7 function leads to increased collagen type I synthesis in livers cells of CCl_4 treated S7$\triangle$E1 mice. (A) Representative photomicrographs of mice liver sections from CD-1 and S7$\triangle$E1 strains treated for 8 weeks with CCl_4 are shown. Untreated tissues of both strains serve as controls. Sirius red staining was performed to measure collagen deposition; magnification x 100. (B) Morphometric quantification of immunohistochemical staining. Ten fields were selected randomly from each section of different groups (6-8 animals/group) to quantify the Sirius red staining, LEICA QWIN software (Germany) was used. The graph shows the percentage of stained areas related to the total area investigated.
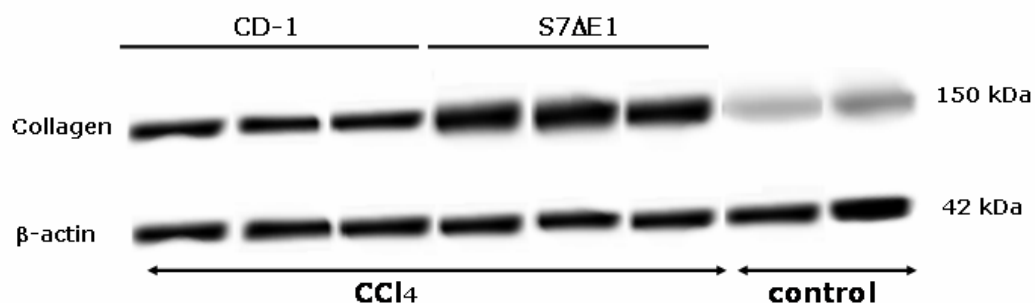
Figure 3.18: Loss of Smad7 by S7ΔE1 mice causes enhanced expression of type I collagen compared to CD-1 wild type mice after CCl₄ dependent liver damage. Liver protein lysates (20 µg) were examined for type I collagen expression by Western blotting as indicated. Representative photomicrographs of results obtained with S7ΔE1 and wild type mice after 8 weeks of CCl₄ intoxication are shown. Blots were reprobed with monoclonal anti-β-actin antibodies to confirm equal protein loading.

3.8 Expression of α-smooth muscle actin as a measure for activated hepatic stellate cells

Pathologically activated HSCs are characterized by the expression of α-smooth muscle actin (α-SMA), the main component of the ECM and the cytoskeleton. Because the amount of α-SMA increases proportional to the part of injured liver, it is a useful marker to detect the fibrosis state of the liver.

To ascertain the effect of transgenic derived Smad7 overexpression in hepatocytes on α-SMA synthesis in damaged liver, sections of experimental animals were analysed by immunohistochemical staining (figure 3.19 and 3.21). Immunostaining with monoclonal anti-α smooth muscle actin antibodies shows increased α-SMA synthesis being accompanied with increased liver damage in all CCl₄ treated mice compared to untreated animals. S7ΔE1 mice (n = 8) exhibit the highest peak of α-SMA expression (figure 3.21). α-SMA expression varies from 3.9 ± 0.7% to 12.1 ± 1.1% synthesized by CD-1 and S7ΔE1 strain mice and from 4.02 ± 1.3% to 8.0 ± 1.3% expressed by FVB and S7tg, respectively after CCl₄ treatment (Table 3.3). There is no difference between α-SMA expression of FVB and S7tg mice in the LPS treated group (Figure 3.19). Apparently, LPS administration alone does not induce or inhibit any α-SMA expression. A significant difference in α-SMA expression appears after CCl₄ + LPS treatment. S7tg mice show reduced α-SMA synthesis (1.4 ± 0.5% stained area) in comparison to FVB wild type exhibiting 9.7 ± 0.914% of stained area (figure 3.19). This corresponds to a 6.9 fold reduction. Another significant, 8.7-fold reduction of α-SMA expression show tissue sections of S7tg mice after CCl₄ + LPS treatment compared to CCl₄ treated S7ΔE1 mice. CCl₄ treated

S7ΔE1 mice produce the highest amount of α-SMA, i.e. 12.1 ± 1.1% stained area in immunohistchemical stainings (Table 3.3).

The comparison between α-SMA contents of liver tissues of FVB wild type, S7tg and S7ΔE1 mice after treatment with CCl$_4$ or CCl$_4$ + LPS suggests that a reduction or elevation of α-SMA synthesis in transgenic mice can be attributed either to Smad7 overexpression or lack of Smad7 synthesis respectively..

These results were confirmed by Western blot analysis of protein lysates of liver tisssues (figure 3.20, 3.22). Comparing bands after antibody treatment of nitrocellulose membranes reveals, that the amount of α-SMA in CCl$_4$ + LPS treated S7tg mice is significantly reduced compared to equally treated FVB mice and CCl$_4$ treated S7ΔE1 mice. This reduction of α-SMA synthesis can be attributed to an inhibition of HSC activation, the main cause of α-SMA production, and is due to ectopic Smad7 overexpression.

Table 3.3: Quantification of α-smooth muscle actin contents. Percentages give the size of stained areas compared to the total area investigated. n=number of animals investigated, n. d.: not determined. For more detail see legend of figures 3.19 and 3.21.

Experimental mice	Control (%)	CCl$_4$ (%)	LPS (%)	CCl$_4$ + LPS (%)
FVB (n = 10)	0.002	8.0 ± 1.3	0.003 ± 0.04	9.7 ± 0.914
S7tg (n = 10)	0.001	4.02 ± 0.8	0.001 ± 0.05	1.4 ± 0.5
CD-1 (n = 8)	0.003	3.9 ± 0.7	n. d.	n. d.
S7ΔE1 (n = 8)	0.002	12.1 ± 1.1	n. d.	n. d.

(A)
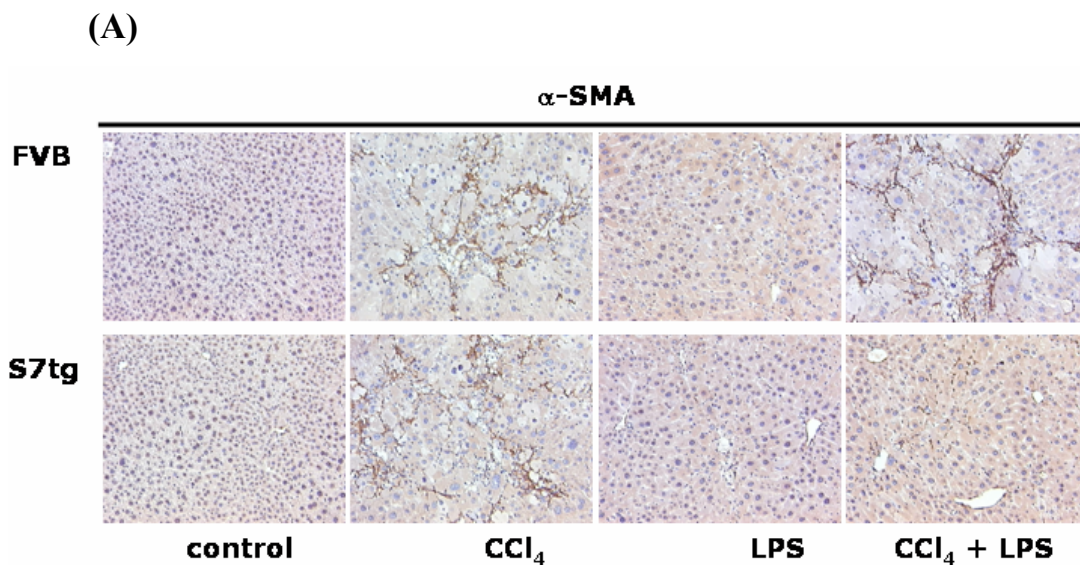
(B)
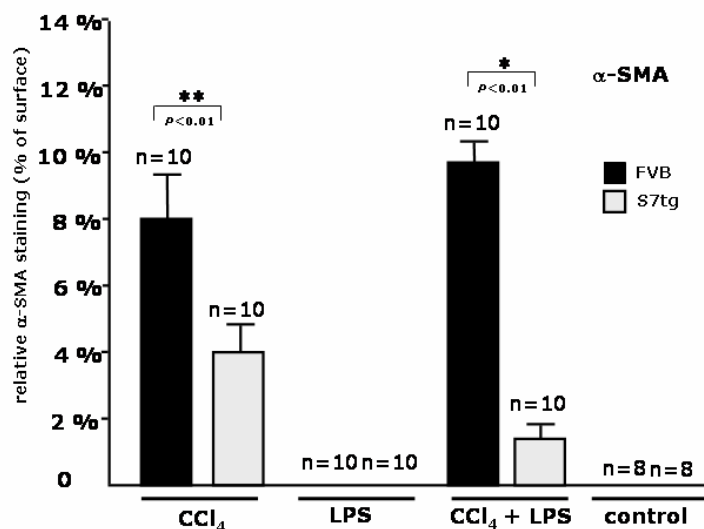
Figure 3.19: Smad7 overexpression leads to a reduction of TGF-β signaling and a decrease of α-SMA synthesis in liver cells of CCl$_4$ treated S7tg mice. (A) Immunohistochemical staining of alpha smooth muscle actin (α-SMA) as a marker for activated HSCs. Representative photomicrographs of mice liver sections from S7tg and FVB wild type strains treated for 8 weeks with CCl$_4$ and/or LPS are shown. Untreated cells serve as controls; magnification x 100. (B) Morphometric quantification of immunohistochemical staining of α-SMA. Ten fields were selected randomly from each section of different groups (8-10 animals/group); LEICA QWIN software (Germany) was used. The graph shows the percentage of stained areas related to the total area investigated.

Figure 3.20: Smad7 overexpression in S7tg mice decreases the expression of α-SMA compared to FVB wild type mice after CCl_4 dependent liver damage. Liver protein lysates (20 μg) were examined for expression of α-SMA by Western blotting as indicated. Representative photomicrographs of results obtained with 10 S7tg and FVB wild type mice after 8 weeks of CCl_4 intoxication. Blots were reprobed with a monoclonal anti-β-actin antibodies to confirm equal protein loading.

(A)   **(B)**
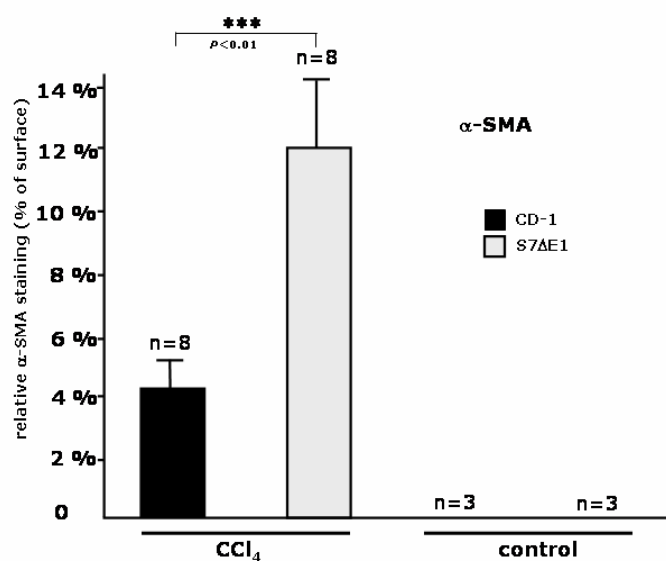
Figure 3.21: Loss of Smad7 function leads to increased α-SMA synthesis in liver cells of CCl_4 treated S7△E1 mice. (A) Immunohistochemical staining of alpha smooth muscle actin (α-SMA) as a marker for activated HSCs. Representative photomicrographs of mice liver sections from CD-1 and S7△E1 strains treated for 8 weeks with CCl_4.are shown. Untreated cells of both strains are controls; magnification x 100 (B) Morphometric quantification of immunohistochemical stainings. Ten fields were selected randomly from each section of different animal groups (3-8 animals/group) for quantification of α-SMA staining, LEICA QWIN software (Germany) was used. The graph shows the percentage of stained areas related to the total area investigated.
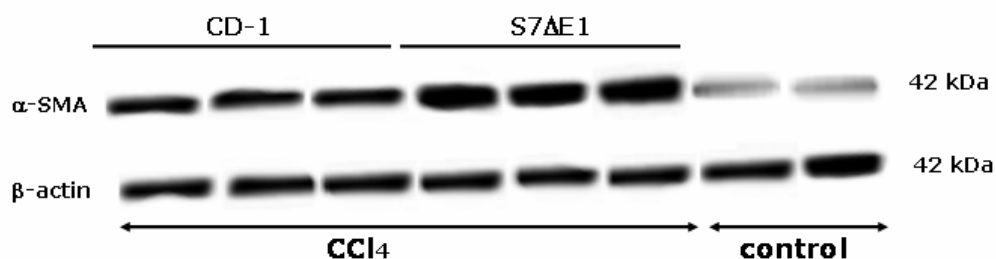
Figure 3.22: Loss of Smad7 in S7ΔE1 mice causes enhanced expression of α-SMA compared to CD-1 wild type mice after CCl₄ dependent liver damage. Liver protein lysates (20 µg) were examined for expression of α-SMA by Western blotting as indicated. Rep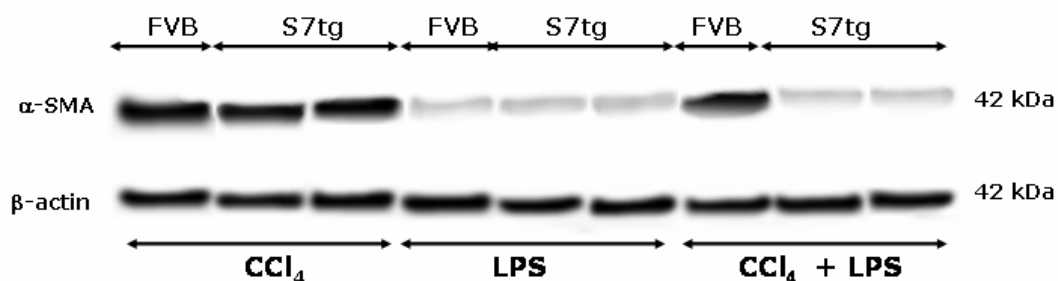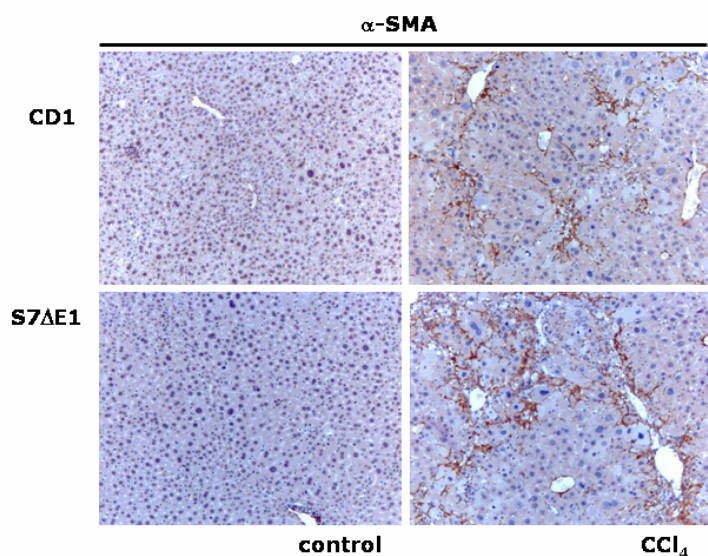resentative photomicrographs of results obtained with S7ΔE1 and wild type mice after 8 weeks of CCl₄ intoxication are shown. Blots were reprobed with a monoclonal anti-β-actin antibodies to confirm equal protein loading.

3.9 Smad7 overexpression in hepatocytes reduces levels of hyaluronic acid in CCl₄ treated mice

Increased amounts of hyaluronic acid (HA) in the serum of experimental animals provide indirect evidence for the extent of liver damage and fibrosis. HA is a polymer composed of repeating dimeric units of glucuronic acid and N-acetyl-glucosamine. It forms the core of complex proteoglycan aggregates found in the extracellular matrix (ECM).

Analysis of hyaluronic acid concentrations was carried out using the "Hyaluronic Acid Test Kit, CORGENIX after 8 weeks of induction of liver damage by i.p. CCl₄ injections or combined CCl₄ + LPS treatment. For this purpose serum of experimental mice was examined, which was obtained from 1 ml blood by a needle prick in the eye of anaesthetized animals.

Immunohistochemical staining of liver sections suggests that CCl₄ treated CD-1, FVB and S7tg mice have approximately the same concentration of HA in the serum (355 ± 22.5, 392.2 ± 21 and 411 ± 31 µg/ml respectively) (Table 3.4, figure 3.23). CCL₄ treated S7△E1 mice instead exhibit an increased concentration of HA (562.2 ± 30.2 µg/ml). LPS treated animals produce as little HA as the control group presenting no fibrotic state. A remarkable difference in HA concentrations measured appears in the group of CCl₄ + LPS treated animals. S7tg mice show a reduced level of HA synthesis of 200.5 ± 18.8 µg/ml, in comparison to FVB mice with an increased level of HA synthesis of 440.06 ± 44.081 ng/ml. This implies a more than twofold reduction of HA synthesis. From these results it can be concluded that Smad7 overexpression in hepatocytes triggered by LPS co-administration under CCL₄ induced fibrotic conditions leads to a significant reduction of HA synthesis in S7tg mice.

(A)   **(B)**
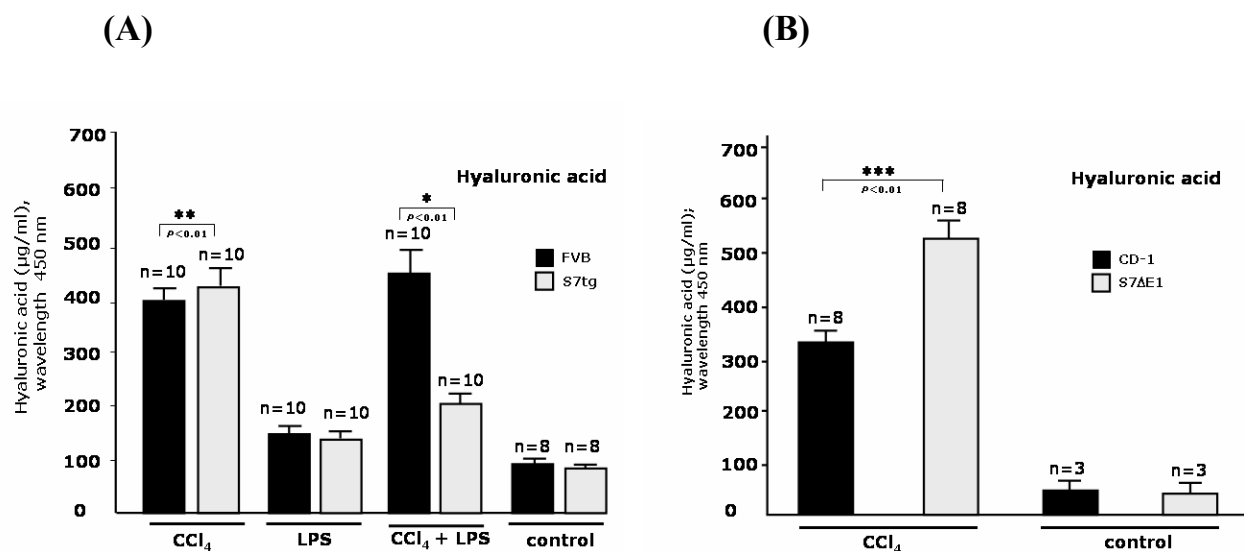
Figure 3.23: Analysis of the concentrations of hyaluronic acid in the serum of mice was carried out using the Hyaluronic Acid Test Kit from CORGENIX. Samples were taken after 8 weeks of treatment with CCl_4 and/or LPS as indicated. Untreated mice served as controls. **(A)** Smad7 overexpression decreases the sensitivity for liver damage and fibrogenesis after CCl_4 intoxication in S7tg mice. (B) Loss of Smad7 leads to enhanced TGF-β signaling and increased concentrations of hyaluronic acid in the serum of S7△E1 mice compared to CD-1 wild type animals after CCl_4 intoxication.

Table 3.4: Effect of Smad7 overexpression on hyaluronic acid levels in the serum of mice as indicated (μg/ml). n=number of animals investigated, n. d.: not determined.

Experimental mice	Control	CCl_4	LPS	CCl_4 + LPS
FVB (n = 10)	89 ± 10.8	392.2 ± 21	146 ± 23.5	440 ± 44
S7tg (n = 10)	84 ± 9.2	411 ± 31	138 ± 14	200.5 ± 18.8
CD-1 (n = 8)	86 ± 7.5	355 ± 22.5	n. d.	n. d.
S7△E1 (n = 8)	91 ± 8.6	562 ± 30.2	n. d.	n. d.

3.10   Smad7 overexpression in hepatocytes reduces the level of hydroxyproline in CCl$_4$ treated mice

Because hydroxyproline (HP) is the main component of collagen, HP levels in liver tissues provide indirect information about the level of collagen synthesis and the fibrotic state of liver cells.

In order to determine the HP concentration in the serum of experimental mice a HP assay was carried out (2.11). Approximately 0.5 g liver tissue from the right and left liver lobes was analysed. The data obtained indicates that CCl$_4$ induced liver damage causes increased HP synthesis in all experimental mice. S7$\triangle$E1 strain mice (n = 8) show the highest HP concentration (463.3 $\pm$ 19.8 µg/g liver), (Table 3.5 and figure 3.24). No significant difference of HP levels between FVB wild type mice (n = 10) and S7tg mice (n = 10) could be determined (figure 3.24). A significant reduction of HP synthesis can be seen in S7tg mice after CCl$_4$ + LPS treatment (129.4 $\pm$ 19.2 µg/g liver) (figure 3.24). In comparison the HP concentration of FVB wild type animals was 331.7 $\pm$ 27.1 µg/g liver under the same fibrotic conditions. This effect can be explained as a result of ectopic Smad7 overexpression triggered by simultaneous LPS injection.

In summary, it can be concluded that S7tg mice exhibit a 50% reduced HP concentration caused by ectopic Smad7 overexpression in hepatocytes (table 3.5, figure 3.24A). The absence of Smad7 in S7$\triangle$E1 mice in contrast leads to an elevated HP level (Table 3.5, figure 3.24B).

Table 3.5: Effect of Smad7 overexpression on serum concentrations of Hydroxyproline in mice (µg/g liver). n=number of animals investigated, n. d.: not determined.

Experimental mice	Control	CCl$_4$	LPS	CCl$_4$ + LPS
FVB (n = 10)	67 $\pm$ 9	306.6$\pm$ 26	102 $\pm$ 10	331.7 $\pm$ 27
S7tg (n = 10)	60 $\pm$ 7.2	276.3 $\pm$ 16	101 $\pm$ 10	129.4 $\pm$ 19
CD-1 (n = 8)	64 $\pm$ 4.5	274.3 $\pm$ 12	n. d.	n. d.
S7$\triangle$E1 (n = 8)	70 $\pm$ 3.6	463.3 $\pm$ 20	n. d.	n. d.

(A)

(B)
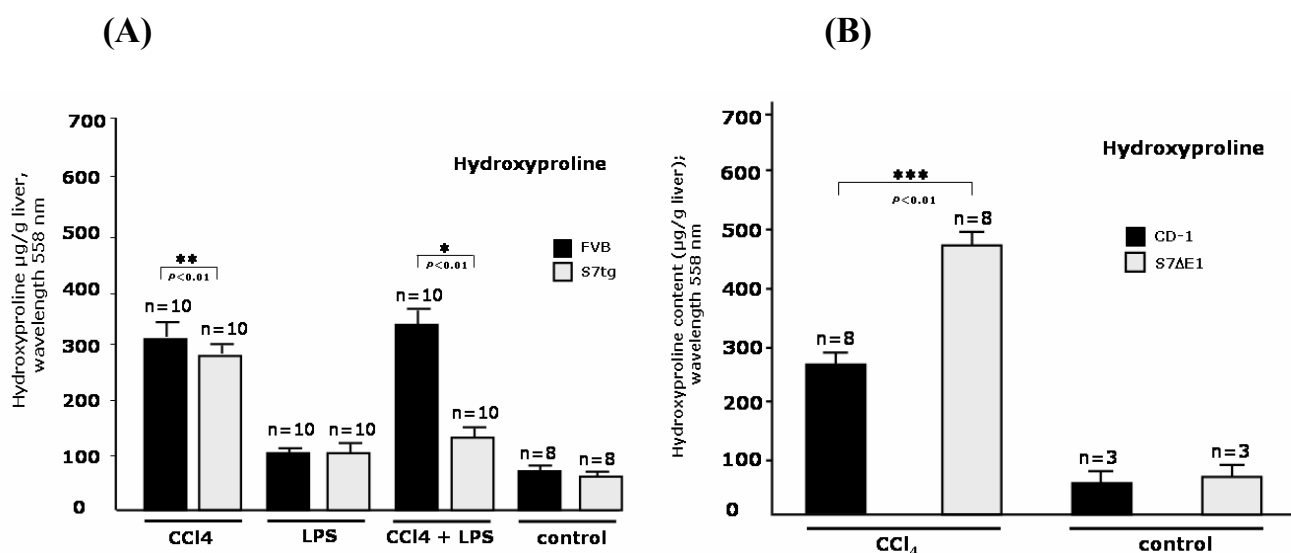
Figure 3.24: Spectrophotometrical analysis (Pharmacia Biotech, Ultraspec 2000; wavelength of 558 nm) of hydroxyproline concentrations was carried out as a measure for the degree of fibrosis in liver tissue samples after 8 weeks treatment with CCl_4 and/or LPS as indicated. (A) Smad7 overexpression decreases the sensitivity for liver damage and fibrogenesis after CCl_4 intoxication. Serum analysis of S7tg and FVB mice were compared. (B) Loss of Smad7 leads to an enhanced TGF-β signaling and an increased level of hydroxyproline after CCl_4 intoxication. Serum concentrations of S7$\triangle$E1 and CD-1 mice were analysed.

3.11 Smad7 overexpression desensitizes hepatocytes for TGF-β/Smad signaling

Smad7 is known to antagonize the TGF-β signal pathway. Binding of Smad7 to the TGF-β type I receptor (TβRI) hinders its subsequent phosphorylation by the TGF-β type II receptor (TβRII). An important measure of function of the TGF-β/Smad signal pathway is the relative presence or absence of Phospho-Smad2 in cell nucleus.

In order to substantiate the effect of Smad7 overexpression in hepatocytes, immunohistological staining of Phospho-Smad2 in liver sections of differently treated mice was carried out as described in 2.9.5.

After treatment with CCl_4 an intensified staining of the nucleus in liver sections can be observed in all mouse groups (figure 3.25 and 3.27). Quantification reveals that FVB (n = 10), S7tg (n = 10) and CD-1 (n = 8) mice exhibit a similar level of nucleus staining i.e. $78.5 \pm 4.8\%$, $78.3 \pm 4.7\%$ and $74.8 \pm 7.2\%$ respectively, whereas liver sections of S7$\triangle$E1 (n = 8) show the highest level of staining ($92.5 \pm 4.2\%$), (figure 3.25 and 3.27). There is no significant difference of Phospho-Smad2 expression in different mice strains after LPS treatment. A significant difference in Phospho-Smad2 staining in the nuclei can be observed in the CCl_4 + LPS treated group. As shown in table 3.6 and figure 3.25, co-

injection of CCl_4 + LPS result in a threefold reduction of nucleus staining of liver cells of S7tg mice ($26.6 \pm 5.6\%$) compared to cells of FVB wild type animals ($77.4 \pm 7\%$) under the same fibrotic conditions. The significant reduction of nucleus staining of S7tg cells can be explained as an effect of transgenic derived Smad7 overexpression, which is triggered by LPS administration.

The immunohistochemical results are in line with Western blot analysis of Phospho-Smad2 in liver cell lysates. Lysates of S7tg mice show weaker bands for Phospho-Smad2 than lysates of FVB wild type and S7△E1 mice (figure 3.26 and 3.28).

In summary one can conclude that Smad7 overexpression in hepatocytes interrupts the TGF-β signal pathway by blocking R-Smad (Smad2/3) phosphorylation and thus their subsequent translocation into the nucleus of hepatocytes. Western Blot analysis and immunohistochemical staining gave evidence for that scenario by showing that under the same CCl_4 induced fibrotic conditions S7tg mice exhibit drastically reduced fibrotic characteristics and less Phospho-Smad2 signaling in comparison to S7△E1 mice and FVB wild type animals.

Table 3.6: Effect of Smad7 overexpression on the level of Phospho-Smad2 in cell nuclei (%).The percentage gives the size of stained areas compared to the total area investigated. n=number of animals investigated, n. d.: not determined. For more information see legend of figure 3.25 and 3.27.

Experimental mice	Control	CCl_4	LPS	CCl_4 + LPS
FVB (n = 10)	0.3	78.5 ± 4.9	8.5 ± 2.8	77.4 ± 7.1
S7tg (n = 10)	0.1	78.3 ± 4.8	5.4 ± 2.4	26.6 ± 5.6
CD-1 (n = 8)	0.2	74.9 ± 7.2	n. d.	n. d.
S7△E1 (n = 8)	0.4	92.5 ± 4.2	n. d.	n. d.

(A)

(B)
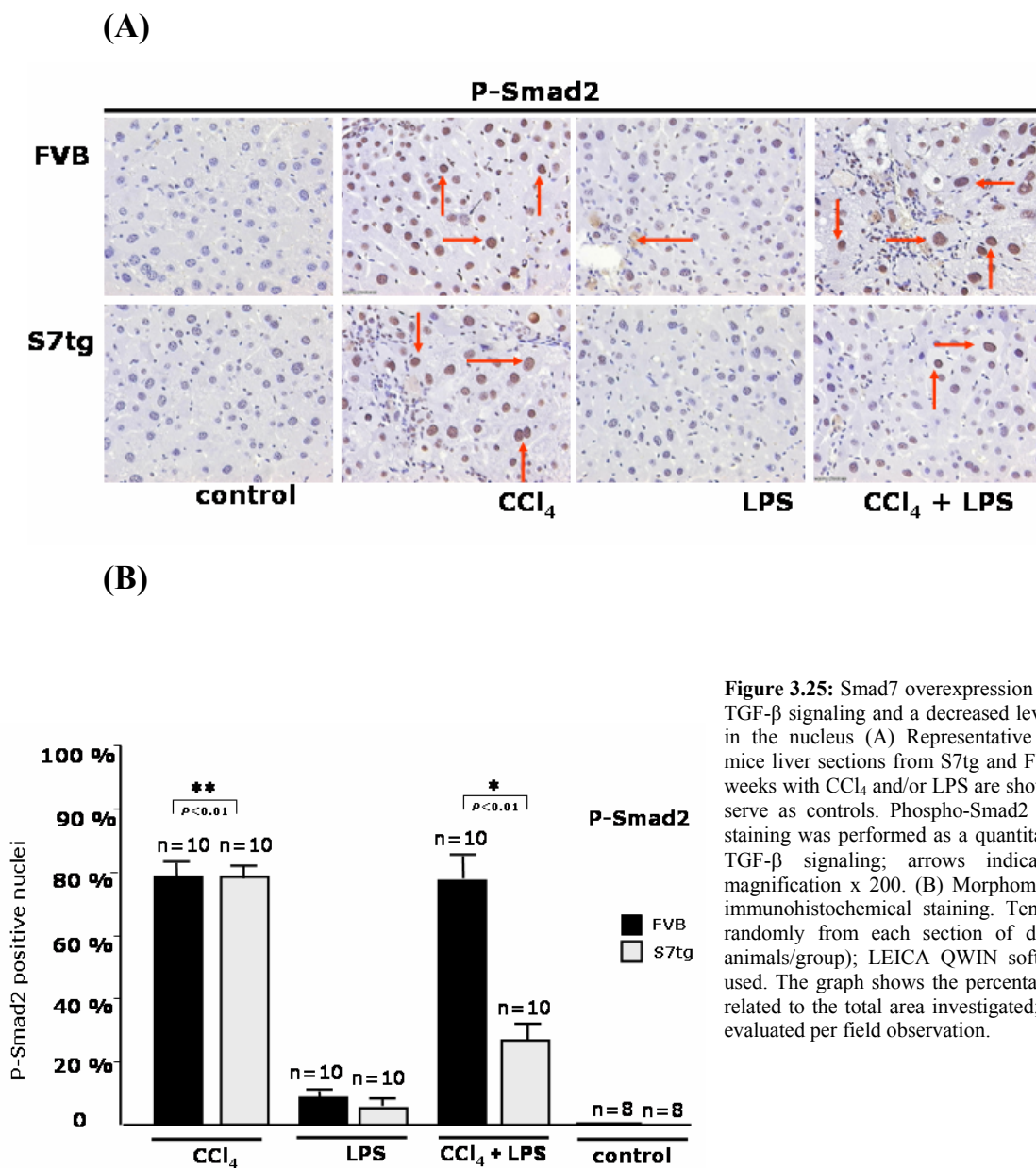
Figure 3.25: Smad7 overexpression leads to a blockade of TGF-β signaling and a decreased level of Phospho-Smad2 in the nucleus (A) Representative photomicrographs of mice liver sections from S7tg and FVB mice treated for 8 weeks with CCl_4 and/or LPS are shown. Untreated animals serve as controls. Phospho-Smad2 immunohistochemical staining was performed as a quantitative measurement for TGF-β signaling; arrows indicate positive signals; magnification x 200. (B) Morphometric quantification of immunohistochemical staining. Ten fields were selected randomly from each section of different groups (8-10 animals/group); LEICA QWIN software (Germany) was used. The graph shows the percentage of nuclear staining related to the total area investigated; about 200 cells were evaluated per field observation.
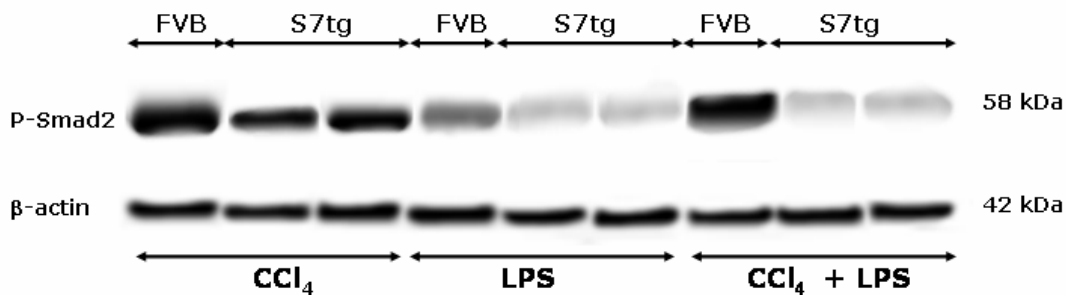
Figure 3.26: Smad7 overexpression leads to reduced levels of Phospho-Smad2 compared to FVB wild type mice after CCl₄ dependent liver damage. Liver protein lysates (20 μg) were examined for Phospho-Smad2 by Western blot analysis as indicated. Representative photomicrographs of results obtained with lysates of 10 S7tg and FVB wild type mice after 8 weeks of CCl₄ intoxication and LPS treatment as indicated are shown. Blots were reprobed with a monoclonal anti-β-actin antibodies to confirm equal protein loading.

(A)

(B)
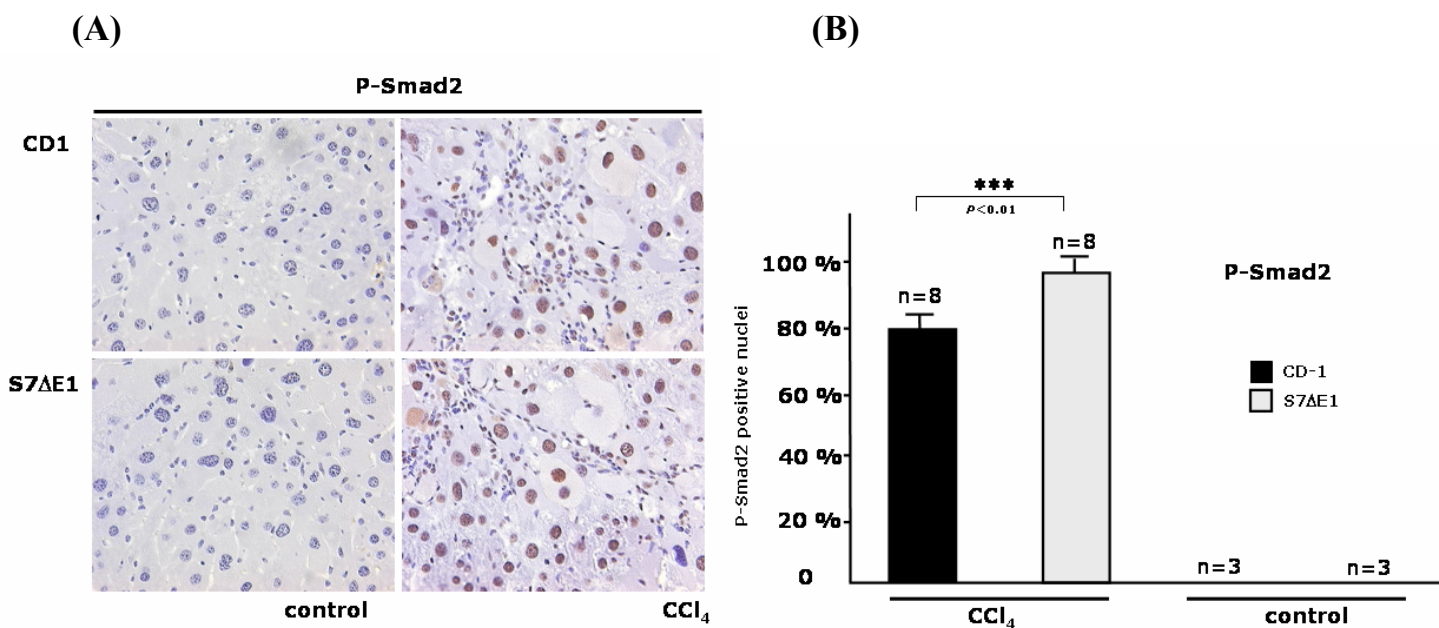
For description of figure 3.37 see next page.

Figure 3.27: Loss of Smad7 function leads to enhanced TGF-β signaling and increased amount of Phospho-Smad2 in the nucleus after CCl$_4$ intoxication. S7△E1 and CD-1 wild type mice were compared. (A) Representative photomicrographs of mice liver sections from CD-1 wild type and S7△E1 mice treated for 8 weeks with CCl$_4$ are shown; untreated animals serve as controls. Phospho-Smad2 immunohistochemical staining as a quantitative measurement for TGF-β signaling was performed; brown staining indicates positive signals; magnification x 200. (B) Morphometric quantification of immunohistochemical staining. Ten fields were selected randomly from each section of different groups (3-8 animals/group) for Phospho-Smad2 staining, LEICA QWIN software (Germany) was used. The graph shows the percentage of nuclear staining related to the total area investigated. About 200 cells were evaluated per observation field, stained cells were counted and expressed as percentage of total cells investigated.
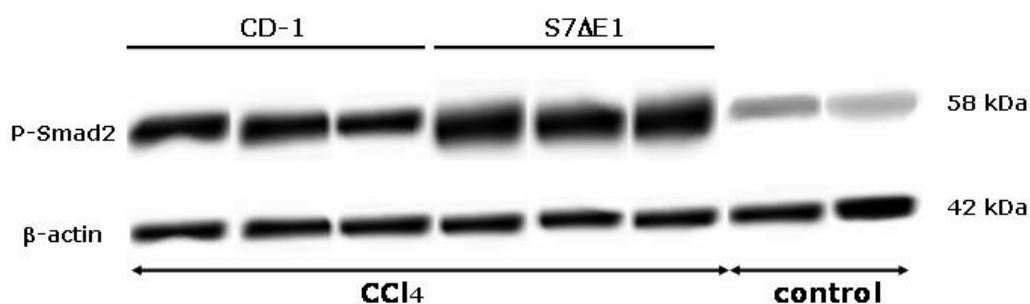

Figure 3.28: Loss of Smad7 in S7ΔE1 mice causes enhanced Smad2 phosphorylation compared to CD-1 wild type mice after CCl$_4$ dependent liver damage. Liver protein lysates (20 μg) were examined for Phospho-Smad2 by Western blot analysis as indicated. Representative photomicrographs of results obtained with S7ΔE1 and wild type mice after 8 weeks of CCl$_4$ intoxication are shown. Blots were reprobed with a monoclonal anti-β-actin antibody to confirm equal protein loading.

Direct determination of Smad7 expression in liver tissues of experimental mice by immunohistochemical staining and Western blotting analysis confirms the conclusion that the interruption of TGF-β/Smad signaling is due to the stimulation of transgenic derived Smad7 overexpression in hepatocytes. Both methods demonstrate the excess of ectopic Smad7 production in transgenic mice, compared to basal Smad7 expression of wild type animals (figures 3.29 and 3.30). Quantification of Smad7 immunostaining indicates (figure 3.29) an invert proportion between overexpression of Smad7 and the extent of liver damage (Table 3.7). In liver tissue sections of different mouse strains Smad7 signals appear predominantly in undamaged regions. Western blot analysis confirms the result with exception of relative high Smad7 expression in CD-1 mice (figure 3.30-31). Because FVB wild type and S7△E1 mice have developed much more fibrotic tissues than S7tg under the same fibrotic condition, the reduction of liver damage in CRP-Smad7 transgenic mice can be interpreted as an evidence for blocking of the TGF-β signal pathway.

Table 3.7: Quantification of immunohistochemical staining of Smad7 in liver sections (%).The percentage gives the size of stained areas compared to the total area investigated. n=number of animals investigated, n. d.: not determined. For more information see legend of figure 3.29 and 3.31.

Experimental mice	Control	CCl$_4$	LPS	CCl$_4$ + LPS
FVB (n = 10)	0.13	1.25 ± 0.5	0.75 ± 0.5	2.4 ± 0.7
S7tg (n = 10)	0.12	4.6 ± 1.1	5.9 ± 1.1	7.4 ± 0.7
CD-1 (n = 8)	0.15	4.5 ± 1.1	n. d.	n. d.
S7△E1 (n = 8)	0	0 ± 0	n. d.	n. d.

(A)
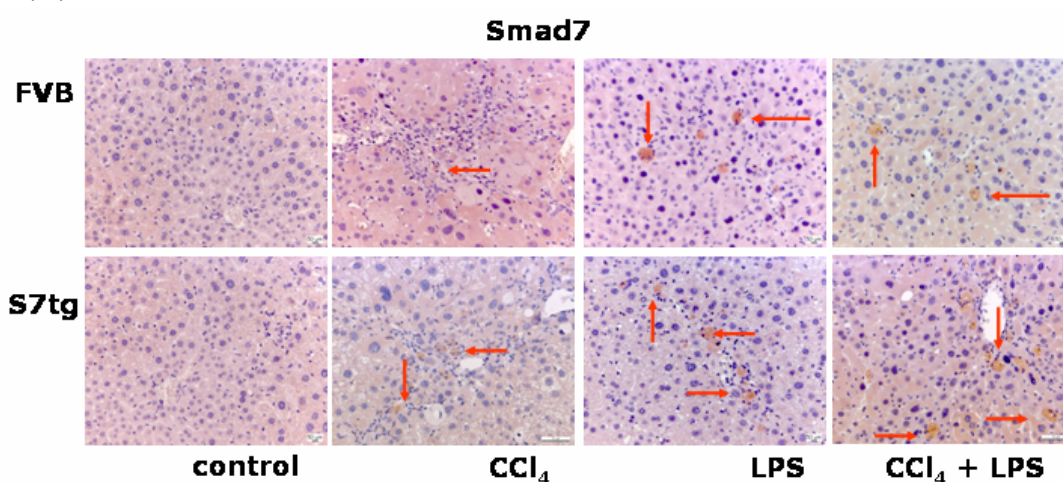
(B)
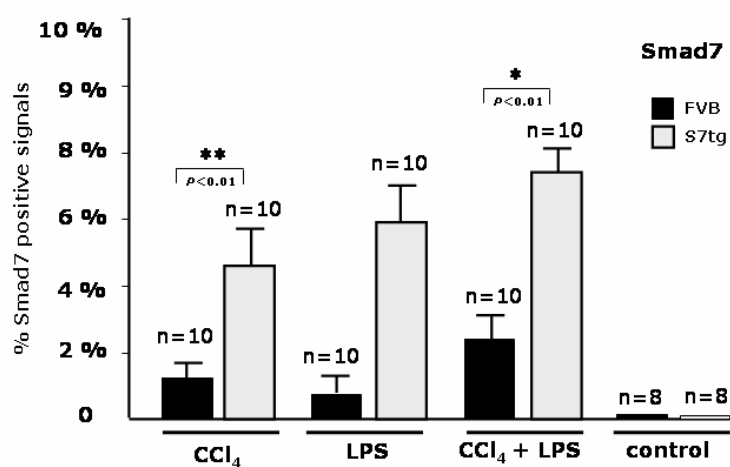
Figure 3.29 Smad7 overexpression in CRP-Smad7 transgenic mice is induced by LPS administration. (A) Smad7 immunostaining was used as a quantitative measurement for blockade of TGF-β activity and the effect of LPS. Representative photomicrographs of mice liver sections from S7tg and FVB mice treated for 8 weeks with both CCl$_4$ and LPS are shown. Untreated cells serve as controls. Arrows indicate positive signals; magnification x 200. (B) Morphometric quantification of immunohistochemical staining of Smad7. Ten fields were selected randomly from each section of different groups (8-10 animals/group); LEICA QWIN software (Germany) was used. The graph shows the percentage of stained area related to the total area investigated. About 200 cells were evaluated per observation field. Stained cells were counted and expressed as percentage of total cells investigated.
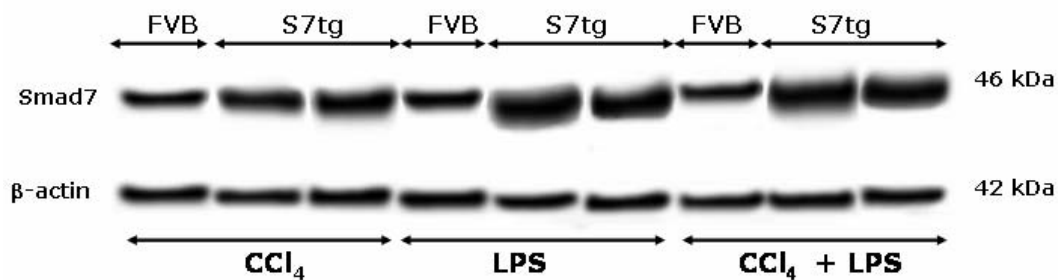
Figure 3.30: Transgenic derived Smad7 is overexpressed after LPS administration in S7tg mice compared to FVB wild type mice. Liver protein lysates (20 µg) of mouse strains as indicated were examined for Smad7 expression by Western blot analysis. Representative photomicrographs of results obtained with 10 S7tg and FVB wild type mice after 8 weeks of treatment as indicated are shown. Blots were reprobed with a monoclonal anti-β-actin antibodies to confirm equal protein loading.

(A)   **(B)**
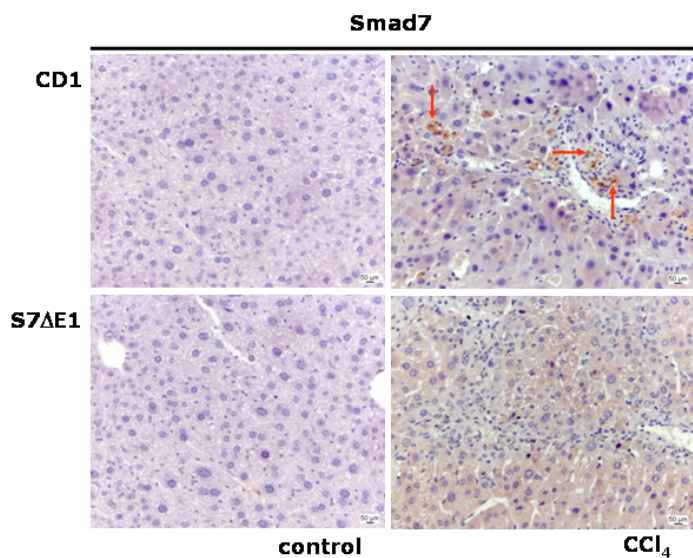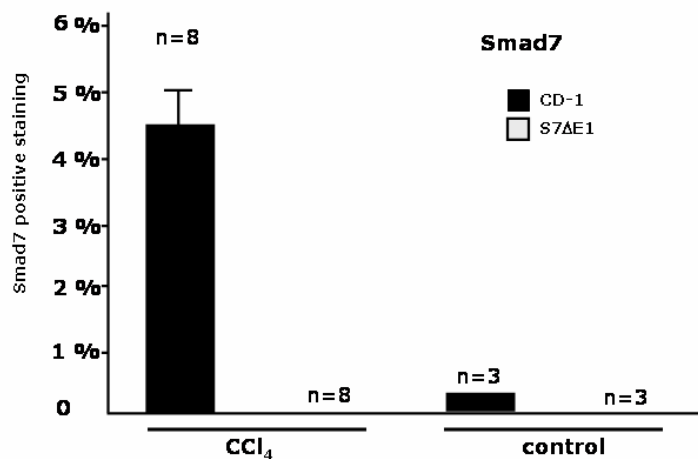
For description of figure 3.31 see next page.

Figure 3.31: TGF-β activity causes Smad7 synthesis as a negative feedback regulation in CD-1 wild type mice but not in S7△E1 mice. (A) Immunohistochemical staining of Smad7. Representative photomicrographs of mice liver sections from S7△E1 and CD-1 wild type mice treated or not (control) for 8 weeks with CCl$_4$ are shown; arrows indicate positive signals; magnification x 200. (B) Morphometric quantification of immunohistochemical staining of Smad7 as a measurement for negative feedback regulation of TGF-β activity in CD-1 wild type and S7△E1 mice treated with CCl$_4$. Ten fields were selected randomly from each section of different animal groups (3-8 animals/group); LEICA QWIN software (Germany) was used. The graph shows the percentage of stained areas related to the total area investigated. About 200 cells were evaluated per observation field. Stained cells were counted and expressed as percentage of total cells investigated.

Smad7 overexpression does not affect Smad2 and Smad3 synthesis

To investigate the effect of Smad7 overexpression in hepatocytes on the level of endogenous derived Smad2 and Smad3, immunohistochemical staining and Western blot analysis was carried out. Immunohistochemical staining points to a constant expression of Smad2 and Smad3 distributed evenly in the cell cytoplasm of S7tg, FVB as well as S7△E1 mice and CD-1 mice (figure 3.32 and 3.35). These results suggest that Smad7 overexpression in hepatocytes has no effect on endogenous Smad2 and Smad3 expression which could be confirmed by Western blot analysis of protein lysates of experimental animals (figure 3.33 and 3.34). Both proteins could be detected in similar amounts in all lysates.

(A)

(B)
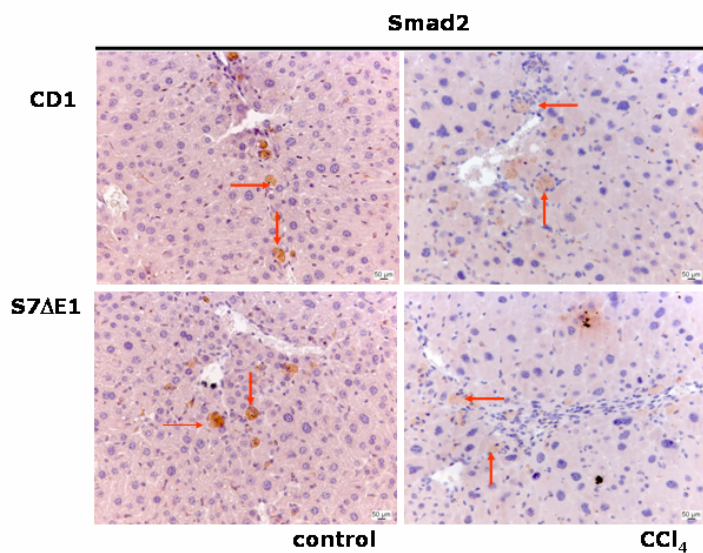
Figure 3.32: Representative photomicrographs of mice liver sections from mouse strains as indicated after treatment with CCl_4 and/or LPS. Untreated cells serve as controls. Immunohistochemical staining of Smad2 was performed; the arrows indicate positive signals; magnification x 200.
(A) Smad7overexpression does not affect constitutive expression of Smad2 in S7tg mice. (B) Loss of Smad7 does not affect constitutive expression of Smad2 by S7ΔE1 mice when compared to CD-1 wild type mice after CCl_4 dependent liver damage.

FVB S7tg CD-1 S7ΔE1 FVB S7tg FVB CD-1   FVB

Smad2   52,3 kDa

β-actin   42 kDa

CCl₄   LPS   CCl₄ + LPS control
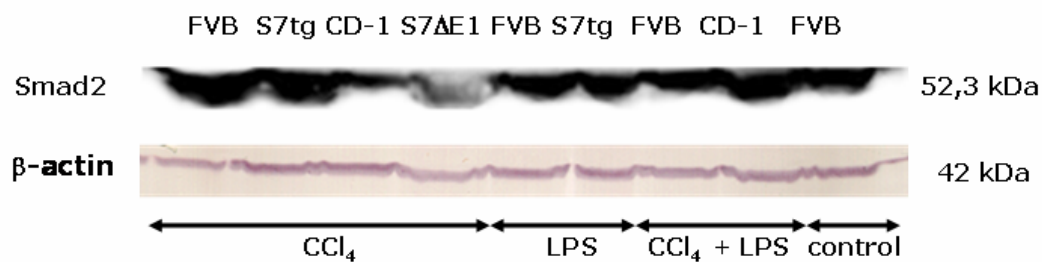
Figure 3.33: Smad7 overexpression or loss of Smad7 does not affect constitutive expression of Smad2. Liver protein lysates (20 µg) of treated mouse strains as indicated were examined for Smad2 expression by Western blot analysis. Representative photomicrographs of results obtained after 8 weeks of CCl₄ and LPS intoxication are shown. Blots were reprobed with a monoclonal anti-β-actin antibodies to confirm equal protein loading.

FVB S7tg CD-1 S7ΔE1 FVB S7tg FVB S7tg FVB

Smad3   48 kDa

β-actin   42 kDa

CCl₄   LPS   CCl₄ + LPS control
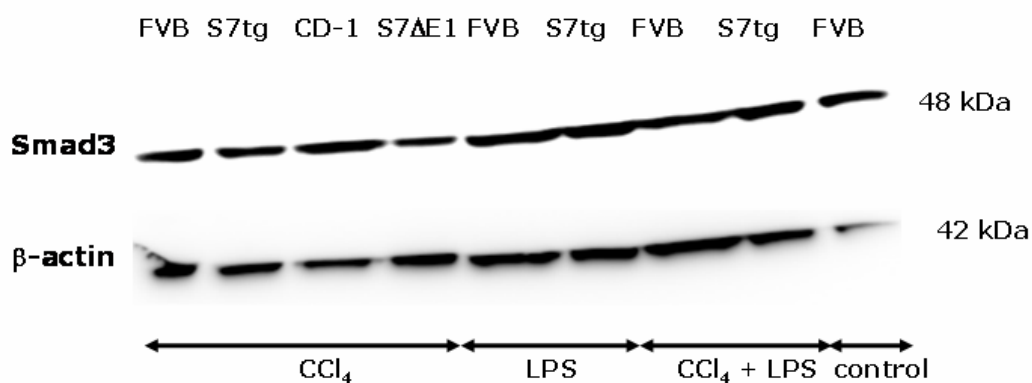
Figure 3.34: Smad7 overexpression or loss of Smad7 does not affect constitutive expression of Smad3. Liver protein lysates (20 µg) of differently treated mouse strains as indicated were examined for Smad3 expression by Western blots analysis. Representative photomicrographs of results are shown. Blots were reprobed with a monoclonal anti-β-actin antibodies to confirm equal protein loading.

(A)
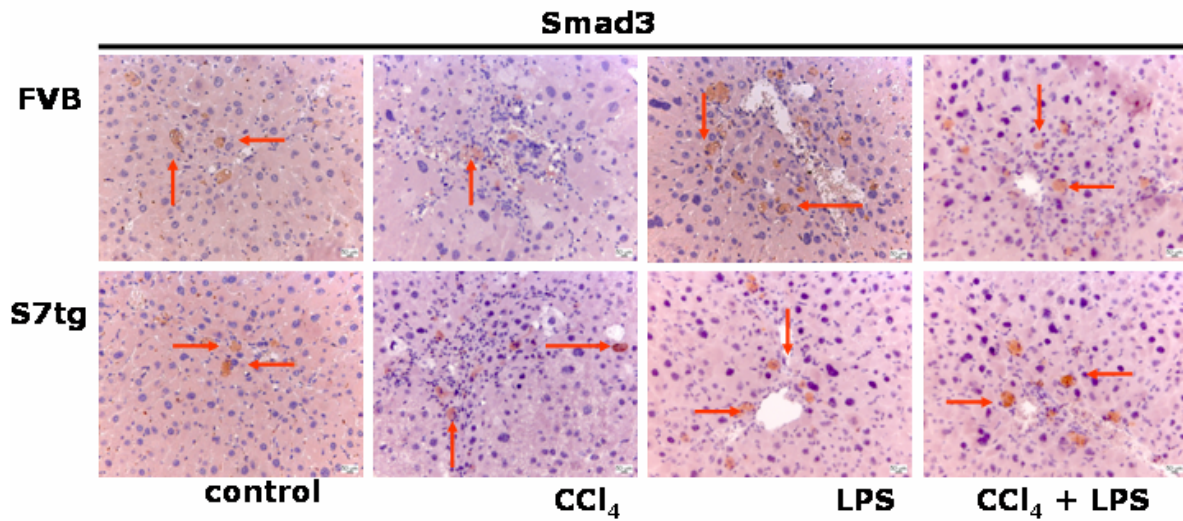
(B)

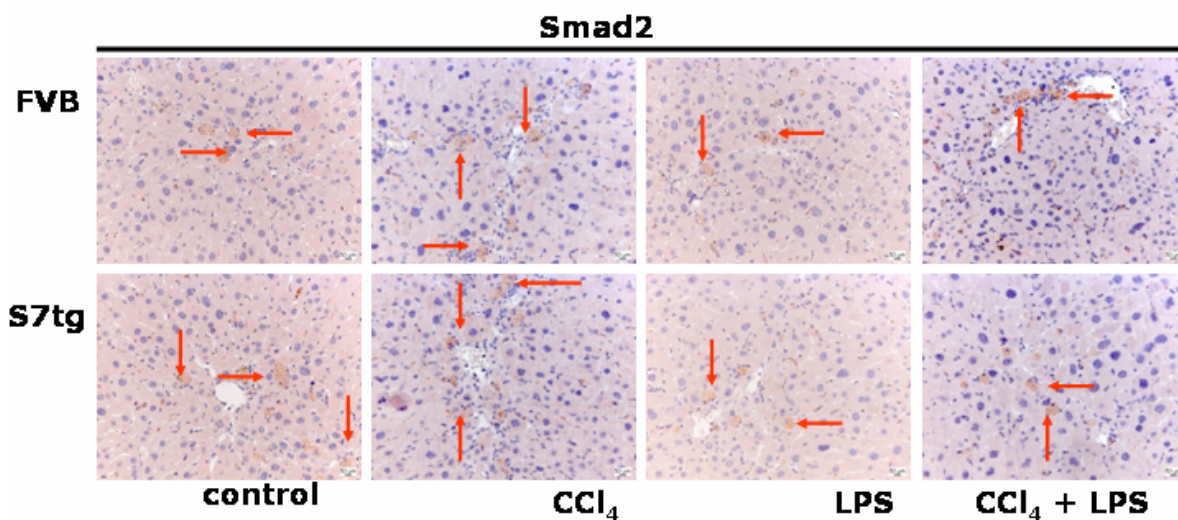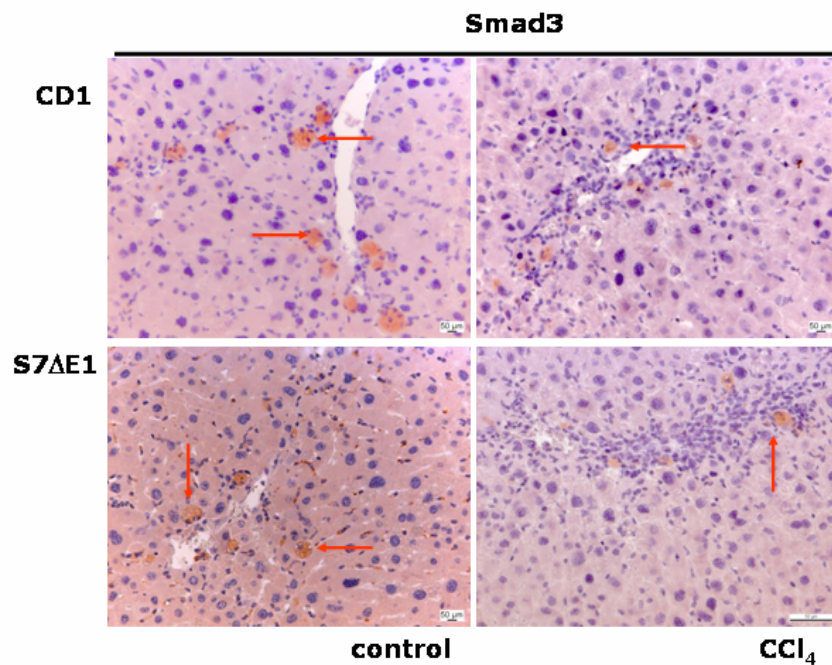**Figure 3.35:** Immunohistochemical staining of Smad 3 in liver tissue sectionsa of different mouse strains after CCl_4 and/or LPS treatment as indicated. Representative photomicrographs are shown. Arrows indicate Smd3 positive signals; magnification x 200. (A) Smad7 overexpression does not affect constitutive expression of Smad3 by S7tg compared to FVB wild types mice after CCl_4 dependent liver damage. (B) Loss of Smad7 does not affect constitutive expression of Smad3.

3.12   Smad7 overexpression in hepatocytes decrease the serum levels of liver enzymes in CCl$_4$ treated mice

Analysis of serum levels of liver enzymes reveals important parameters of the state of liver fibrosis. For example aspartate aminotransferase (AST) present in hepatocytes and myocytes catalyses the reversible transfer of an amino group from L-glutamic acid to oxaloacetic acid, forming alpha-oxoglutaric acid and L-aspartic acid. Its concentration raises proportional to the damage of inner organs e.g. due to liver fibrosis and heart myocardial infraction. Following a damage of those cells, AST is released into the blood. Measuring the concentration of AST in the serum can thus give important information about the state of organ damage.

Alanin aminotransferase (ALT) found primarily in the liver, is also released into the bloodstream as a result of liver damage. Its increased level in the serum is a marker of liver fibrosis. Further alkaline phosphatase (AP) a liver enzyme which splits phosphate groups from nucleotides and proteins shows increased serum concentrations at liver fibrosis. To measure concentrations of AST, ALT and AP serum was prepared from 1 ml blood by needle prick into the eyes of anesthetized experimental mice.

Analysis showed that AST, ALT and AP levels increase rapidly with CCl$_4$ induced liver damage in experimental mice. Serum analysis in this study reveals that AST concentration of CCl$_4$ treated S7tg mice (n = 10) is 132.9 ± 18.9 U/L. This is slightly reduced in comparison to AST levels in equally treated FVB wild type animals (n = 10) (167.6 ± 13.6 U/L) (figure 3.36). CD-1 mice (n = 8) release approximately the same amount of AST (121.3 ± 18.8 U/L) as S7tg mice but only half as much as S7ΔE1 strain mice (n = 8) (Table 3.8 and figure 3.37). No remarkable difference between AST levels in the serum of FVB and S7tg mice could be measured in LPS treated group. A significant reduction of the AST level in the serum of S7tg mice can be observed in the CCl$_4$ + LPS treated group. After this medication FVB wild type mice produced approximately threefold more serum AST (i.e. 151.5 ± 6.7 U/L) than S7tg mice (figure 3.36). A comparison between CCl$_4$ treated S7ΔE1 mice and S7tg mice after CCl$_4$ + LPS treatment demonstrates that S7tg mice exhibit heavily reduced AST serum concentrations. Although both groups are treated differently this result proves that transgenic Smad7 overexpression in hepatocytes triggers a strong reduction of AST in the serum of experimental mice. That effect can be correlated to a lower state of liver damage due to Smad7.

Table 3.8: Serum concentrations of liver enzymes in experimental miceas indicated. For comparison the data of hyaluronic acid are showed repeatedly. See figure 3.23 and Table 3.4. n=number of animals investigated.

Experimental mice	treatment	AST (U/L)	ALT (U/L)	AP (U/L)	Hyaluronic acid (μg/ml)
FVB (n = 10)	CCl_4	167.6 ± 13.6	428.8 ± 23.6	198.4 ± 15.	392.2 ± 21
S7tg (n = 10)	CCl_4	132.9 ± 18.9	413.1 ± 24.7	191.4 ± 11.8	411 ± 31
CD-1(n = 8)	CCl_4	121.3 ± 16.8	362.7 ± 15.4	191.3 ± 13.3	355 ± 22.5
S7△E1 (n = 8)	CCl_4	262.3 ± 16.6	605.5 ± 22.3	247.3 ± 9.8	562 ± 30.2
FVB (n = 10)	LPS	25.13 ± 6.7	91.12 ± 9.5	108.25 ± 20.9	146 ± 23.5
S7tg (n = 10)	LPS	28.4 ± 4.2	87.9 ± 11.8	81.5 ± 11.2	138 ± 14
FVB (n = 10)	CCl_4 + LPS	151.5 ± 6.7	307.4 ± 27.7	190.6 ± 8.4	440 ± 44
S7tg (n = 10)	CCl_4 + LPS	50.4 ± 12.6	151.1 ± 26.1	134.9 ± 14.9	200.5 ± 18.8
FVB (n = 8)	without	24.04 ± 9.01	54.5 ± 4.3	64.5 ± 9.7	89 ± 10.8
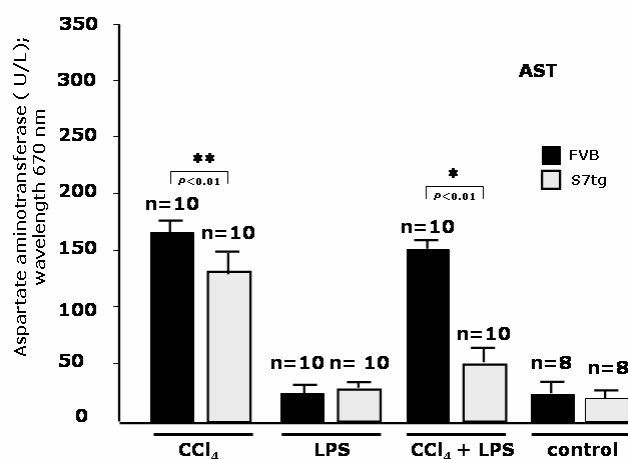
Figure 3.36   **Figure 3.37**

Figure 3.36: Smad7 overexpression decreases serum levels of AST i.e. the sensitivity for liver damage and fibrogenesis after CCl_4 intoxication. S7tg mice were compared to FVB wild type animals. Evaluation of asparate aminotransferase (AST) concentrations in the serum was measured after 8 weeks of treatment as indicated at 670 nm with VITROS Chemistry Products; n = number of animals investigated in triplicate measurements. S7tg mice exhibit significantly more AST in the serum than FVB mice after CCL_4 + LPS treatment. This can be correlated to a lower state of liver damage.
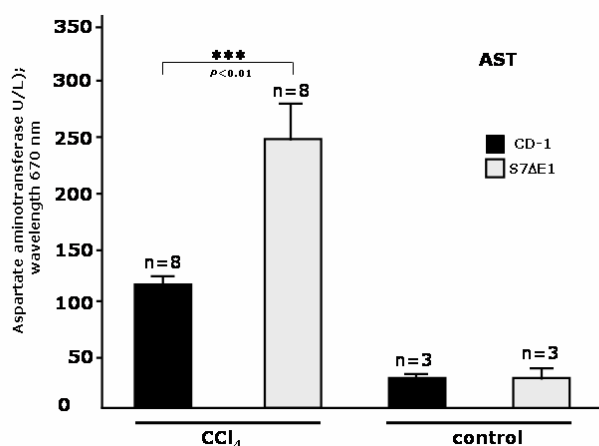
Figure 3.37: Loss of Smad7 increases serum levels of AST i.e. the sensitivity for liver damage and fibrogenesis after CCl_4 intoxication. S7ΔE1 mice were compared to CD-1 wild type animals. Asparate aminotransferase (AST) serum concentration was measured at 670 nm with VITROS Chemistry Products after 8 weeks of CCl_4 treatment; n = number of animals investigated in triplicate measurements.

In line with AST levels indicating increased liver damage as a result of CCl_4 induced fibrosis, ALT concentrations are elevated after CCl_4 treatment in all mouse strains tested. Nevertheless, in early stages of liver damage the AST concentration is approximately half of that of ALT. The inverse scenario only occurs in the case of cirrhosis.

Measurement of ALT concentrations in the sera shows only slight differences between FVB (n = 10) (428.8 ± 23.6 U/L), CD-1 (n = 8) (362.7 ± 15.4 U/L) and S7tg mice (n = 109) (413.1 ± 24.7 U/L) under CCl_4 induced fibrotic conditions (Table 3.9 and figure 3.38 and 3.39). This difference increases significantly if experimental mice were exposed to additional LPS co-injunction. Figure 3.38 shows that in S7tg mice then only ALT concentrations of 151.1 ± 26.2 U/L could be detected. In comparison FVB mice produced a twofold higher serum concentration of ALT (307.4 ± 27.7 U/L). A comparison between ALT serum concentrations of S7ΔE1 mice and S7tg mice reveals that S7ΔE1 animals synthesize the highest amount of serum ALT i.e. 605.5 ± 22.3 U/L. This amount is fourfold higher than the one measured in S7tg mice (figure 3.38-3.39).

Table 3.9: Effect of Smad7 overexpression on ALT serum concentrations (U/L). n=number of animals investigated, n. d.: not determined.

| Experimental mice	Control	CCl₄	LPS	CCl₄ + LPS
FVB (n = 10)	54.5 ± 4.3	428.8 ± 23.6	91.12 ± 9.5	307.4 ± 27.7
S7tg (n = 10)	50.3 ± 3.3	413.1 ± 24.7	87.9 ± 11.8	151.1 ± 26.1
CD-1 (n = 8)	48.2 ± 2.4	362.7 ± 15.4	n. d.	n. d.
S7ΔE1 (n = 8)	55.2 ± 3.6	605.5 ± 22.3	n. d.	n. d.
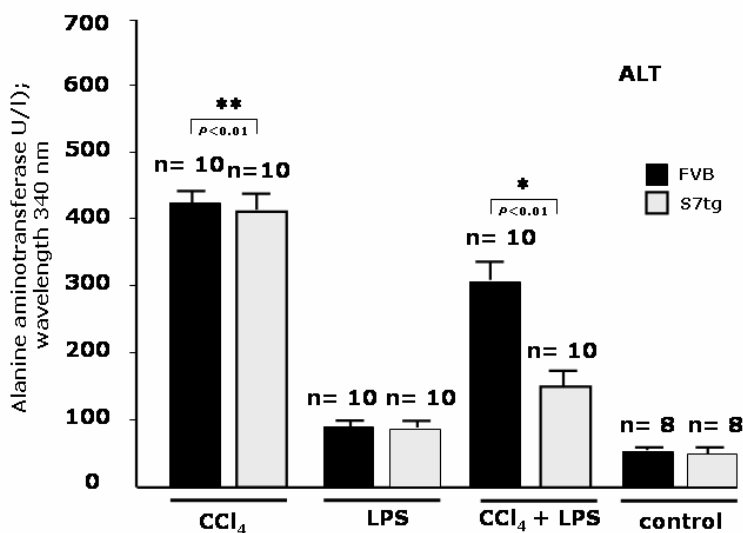
Figure 3.38: Smad7 overexpression decreases serum levels of ALT i.e. reduces the sensitivity for liver damage and fibrogenesis after CCl_4 intoxication. S7tg mice were compared to FVB wild type animals after different treatsments as indicated. Alanine aminotransferase (ALT) concentrations in the serum were measured at 340 nm with VITROS Chemistry Products; n, number of animals investigated in triplicate measurements.
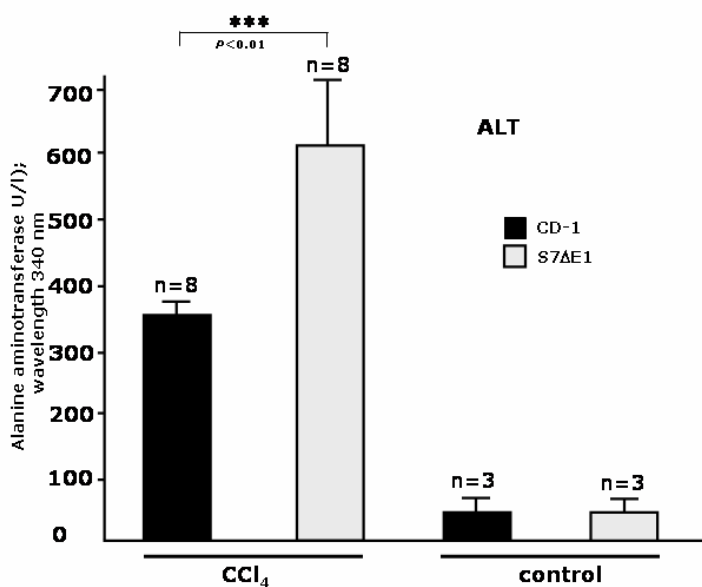
Figure 3.39: Loss of Smad7 increases the serum level of ALT i.e. enhances the sensitivity for liver damage and fibrogenesis after CCl_4 intoxication. S7ΔE1 mice were compared to CD-1 wild type animals after 8 weeks of CCl_4 treatment. Serum concentrations of alanine aminotransferase (ALT) were measured at 340 nm with VITROS Chemistry Products; n = number of animals investigated in triplicate measurements.

As expected based on the results of AST and ALT measurements, alkaline phosphatase (AP) serum levels do not show significant differences between FVB, S7tg and CD-1 mice after CCl_4 treatment. Again in the serum of S7ΔE1 mice (n = 8) the highest concentration of the fibrosis marker enzyme was detected. AP levels were measured to be 247.3 ± 9.8 U/L (Table 3.10, figure 3.40 and 3.41). LPS treatment and the resulting Smad7 overexpression causes the reduction of AP levels in S7tg mice to 81.5 ± 11.2 (U/L). In comparison, FVB mice produce up to 108.25 ± 20.9 U/L serum after the same treatment. A reduction of AP levels (134.9 ± 14.9 U/L) is observed in the serum of S7tg mice after CCl_4 + LPS treatment in comparison to CCl_4 treated mice. In contrast FVB mice showed AP levels of 190.6 ± 8.4 U/L (figure 3.40).

Table 3.10: Effect of Smad7 overexpression on serum concentrations of alkaline phosphatase (U/L). n=number of animals investigated, n. d.: not determined.

Experimental mice	Control	CCl_4	LPS	CCl_4 + LPS
FVB (n = 10)	64.5 ± 9.7	198.4 ± 15.7	108.25 ± 20.9	190.6 ± 8.4
S7tg (n = 10)	60.3 ± 2.3	191.4 ± 11.8	81.5 ± 11.2	134.9 ± 14.9
CD-1 (n = 8)	58.2 ± 4.3	191.3 ± 13.3	n. d.	n. d.
S7△E1 (n = 8)	65 ± 4.5	247.3 ± 9.8	n. d.	n. d.
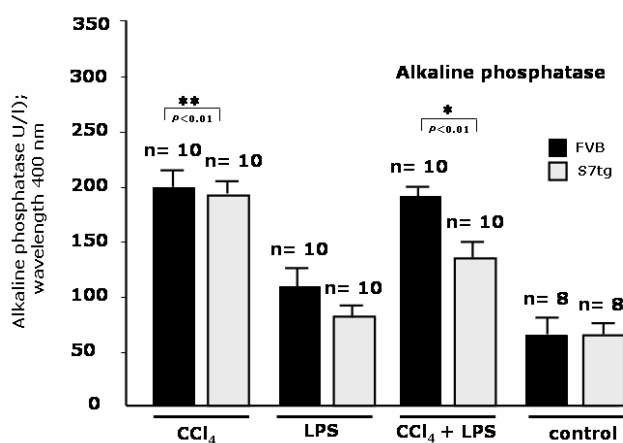
Figure 3.40
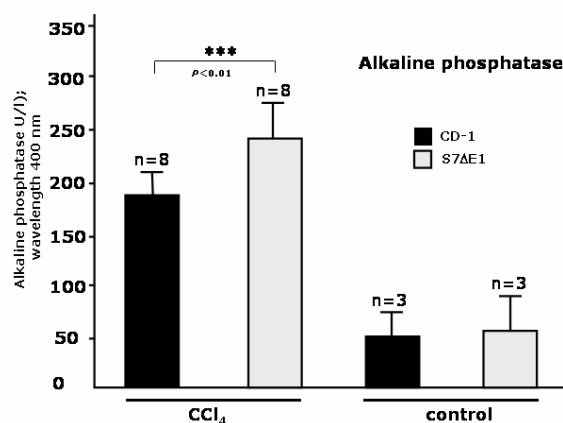
Figure 3.41

For description of figures 3.40 and 3.41 see next page.

Figure 3.40: Smad7 overexpression decreases the serum level of AP i.e. decreases the sensitivity for liver damage and fibrogenesis. S7tg mice were compared to FVB wild type animals after different intoxication treatments as indicated. Alkaline phosphatase serum concentrations were measured at 400 nm with VITROS Chemistry Products; n, number of animals investigated in triplicate measurements.

Figure 3.41: Loss of Smad7 increases serum concentrations of AP i.e. increases sensitivity for liver damage and fibrogenesis after CCl_4 intoxication. S7ΔE1 mice were compared to CD-1 wild type animals after CCl_4 treatment. Evaluation of Alkaline phosphatase in the serum was measured at 400 nm with VITROS Chemistry Products; n, number of animals investigated in triplicate measurements.

In summary the measurements of AST, ALT and AP serum concentrations in differently treated mice reveals that Smad7 expression reduces the amount of fibrosis marker enzymes in the serum. Thus it can be interpreted, that Smad7 overexpression in hepatocytes can reduce liver damage in CCl_4 exposed animal.

3.13   Smad7 overexpression reduces apoptosis of liver cells in CCl_4 treated mice

Apoptosis is applied to a group of characteristic structural and molecular events that separate this type of cell deletion from necrosis. In contrast to necrosis which involves death of a group of cells simultaneously, apoptosis can occur in a single cell surrounded by a group of viable cells. There is a distinct and precisely localized control over the fate of specific cells in a mixed cell population that undergo apoptosis. Diverse groups of specific molecules are involved in the apoptosis pathway. One set of mediators implicated in apoptosis belong to the asparate-specific cysteinyl proteases or caspases. A member of this family, caspase-3 (CPP32, apopain, YAMA) has been identified as being a key mediator of apoptosis of mammalian cells. Determining the amount of caspase-3 in a cell gives indirect evidence whether it is apoptotic.

In order to determine the effect of Smad7 overexpression on apoptosis immunostaining analysis was carried out using anti-caspase-3 antibodies. The result obtained suggests that CCl_4 induced fibrosis causes an increasing number of apoptotic cells in fibrotic regions of the liver. In contrast non-fibrotic liver regions were not affected by apoptosis. Based on the effects of Smad7 overexpression described earlier in this thesis less apoptotic cells were expected in tissue sections of S7tg mice compared to wild type animals. Quantitative analysis of anti-caspase-3 immunohistochemical staining based on direct cell counting under a light microscope (figure 3.42 and 3.43) confirms that expectation. In sections of CCl_4 treated animals equally low anti-caspase-3 stainings could be detected i.e. $3 \pm 0.9\%$, $2.3 \pm 0.7\%$ and $2.12 \pm 0.8\%$ in cells of FVB (n = 10), S7tg (n = 10) and CD-1 (n = 8) mice respectively (Table 3.11). In contrast liver sections of S7ΔE1 mice showed a higher amount of apoptotic caspase-3 signals. Additional treatment with LPS causes a drastic reduction of anti-caspase-3 signals in cells of S7tg mice to 0.6%. In comparison FVB wild type cells exhibit an apoptotic signal rate of $2.8 \pm 0.8\%$ under similar CCl_4 fibrotic condition with LPS co-administration. That implies a 4.8-fold reduction of apoptosis in S7tg mice, most probably as a result of Smad7 overexpression in hepatocytes.

Table 3.11: Effect of Smad7 overexpression on apoptosis. Anti-caspase-3 immunohistochemical staining of liver sections of mouse strains as indicated was quantified. n=number of animals investigated, n. d.: not determined. Percentages give the amount of stained areas in relation to the total area investigated. For more information see legend of figures 3.42 and 3.43.

Experimental mice	Control (%)	CCl_4 (%)	LPS (%)	CCl_4 + LPS (%)
FVB (n = 10)	0.25	3 ± 0.92	0.5 ± 0.5	2.8 ± 0.8
S7tg (n = 10)	0.2	2.3 ± 0.7	0.5 ± 0.5	0.6 ± 0.7
CD-1 (n = 8)	0.3	2.1 ± 0.8	n. d.	n. d.
S7△E1 (n = 8)	0.3	5 ± 0.5	n. d.	n. d.

(A)

(B)
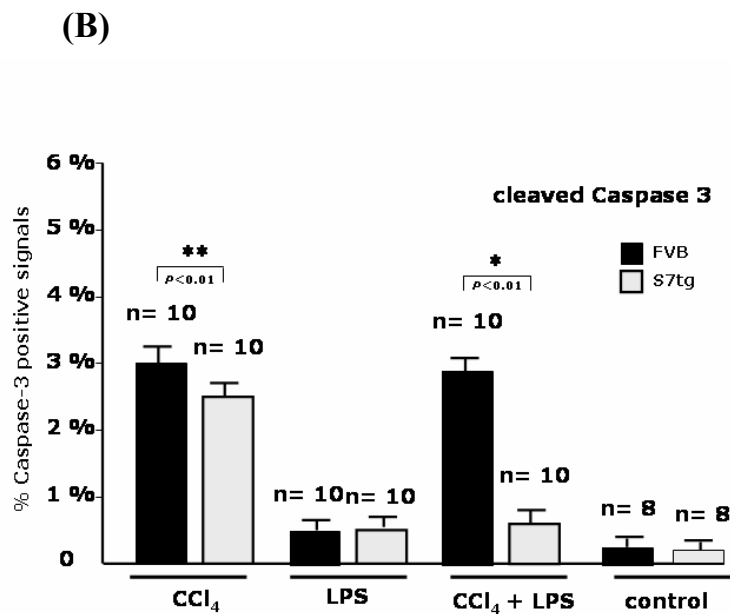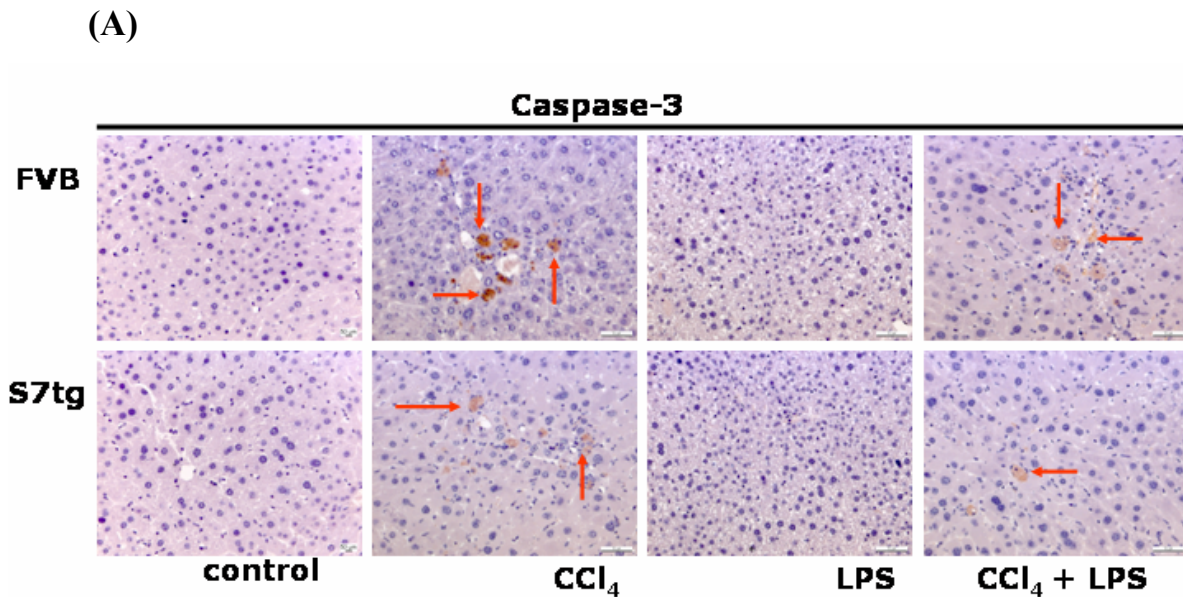
Figure 3.42: Smad7 overexpression leads to a blockade of TGF-β signaling and a reduction of hepatocyte apoptosis in mice. S7tg mice were compared to FVB wild type animals. (A) Immunohistochemical staining of cleaved caspase 3 was performed to identify apoptotic cells. Representative photomicrographs of mice liver sections treated for 8 weeks as indicated are shown. Untreated cells serve as controls. Arrows indicate positive signals; magnification x 200. (B) Morphometric quantification of immunohistochemical stainings depicted in A. Ten fields were selected randomly from each section of different groups (8-10 animals/group); LEICA QWIN software (Germany) was used. The graph shows the percentage of stained areas related to the total area investigated; about 200 cells were evaluated per observation field, stained cells were counted and expressed as percentage of total cells investigated.

(A)
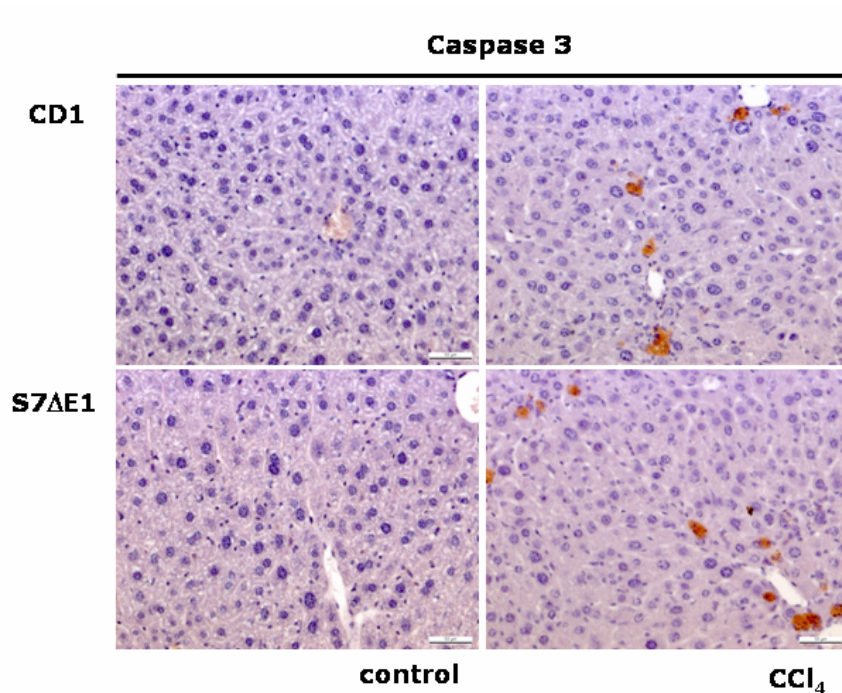
(B)

Figure 3.43: Loss of Smad7 leads to an intensification of TGF-β signaling and an increase of hepatocyte apoptosis. S7ΔE1 mice were compared to CD-1 wild type animals. (A) Immunohistochemical staining of cleaved caspase 3 was performed to identify apoptotic cells. Representative photomicrographs of mice liver sections from S7ΔE1 and CD-1 mice as indicated are shown; untreated cells serve as controls; Brown staining indicates positive signals; magnification x 200. (B) Morphometric quantification of immunohistochemical staining of cleaved caspase 3. Ten fields were selected randomly from each section of different groups (3-8 animals/group); LEICA QWIN software (Germany) was used. The graph shows the percentage of stained areas related to the total area investigated; about 200 cells were evaluated per observation field, stained cells were counted and expressed as percentage of total cells investigated.

3.14   Smad7 overexpression reduces proliferation of hepatocytes in CCl$_4$ treated mice

Proliferating cell nuclear antigen (PCNA, 36 kDa), also known as cyclin, is an auxiliary protein of DNA polymerase that is essential for DNA replication during S phase of the cell cycle. The protein is present in the nucleoplasm of continually cycling cells throughout the cell cycle (Waseem, N., and Lane, D., 1990). PCNA begins to accumulate during G1 phase of the cell cycle, is most abundant during S phase, and declines during G2/M phase. The predominant distribution of PCNA also appears to change within the stages of the cell cycle.

Monoclonal anti-proliferating cell nuclear antigen (PCNA) (mouse IgG2a isotype) antibodies were used to analyse cell proliferation and its relation with Smad7 overexpression. The results suggest a proportional correlation between the degree of tissue damage and cell proliferation (figure 3.44). As figure 3.44 indicates anti-PCNA signals appear predominantly in fibrotic areas after CCl$_4$ treatment. Quantitative analysis of PCNA immunohistochemical staining shows only small differences of PCNA signals in cells of CCl$_4$ treated animals. 15.1 ± 1.5 %, 17.5 ± 1.6% and 14 ± 2.3% of immunostained areas in cell sections of FVB (n = 10), S7tg (n = 10) and CD-1 (n = 8) mice could be detected respectively. Tissue sections of S7ΔE1 mice show the highest amount of anti-PCNA signals i.e. 34.9 ± 3.3% (figure 3.45). LPS treatment alone did not induce any proliferation. Immunohistochemical staining with anti-PCNA antibodies revealed no difference of LPS treated cells to untreated cells of the control. After CCl$_4$ + LPS treatment in contrast, S7tg cell sections exhibit 6.6 ± 1.3% of immunostained areas, whereas sections of FVB wild type mice show threefold more anti-PCNA signals i.e., 18.8 ± 2.1%. This reduction can be attributed to transgenic derived Smad7 overexpression in hepatocytes triggered by LPS administration (Table 3.12 and figure 3.44).

Table 3.12: Quantification of immunohistochemical staining of PCNA in mouse liver sections as indicated. n=number of animals investigated, n. d.: not determined. Percentages give the relation between stained areas and the total area investigated.

Experimental mice	Control (%)	CCl$_4$ (%)	LPS (%)	CCl$_4$ + LPS (%)
FVB (n = 10)	0.3 ± 0.4	15.1 ± 1.5	0.5 ± 0.5	18.6 ± 2.1
S7tg (n = 10)	0.21	17.5 ± 1.6	0.3 ± 0.4	6.6 ± 1.3
CD-1 (n = 8)	0.31	14 ± 2.3	n. d.	n. d.
S7ΔE1 (n = 8)	0.32	34.9 ± 3.3	n. d.	n. d.

(A)

(B)

Figure 3.44: Smad7 overexpression leads to a blockade of TGF-β signaling and a decrease of hepatocyte proliferation after CCl$_4$ induced liver damage. (A) Representative photomicrographs of mouse liver sections of S7tg and FVB mice treated for 8 weeks with CCl$_4$ and LPS are shown. Untreated cells serve as a control. Immunohistochemical staining of PCNA was performed to analyse hepatocyte proliferation. Arrows indicate positive signals. Magnification x 200. (B) Morphometric quantification of anti-PCNA immunostaining. Ten fields were selected randomly from each section of different groups (8-10 animals/group); LEICA QWIN software (Germany) was used. The graph shows the percentage of stained areas related to the total area investigated; about 200 cells were evaluated per observation field, stained cells were counted and expressed as a percentage of total cells investigated.
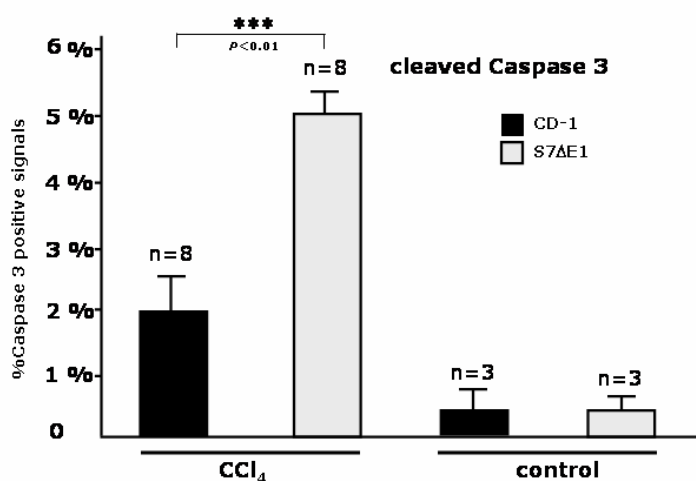
(A)

(B)

Figure 3.45: Loss of Smad7 leads to an intensification of TGF-β signaling and an increase of hepatocyte proliferation after CCl_4 induced liver damage. (A) Representative photomicrographs of mice liver sections from S7ΔE1 and CD-1 animals treated for 8 weeks with both CCl_4 and LPS are shown. Untreated cells serve as a control. Anti-PCNA immunohistochemical staining was performed to assay hepatocyte proliferation. Brown staining indicates positive signals; magnification x 200. (B) Morphometric quantification of immunohistochemical staining of PCNA. Ten fields were selected randomly from each section of different groups (3-8 animals/group); LEICA QWIN software (Germany) was used. The graph shows the percentage of stained area related to the total area investigated; about 200 cells were evaluated per observation field, stained cells were counted and expressed as a percentage of total cells investigated.

3.15 Smad7 overexpression in hepatocytes blunts inflammation in CCl$_4$ treated mice

An important marker for determination of inflammation states is CD43, expressed on peripheral T cells (Baecher et al; 1988 and Gulley et al 1988), on thymocytes (Jones et al 1994), and on early myeloid and lymphoid hematopoietic precursors within the bone marrow (Moore et al 1994). CD43 has been shown to be involved in a number of T cell-mediated responses, including co-stimulation of proliferation (Rosenstein et al 1991), enhanced cytotoxicity of CD8 and T cells (Mosley et al 1994) and leukocyte adhesion (Axelsson et al 1988 and Nong et al 1989).

In order to determine the effect of Smad7 overproduction in hepatocytes on inflammations, an accompanying symptom of fibrosis, immunohistochemical staining with anti-CD43 antibodies (BD Pharmingen) was performed (table 3.13 and figure 3.46 and 3.47). The analysis indicates that CCl$_4$ treatment of mice causes strong CD43 expression. CD43 could be detected predominantly in damaged regions of liver tissues. Tissue sections of S7ΔE1 mice (n = 8) exhibit most anti-CD43 signals, i.e. 29 ± 0.92 %. (Table 3.13 and figure 3.47). Unexpectedly, FVB wild type (n = 10) shows little less CD43 signals than S7tg (n = 10), i.e. 13.8 ± 1.7 % and 17 ± 1.1 %, respectively. But in cells of CCl$_4$ + LPS treated S7tg mice significantly less CD43 signals were detected (3 ± 0.92%). In contrast, the amount of CD43 signals in FVB wild type cells remained unchanged after LPS co-injection. It is threefold higher than in cells of S7tg mice (12.75 ± 1.4 %). S7ΔE1 strain mice show most CD43 signals, i.e. (29 ± 0.92%). The corresponding CD-1 wild type cells show only 16.8 ± 1.2 % of CD43 staining. This result points out the enormous decrease of CD43 signals in S7tg mice in comparison to S7ΔE1 mice exhibiting six fold as many CD43 signals. This peak can be correlated to highest extent of liver damage in this mouse strain.

Further, this finding confirms that Smad7 overexpression in hepatocytes can inhibit CCl$_4$ induced liver fibrosis and blunts the inflammatory state of the liver of those animals.

Table 3.13: Quantification of immunohistochemical staining of CD43. n=number of animals investigated, n. d.: not determined. Percentages give the amount of stained area in relation to the total area investigated. For more information see legends of figures 3.46 and 3.47.

Experimental mice	Control (%)	CCl$_4$ (%)	LPS (%)	CCl$_4$ + LPS (%)
FVB (n = 10)	0.12	13.8 ± 1.7	0.5	12.8 ± 1.4
S7tg (n = 10)	0.13	17 ± 1.06	0.3	3 ± 0.9
CD-1 (n = 8)	0.2	16.8 ± 1.2	n. d.	n. d.
S7$\triangle$E1 (n = 8)	0.3	29 ± 0.9	n. d.	n. d.

(A)

(B)
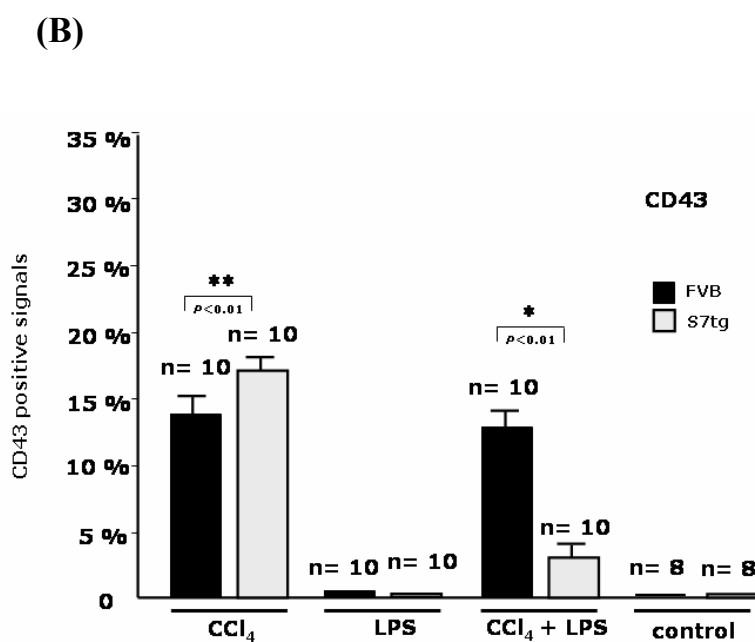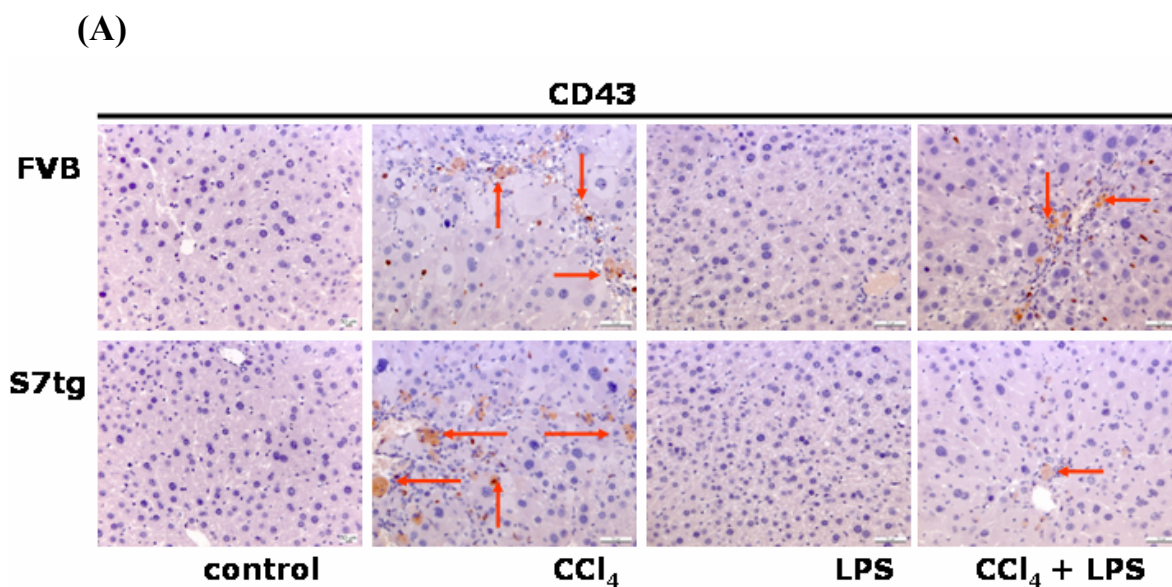
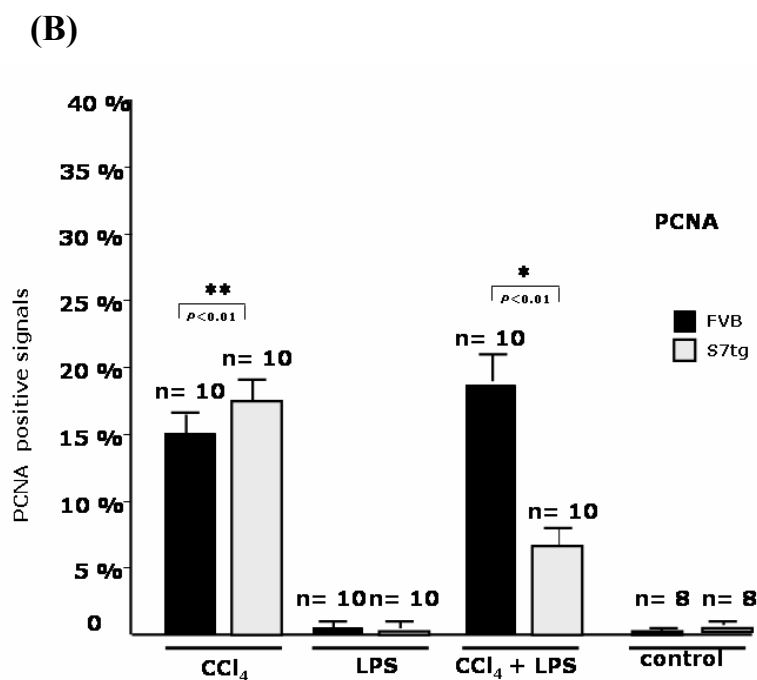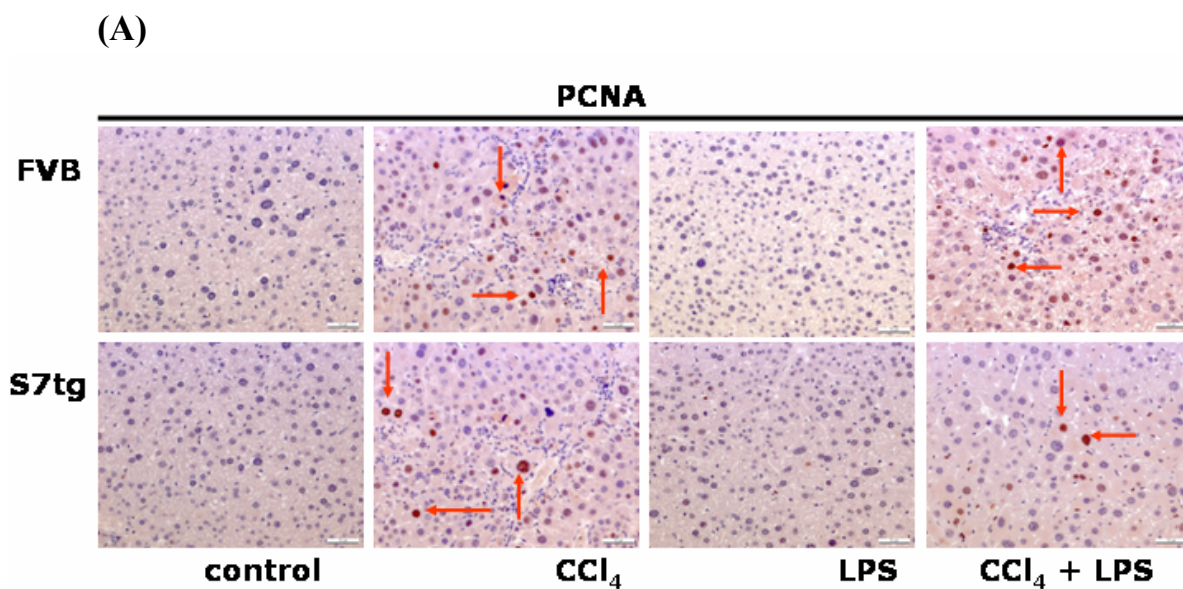**Figure 3.46:** Smad7 overexpression leads to a blockade of TGF-β signaling and a decrease of inflammation after CCl$_4$ induced liver damage. (A) Representative photomicrographs of mouse liver sections of S7tg and FVB mice treated for 8 weeks with both CCl$_4$ and LPS as indicated are shown. Untreated cells serve as a control. Immunohistochemical staining of CD43 was performed to indicate inflammation. Arrows indicate positive signals; magnification x 200. .(B) Morphometric quantification of immunohistochemical staining of CD43. Ten fields were selected randomly from each section of different groups (8-10 animals/group); LEICA QWIN software (Germany) was used. The graph shows the percentage of stained areas related to the total area investigated. About 200 cells were evaluated per observation field, stained cells were counted and expressed as a percentage of total cells investigated.
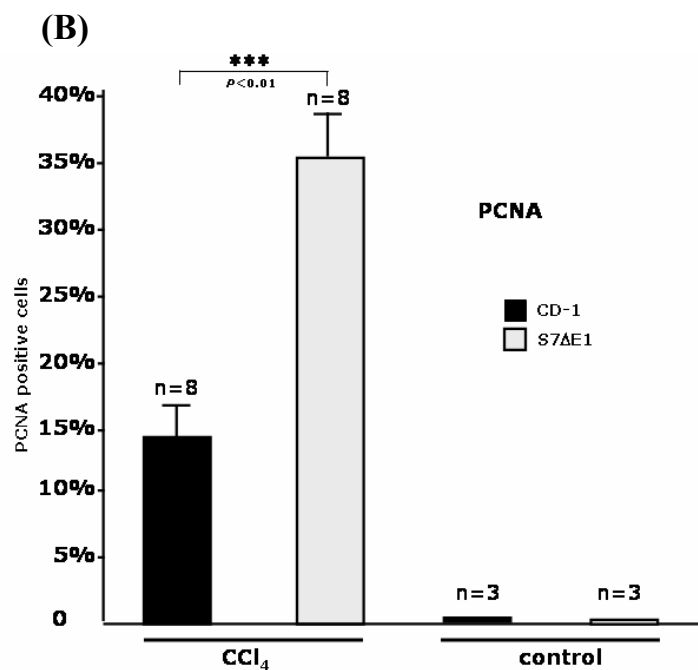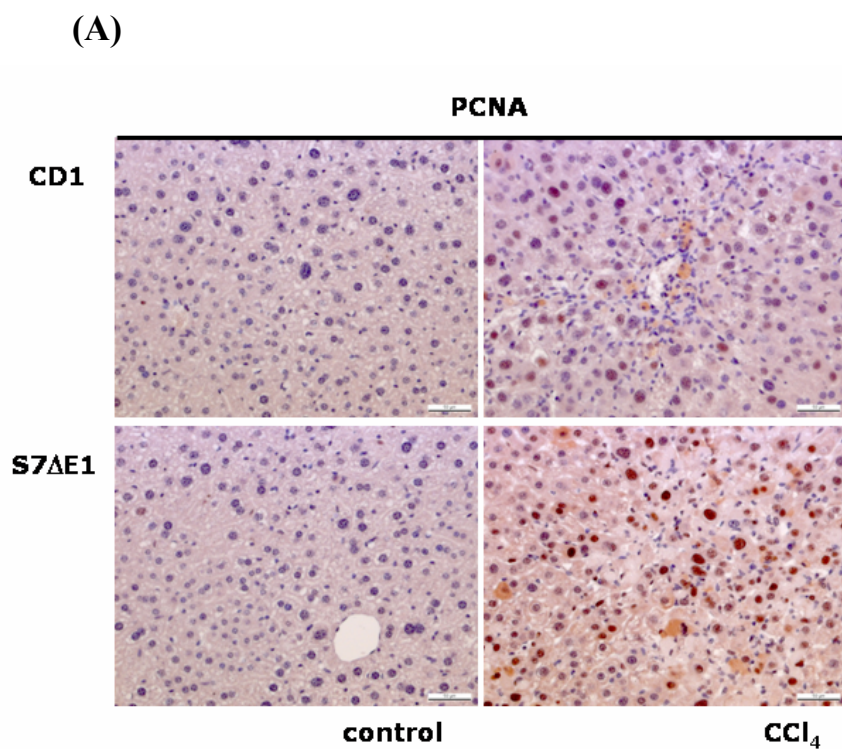
(A)

(B)
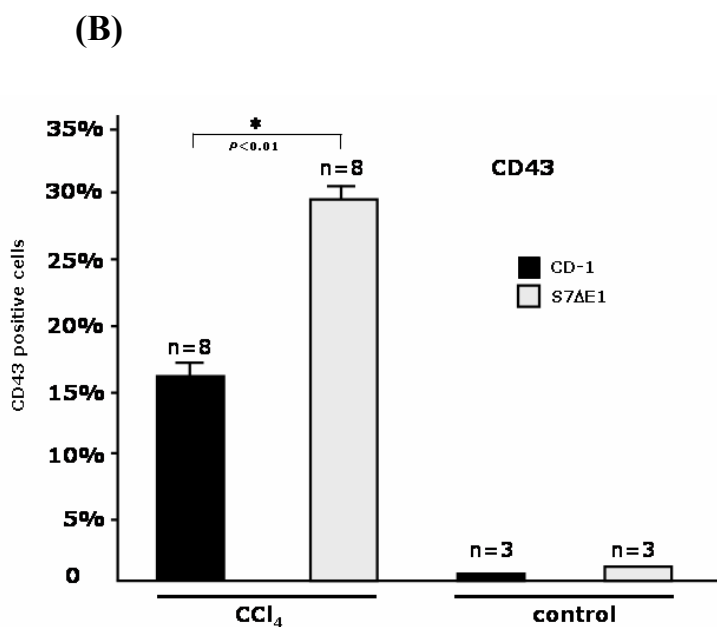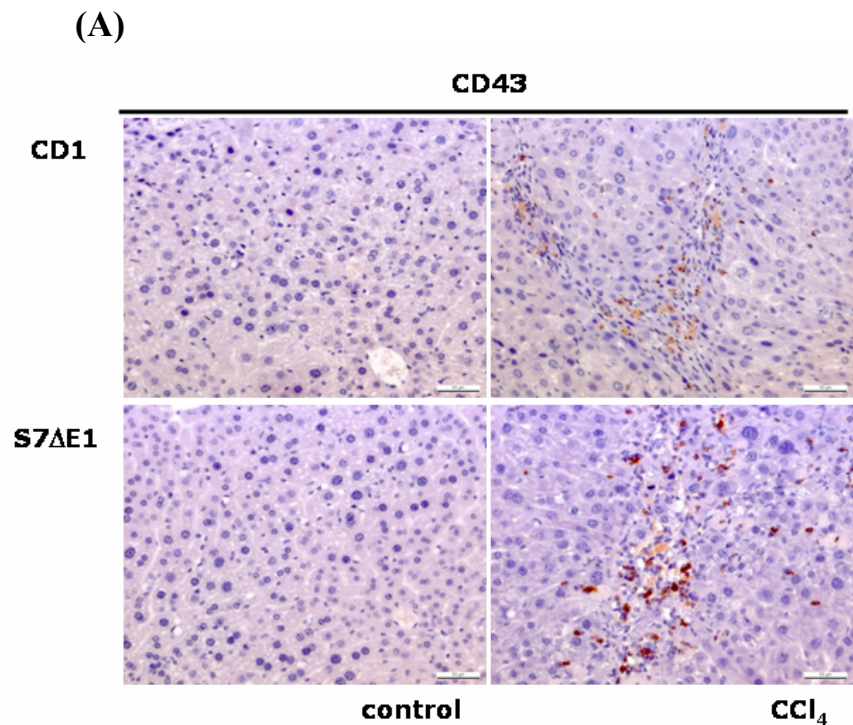
Figure 3.47: Loss of Smad7 leads to an intensification of TGF-β signaling and an increase of hepatocyte inflammation after CCl_4 induced liver damage. (A) Representative photomicrographs of mice liver sections of S7ΔE1 and CD-1 mice treated for 8 weeks with both CCl_4 and LPS as indicated are shown. Untreated cells serve as a control. Immunohistochemical staining of PCNA was performed to analyse hepatocyte proliferation. Brown staining indicates positive signals; magnification x 200. (B) Morphometric quantification of immunostaining of CD43. Ten fields were selected randomly from each section of different groups (3-8 animals/group); LEICA QWIN software (Germany) was used. The graph shows the percentage of stained areas related to the total area investigated; about 200 cells were evaluated per observation field, stained cells were counted and expressed as percentage of total cells investigated.

4   Discussion

TGF-β is known to play a central role in fibrogenesis. Therefore numerous antifibrotic strategies aim to block action of this cytokine or reduce its synthesis. One strategy is application of antisense mRNA, as reported by Arias et al., [4]. Thus, synthesis and autocrine signaling of TGF-β was suppressed in HSCs by an adenovirus expressing antisense mRNA (Ad5-CMV-asTGF-β1) targeting the 3´coding sequence of TGF-β1. In that study, Col1A1, α-SMA, LTBP-1, TβRI, and TβRII, which are increased during fibrogenesis, decreased after expression of antisense mRNA.

As a model of irreversible fibrosis in rats Qi et al., [94] and Ueno et al., [120] used dimethylnitrosamine (DMN). Both groups successed in blocking the TGF-β signaling pathway using expression of either a dominant negative or a soluble type II TGF-β receptor (TβRII) . Rats infected with adenoviruses expressing these constructs survived the harmful effect of DMN, whereas control rats died of fibrosis. The authors concluded that anti-TGF-β treatment prevents fibrosis and preserves organ function, thus being therapeutically useful. Similarly, fibrosis induced by chronic bile duct ligation (BDL) was suppressed by ectopic expression of a fusion protein consisting of the Fc domain of immunoglobin G and the extracellular portion of TβRII [43].

Since Smad7 represents an efficient inhibitor of TGF-β signaling, it is conceivable that hyperexpression of Smad7 is an additional means to antagonize TGF-β in fibrogenesis. Thus, bleomycin-induced lung fibrosis was reduced by intratracheal injection of a recombinant adenovirus containing Smad7 cDNA [82]. Furthermore, gene transfer of Smad7 into obstructive kidney fibrosis prevented accumulation of ECM in this organ [113], confirming the above mentioned hypothesis.

In a part of my own work, we studied the effect of Smad7 overexpression after adenoviral gene transfer (AdSmad7) in primary cultured HSCs and in vivo after BDL of rats [34]. Exogenous Smad7 overexpression prevented BDL dependent activation of HSCs and liver fibrosis. Collagen I deposition and hydroxyproline content were significantly reduced in Smad7 overexpressing livers. Although Smad7 overexpression did not reduce expression of α-SMA, a marker for HSC transdifferentiation, in cultured HSCs, it was strongly reduced in Smad7 overexpressing rats. We concluded that Smad7 overexpression completely inhibits autocrine and paracrine TGF-β signaling in HSCs, leading to abrogation of Smad2/3 activation and subsequent downstream events. Our results further indicate that HSCs remained in a quiescent stage after Smad7 overexpression confirming the important role of TGF-β signaling during the early phase of HSC activation.

As AdSmad7 viruses infected and resided in all cell types of the liver, specificity of its effect could not be related to a single cell type. Even an influence on other organs could not be excluded.

In my thesis I therefore established an animal model with inducible overexpression of transgenic Smad7 in hepatocytes (S7tg mice) and studied its effect on fibrogenesis after CCl$_4$ induced liver damage. In contrast to albumin/TGF-β1 transgenic mice of Sanderson and colleagues [103], the mortality rate of S7tg mice was infinitely small during the CCl$_4$ treatment protocol I used.

In S7tg mice the Smad7 gene was expressed under the control of the human CRP promoter. CRP is a component of the congenital immune system stimulated by LPS. Binding of LPS to cell surface receptors triggers the synthesis of inflammatory cytokines including IL-6, which then induces expression of CRP [1]. Because CRP and its transcription factors are mainly expressed in hepatocytes, this new mouse model leads to specific Smad7 expression in hepatocytes.

Liver histology analysis pointed to similar morphology of liver tissues in untreated S7tg mice and corresponding FVB wild type mice. LPS, used to induce the CRP promoter, is known to trigger expression of cytokines like TNF-α, thereby strengthening the profibrotic effect of TGF-β1[101] and [48]. Further, it was previously reported that LPS treatment may result in activation of Kupffer cells to release various kinds of cytokines and inflammatory mediators, thus inducing liver injury [88], [45], [31] and [125]. Even exposure to smaller LPS doses can result in a modest, noninjurious inflammatory response [42]; [76] and [74]. On the other hand it was recently shown that LPS treated animals can develop endotoxin tolerance taking advantage of the scavenger character of kupffers cells and liver sinusoidal endothelial cells clearing circulating blood from LPS [121]. Moreover, production and signaling of IL-10 have been proven to be important for protection against liver injury in mice [33] and [53]. In summary, the initial burst of proinflammatory gene expression in response to LPS is proposed to be short-lived and replaced by the prolonged expression of various anti-inflammatory genes. This can lead to an immunosuppressed state which is characterized by LPS tolerance [23], [37] and [129]. In order to reduce stress, liver damage and mortality due to LPS treatment, but nevertheless avoid simultaneous development of LPS tolerance, I started to treat the animals with a relatively small dosage of LPS (10 μg/injection; being sufficient to stimulate CRP-Smad7 construct), and increased it after 6 weeks to 25 μg/injection. In comparison, other authors worked with dosages up to 100 mg/kg, i.p. [140]. Despite very low doses of LPS, I could show expression of Smad7 in S7tg mice both, directly and indirectly by detecting the Flag-tag. This indicates LPS dependent activation of the ectopic CRP promoter and subsequent transgene expression specifically in hepatocytes.

Although LPS alone had no influence on the state of liver fibrosis in my study, the agent multiplied the harmful, fibrotic effect of CCl$_4$. When both agents were injected simultaneously into FVB mice this could even lead to death. To limit mortality, experimental mice determined for CCl$_4$ and LPS treatment have been injected at alternate days with both agents.

Comparing the extent of liver damage between wild type, S7tg and S7ΔE1 mice caused by CCl$_4$ a significant increase of fibrosis in S7ΔE1 mice was detected, whereas in S7tg mice fibrotic effects were attenuated after LPS induced Smad7 expression. This includes the reduction of collagen I, α-SMA, serum enzymes, hyaluronic acid and hydroxyproline in S7tg mice. Further, immunostaining of liver tissues and Western blot analysis of Phospho-Smad2 and Phospho-Smad3 show a strongly reduced nuclear localization of both proteins. These results can be interpreted to be due to antifibrotic effects of Smad7 overexpression interrupting the TGF-β signaling pathway in hepatocytes.

Although the reduction of serum enzymes might be due to a role of hepatocyte residing TGF-β/Smad7 in liver damage or regeneration, this finding is in contrast to our previous study with adenoviral Smad7 expression. A similar contradicting tendency was reported by Qi et al., Nakamura et al. and Yata et al. who used dominant negative TβRII adenovirus constructs or a soluble TβRII variant as antifibrotic approaches [94], [80] and [139]. The difference of my results to those studies might depend on different methods of fibrosis induction (BDL versus CCl$_4$), cell type specific effects (hepatocyte specific Smad7 versus general delivery of an adenoviral Smad7 construct), or different points of interference with the signaling pathway (ligand itself versus type I receptor/R-Smad activation).

To complete my study after comparing expression of ECM and serum proteins I investigated the influence of Smad7 overexpression in hepatocytes on TGF-β dependent processes like apoptosis, inflammation and cell proliferation. TGF-β is described as one of the most potent inducers of apoptosis in normal hepatocytes [75], [103], Arsura [5]. Hepatocytes protect themselves against the pro-apoptotic effect of TGF-β by morphological transdifferentiation, a process termed epithelial mesenchymal transition (EMT). EMT includes loss of cell cell and cell matrix interactions through downregulation of E-cadherin and β-catenin [104] and [14]), migration, basement membrane degradation through matrix metalloproteinase-2 (MMP-2) [137] and cytoskeletal rearrangements including expression of α-SMA [118] and activation of Snail. All these events are normal parts of tissue repair, however, if occurring unregulated, they may contribute to chronic fibrosis and apoptosis.

In line with this, disrupting the TGF-β signaling pathway in hepatocytes of S7tg mice resulted in reduced apoptosis. A proportional relationship between increased TGF-β signaling and apoptosis was demonstrated by anti-caspase-3 signals appearing mainly in fibrotic areas of liver cells. Blocking TGF-β signaling in hepatocytes by Smad7 overexpression reduced apoptosis in S7tg mice significantly compared to FVB wild type mice and even more drastically in comparison to S7ΔE1 mice.

Determination of hepatocyte proliferation was carried out by immunohistochemical staining of PCNA, a marker for cell proliferation. PCNA staining increased in parallel with the extent of liver damage and was restricted to fibrotic regions. These data contradict the postulated inhibitory effect of TGF-β on cell proliferation; however, they are in line with findings of Date et al. [27], who examined this apparent paradox in more detail. They documented that hepatocytes may

proliferate despite the presence of a powerful antiproliferative stimulus. Date et al. further observed that isolated hepatocytes of CCl_4 treated animals have reduced sensitivity to antiproliferative effects of TGF-β1, compared to hepatocytes from normal rats. Concurrently, a dose dependent induction of fibronectin expression and proliferation inhibition by TGF-β1 in HSCs was observed, which was not differentially regulated by CCl_4 treatment. To explain the different sensitivity of HSCs and hepatocytes to TGF-β after CCl_4 induced injury, binding of radiolabelled TGF-β1 to TGF-β type I receptors in HSCs and hepatocytes from normal and CCl_4 treated livers was examined. They found that in hepatocytes in contrast to HSCs, TGF-β type I and II receptors were downregulated, thus providing an explanation for the observed reduction of TGF-β mediated growth inhibition of hepatocytes.

Finally, the rate of inflammation, usually accompanying liver fibrosis, in dependency of hepatocyte specific Smad7 expression was examined. Immunohistochemical staining with anti-CD43 antibodies points to a dramatic reduction of inflammation in livers of S7tg mice induced with LPS, in parallel with a decrease of detectable fibrosis. As expected the highest level of inflammation was measured in S7ΔE1 mice, indicating a regulatory role of the negative feedback regulation of TGF-β signaling via Smad7 during intrinsic wound healing responses. Similarly, overexpression of Smad7 in kidney inhibits renal inflammation in remnant kidney disease [52] and [84]. A direct anti inflammatory role for Smad7 within hepatocytes might be induction of IκBα, thus inhibiting NF-κB activation and a subsequent NF-κB–driven inflammatory response

Taken together, my thesis demonstrates that TGF-β signaling in hepatocytes is required for progression of chronic liver disease and blocking its signaling pathway in this cell type by ectopic expression of Smad7 is sufficient to obtain a beneficial outcome.

5 Summary

Chronic injury of the liver occurs in response to a variety of damages, including viral hepatitis, alcohol abuse, drugs and metabolic diseases. Liver fibrosis is reversible, whereas cirrhosis, the end-stage consequence, is generally not. Thus, efforts to understand fibrogenesis mechanisms should be focused on initiating events that lead to early accumulation of scar tissue in hope of identifying therapeutic targets to slow down this progression.

Hepatic stellate cells (HSC) are important effectors in the diseased liver. In response to profibrogenic cytokines such as TGF-β1, HSCs undergo an activation process that involves proliferation, exhibition of a myofibroblastic phenotype and enhanced production of ECM proteins. Strategies aiming at blocking TGF-β1 synthesis and/or its signaling pathways significantly decrease fibrosis in experimental models.

In a further approach targeting TGF-β signaling in fibrogenesis, we used TGF-β antagonistic Smad7 and were able to blunt disease progression after adenoviral delivery. To monitor the effect of a cell type specific abrogation of TGF-β signaling in chronic liver disease, transgenic mice were generated, which express mouse Smad7 under the control of the human C-reactive protein (CRP) promoter. In this model, transgenic Smad7 overexpression was induced by lipopolysaccharide injections specifically in hepatocytes. These mice and corresponding controls were treated with CCl_4 for 8 weeks. In addition, mice with a disrupted Smad7 gene (S7ΔE1) were investigated. The S7ΔE1 strain displayed the highest degree of fibrosis, indicating that the presence of a functional negative feedback regulation for TGF-β signaling is controling the degree of fibrogenesis. Interestingly, Smad7 overexpression in hepatocytes of CRP-Smad7 transgenic mice was sufficient to reduce fibrosis and expression of protein markers in the liver, e.g., collagen and α-SMA, as well as in serum, e.g., AST, ALT, AP and HA, by more than 70% in comparison to wild type animals. Further, Smad7 overexpression reduces proliferation, inflammation and apoptotic processes in liver cells of CRP-Smad7 transgenic mice.

6   References

1.   Agrawal A, Cha-Molstad H, Samols D, Kushner I (2001)
        Transactivation of C-reactive protein by IL-6 requires synergistic interaction of CCAAT/enhancer binding protein beta (C/EBP beta)
        and Rel p50.
        J Immunol 166**:** 2378-84

2.   Ala-Kokko L, Pihlajaniemi T, Myers JC, Kivirikko KI, Savolainen ER (1987)
        Gene expression of type I, III and IV collagens in hepatic fibrosis induced by dimethylnitrosamine in the rat.
        Biochem J 244**:** 75-9

3.   Anscher MS, Peters WP, Reisenbichler H, Petros WP, Pharm D, Jirtle RL (1993)
        Transforming growth factor-beta as a predictor of liver and lung fibrosis after autologous bone marrow transplantation for advanced
        breast cancer.
        328**:** 1592-1598

4.   Arias M, Lahme B, Van de Leur E, Gressner AM, Weiskirchen R (2002)
        Adenoviral delivery of an antisense RNA complementary to the 3' coding sequence of transforming growth factor-beta1 inhibits
        fibrogenic activities of hepatic stellate cells.
        Cell Growth Differ 13**:** 265-73

5.   Arsura M, Fitzgerald MJ, Fausto N, Sonenshein GE (1997)
        Nuclear factor-kappa B Rel blocks transforming growth factor beta 1-induced apoptosis of murine hepatocyte cell lines.
        Cell Growth Differ 8**:** 1049-1059

6.   Arthur MJP (1995)
        Collagenases and liver fibrosis.
        22**:** 43-48

7.   Battegay EJ, Raines EW, Seifert RA, Bowen-Pope DF, Ross R (1990)
        TGF-beta induces bimodal proliferation of connective tissue cells via complex control of an autocrine PDGF loop.
        Cell 63**:** 515-524

8.   Benyon RC, Hovell CJ, Da Gaca M, Jones EH, Iredale JP, Arthur MJ (1999)
        Progelatinase A is produced and activated by rat hepatic stellate cells and promotes their proliferation.
        Hepatology 30**:** 977-86

9.   Boigk G, Stroedter L, Herbst H, Waldschmidt J, Riecken EO, Schuppan D (1997)
        Silymarin retards collagen accumulation in early and advanced biliary fibrosis secondary to complete bile duct obliteration in rats.
        Hepatology 26**:** 643-649

10.   Border WA, Brees D, Noble NA (1994)
        Transforming growth factor-beta and extracellular matrix deposition in the kidney.
        Contrib Nephrol 107**:** 140-5

11.   Border WA, Noble NA (1994)
        Mechanisms of disease: transforming growth factor-beta in tissue fibrosis.
        N.Engl.J.Med 331**:** 1286-1292

12.   Border WA, Noble NA (1994)
        Transforming growth factor beta in tissue fibrosis.
        N Engl J Med 331**:** 1286-92.

13.   Bottinger EP, Letterio JJ, Roberts AB (1997)
        Biology of TGF-beta in knockout and transgenic mouse models.
        51: 1355-1360

14.   Boyer B, Valles AM, Edme N (2000)
        Induction and regulation of epithelial-mesenchymal transitions.
        Biochem Pharmacol 60: 1091-9

15.   Brandes ME, Allen JB, Ogawa Y, Wahl SM (1991)
        Transforming growth factor-beta1 suppresses acute and chronic arthritis in experimental animals.
        87: 1108-1113

16.   Breitkopf K, Haas S, Wiercinska E, Singer MV, Dooley S (2005)
        Anti-TGF-beta strategies for the treatment of chronic liver disease.
        Alcohol Clin Exp Res 29: 121S-131S

17.   Breitkopf K, Lahme B, Tag CG, Gressner AM (2001)
        Expression and matrix deposition of latent transforming growth factor beta binding proteins in normal and fibrotic rat liver and transdifferentiating hepatic stellate cells in culture.
        Hepatology 33: 387-96.

18.   Breitkopf K, Sawitza I, Westhoff JH, Wickert L, Dooley S, Gressner AM (2005)
        Thrombospondin-1 acts as a strong promoter of TGF-beta effects via two distinct mechanisms in hepatic stellate cells.
        Gut 54: 673-681

19.   Brown CB, Boyer AS, Runyan RB, Barnett JV (1999)
        Requirement of type III TGF-beta receptor for endocardial cell transformation in the heart.
        Science 283: 2080-2082

20.   Calabro P, Willerson JT, Yeh ET (2003)
        Inflammatory cytokines stimulated C-reactive protein production by human coronary artery smooth muscle cells.
        Circulation 108: 1930-2

21.   Carcamo J, Zentella A, Massague J (1995)
        Disruption of transforming growth factor beta signaling by a mutation that prevents transphosphorylation within the receptor complex.
        Mol Cell Biol 15: 1573-81

22.   Carmeliet P, Schoonjans L, Kieckens L, Ream B, Degen J, Bronson R, De Vos R, van den Oord JJ, Collen D, Mulligan RC (1994)
        Physiological consequences of loss of plasminogen activator gene function in mice.
        Nature 368: 419-24

23.   Cavaillon JM, Fitting C, Adib-Conquy M (2004)
        Mechanisms of immunodysregulation in sepsis.
        Contrib Nephrol 144: 76-93

24.   Christensen H.E. FEJ, Eds, B.S., Carroll R.J. L   ewis, project Coordinators (1976)
        Registry of Toxic Effects of Chemical Substances, Pages
        In: Editor (Hrsg): Book Registry of Toxic Effects of Chemical Substances
        Aufl. Washington, D.C

25.   Ciliberto G, Arcone R, Wagner EF, Ruther U (1987)
        Inducible and tissue-specific expression of human C-reactive protein in transgenic mice.
        Embo J 6: 4017-22

26.   Crawford SE, Stellmach V, Murphy-Ullrich JE, Ribeiro SM, Lawler J, Hynes RO, Boivin GP, Bouck N (1998)
        Thrombospondin-1 is a major activator of TGF-beta1 in vivo.

Cell 93**:** 1159-70

27.   Date M, Matsuzaki K, Matsushita M, Tahashi Y, Sakitani K, Inoue K (2000)
        Differential regulation of activin A for hepatocyte growth and fibronectin synthesis in rat liver injury.
        J Hepatol 32**:** 251-60

28.   Davidson JM (1992)
        Wound repair, 809-819
        In: Gallin J.I., Goldstein I.M. and Snyderman R. (Hrsg.): Inflammation: Basic Principles and Clinical Correlates
        Aufl. Raven Press, Ltd., New York

29.   de Caestecker MP, Hemmati P, Larisch-Bloch S, Ajmera R, Roberts AB, Lechleider RJ (1997)
        Characterization of functional domains within Smad4/DPC4.
        J Biol Chem 272**:** 13690-6

30.   de Gouville AC, Boullay V, Krysa G, Pilot J, Brusq JM, Loriolle F, Gauthier JM, Papworth SA, Laroze A, Gellibert F, Huet S (2005)
        Inhibition of TGF-beta signaling by an ALK5 inhibitor protects rats from dimethylnitrosamine-induced liver fibrosis.
        Br J Pharmacol 145**:** 166-77

31.   Decker K (1990)
        Biologically active products of stimulated liver macrophages (Kupffer cells).
        192**:** 245-261

32.   Dennler S, Itoh S, Vivien D, Tendijke P, Huet S, Gauthier JM (1998)
        Direct binding of Smad3 and Smad4 to critical TGF beta- inducible elements in the promoter of human plasminogen activator inhibitor-type 1 gene.
        EMBO J. 17**:** 3091-3100

33.   Di Marco R, Xiang M, Zaccone P, Leonardi C, Franco S, Meroni P, Nicoletti F (1999)
        Concanavalin A-induced hepatitis in mice is prevented by interleukin (IL)-10 and exacerbated by endogenous IL-10 deficiency.
        Autoimmunity 31**:** 75-83

34.   Dooley S, Hamzavi J, Breitkopf K, Wiercinska E, Said HM, Lorenzen J, Ten Dijke P, Gressner AM (2003)
        Smad7 prevents activation of hepatic stellate cells and liver fibrosis in rats.
        Gastroenterology 125**:** 178-91

35.   Edlund S, Bu S, Schuster N, Aspenstrom P, Heuchel R, Heldin NE, ten Dijke P, Heldin CH, Landstrom M (2003)
        Transforming growth factor-beta1 (TGF-beta)-induced apoptosis of prostate cancer cells involves Smad7-dependent activation of p38 by TGF-beta-activated kinase 1 and mitogen-activated protein kinase kinase 3.
        Mol Biol Cell 14**:** 529-44

36.   El-Youssef M, Mu Y, Huang LJ, Stellmach V, Crawford SE (1999)
        Increased expression of transforming growth factor-beta(1) and thrombospondin-1 in congenital hepatic fibrosis: Possible role of the hepatic stellate cell.
        J Pediat Gastroenterol Nutr 28**:** 386-392

37.   Fan H, Cook JA (2004)
        Molecular mechanisms of endotoxin tolerance.
        J Endotoxin Res 10**:** 71-84

38.   Fibbi G, Pucci M, Grappone C, Pellegrini G, Salzano R, Casini A, Milani S, Del Rosso M (1999)
        Functions of the fibrinolytic system in human Ito cells and its control by basic fibroblast and platelet-derived growth factor.
        Hepatology 29**:** 868-78.

39.   Flanders KC (2004)
        Smad3 as a mediator of the fibrotic response.
        Int J Exp Pathol 85**:** 47-64

40.   Friedman SL (2000)
       Molecular regulation of hepatic fibrosis, an integrated cellular response to tissue injury.
       J Biol Chem 275**:** 2247-50

41.   Gambaro G, Weigert C, Ceol M, Schleicher ED (2001)
       Inhibition of transforming growth factor-beta 1 gene overexpression as a strategy to prevent fibrosis.
       Contrib Nephrol 107-13

42.   Ganey PE, Roth RA (2001)
       Concurrent inflammation as a determinant of susceptibility to toxicity from xenobiotic agents.
       Toxicology 169**:** 195-208

43.   George J, Roulot D, Koteliansky VE, Bissell DM (1999)
       In vivo inhibition of rat stellate cell activation by soluble transforming growth factor beta type II receptor: A potential new therapy for hepatic fibrosis.
       Proc Nat Acad Sci USA 96**:** 12719-12724

44.   Hahn SA, Schutte M, Hoque AT, Moskaluk CA, da Costa LT, Rozenblum E, Weinstein CL, Fischer A, Yeo CJ, Hruban RH, Kern SE (1996)
       DPC4, a candidate tumor suppressor gene at human chromosome 18q21.1.
       Science 271**:** 350-3

45.   Han X, Wilbanks GD, Devaja O, Ruperelia V, Raju KS (1999)
       IL-2 enhances standard IFNgamma/LPS activation of macrophage cytotoxicity to human ovarian carcinoma in vitro: a potential for adoptive cellular immunotherapy.
       Gynecol Oncol 75**:** 198-210

46.   Haouzi D, Lekehal M, Moreau A, Moulis C, Feldmann G, Robin MA, Letteron P, Fau D, Pessayre D (2000)
       Cytochrome P450-generated reactive metabolites cause mitochondrial permeability transition, caspase activation, and apoptosis in rat hepatocytes.
       Hepatology 32**:** 303-11

47.   Hata A, Lo RS, Wotton D, Lagna G, Massague J (1997)
       Mutations increasing autoinhibition inactivate tumour suppressors Smad2 and Smad4 [see comments].
       Nature 388**:** 82-7

48.   Hewett JA, Jean PA, Kunkel SL, Roth RA (1993)
       Relationship between tumor necrosis factor-alpha and neutrophils in endotoxin-induced liver injury.
       Am J Physiol 265**:** G1011-5

49.   Hori Y, Katoh T, Hirakata M, Joki N, Kaname S, Fukagawa M, Okuda T, Ohashi H, Fujita T, Miyazono K, Kurokawa K (1998)
       Anti-latent TGF-beta binding protein-1 antibody or synthetic oligopeptides inhibit extracellular matrix expression induced by stretch in cultured rat mesangial cells.
       Kidney Int 53**:** 1616-1625

50.   Huse M, Chen YG, Massague J, Kuriyan J (1999)
       Crystal structure of the cytoplasmic domain of the type I TGF beta receptor in complex with FKBP12.
       Cell 96**:** 425-436

51.   Imamura T, Takase M, Nishihara A, Oeda E, Hanai J, Kawabata M, Miyazono K (1997)
       Smad6 inhibits signalling by the TGF-beta superfamily [see comments].
       Nature 389**:** 622-6

52.   Kanamaru Y, Nakao A, Mamura M, Suzuki Y, Shirato I, Okumura K, Tomino Y, Ra C (2001)
       Blockade of TGF-beta signaling in T cells prevents the development of experimental glomerulonephritis.
       J Immunol 166**:** 2818-23

53.   Kato M, Ikeda N, Matsushita E, Kaneko S, Kobayashi K (2001)
        Involvement of IL-10, an anti-inflammatory cytokine in murine liver injury induced by Concanavalin A.
        Hepatol Res 20**:** 232-243

54.   Kieczka H, Kappus H (1980)
        Oxygen dependence of CCl4-induced lipid peroxidation in vitro and in vivo.
        Toxicol Lett 5**:** 191-6

55.   Kim SJ, Kehrl JH, Burton J, Tendler CL, Jeang KT, Danielpour D, Thevenin C, Kim KY, Sporn MB, Roberts AB (1990)
        Transactivation of the transforming growth factor beta 1 (TGF-beta 1) gene by human T lymphotropic virus type 1 tax: a potential
        mechanism for the increased production of TGF-beta 1 in adult T cell leukemia.
        J Exp Med 172**:** 121-9

56.   Kim SJ, Park K, Koeller D, Kim KY, Wakefield LM, Sporn MB, Roberts AB (1992)
        Post-transcriptional regulation of the human transforming growth factor-beta 1 gene.
        J Biol Chem 267**:** 13702-7

57.   Knittel T, Dinter C, Kobold D, Neubauer K, Mehde M, Eichhorst S, Ramadori G (1999)
        Expression and regulation of cell adhesion molecules by hepatic stellate cells (HSC) of rat liver - Involvement of HSC in recruitment of
        inflammatory cells during hepatic tissue repair.
        Amer J Pathol 154**:** 153-167

58.   Kondou H, Mushiake S, Etani Y, Miyoshi Y, Michigami T, Ozono K (2003)
        A blocking peptide for transforming growth factor-beta1 activation prevents hepatic fibrosis in vivo.
        J Hepatol 39**:** 742-8

59.   Kopp JB, Factor VM, Motes M, Nagy P, Sanderson N, Bottinger EP, Klotman PE, Thorgeirsson SS (1996)
        Transgenic mice with increased plasma levels of TGF-beta 1 develop progressive renal disease.
        74**:** 991-1003

60.   Kountouras J, Billing BH, Scheuer PJ (1984)
        Prolonged bile duct obstruction: A new experimental model for cirrhosis in the rat.
        Br.J.Exp.Path. 65**:** 305-311

61.   Krag S, Osterby R, Chai Q, Nielsen CB, Hermans C, Wogensen L (2000)
        TGF-beta1-induced glomerular disorder is associated with impaired concentrating ability mimicking primary glomerular disease with
        renal failure in man.
        Lab Invest 80**:** 1855-68

62.   Kulkarni AB, Huh CG, Becker D, Geiser A, Lyght M, Flanders KC, Roberts AB, Sporn MB, Ward JM, Karlsson S (1993)
        Transforming growth factor beta-1 null mutation in mice causes excessive inflammatory response and early death.
        90**:** 770-774

63.   Kurisaki A, Kose S, Yoneda Y, Heldin CH, Moustakas A (2001)
        Transforming growth factor-beta induces nuclear import of Smad3 in an importin-beta1 and Ran-dependent manner.
        Mol Biol Cell 12**:** 1079-91

64.   Kushner I, Jiang SL, Zhang D, Lozanski G, Samols D (1995)
        Do post-transcriptional mechanisms participate in induction of C-reactive protein and serum amyloid A by IL-6 and IL-1?
        Ann N Y Acad Sci 762**:** 102-7

65.   Lan HY, Mu W, Tomita N, Huang XR, Li JH, Zhu HJ, Morishita R, Johnson RJ (2003)
        Inhibition of renal fibrosis by gene transfer of inducible Smad7 using ultrasound-microbubble system in rat UUO model.
        J Am Soc Nephrol 14**:** 1535-48

66.   Lopez-Casillas F, Cheifetz S, Doody J, Andres JL, Lane WS, Massague J (1991)
        Structure and expression of the membrane proteoglycan betaglycan, a component of the TGF-beta receptor system.

Cell 67**:** 785-95

67. Macias-Silva M, Abdollah S, Hoodless PA, Pirone R, Attisano L, Wrana JL (1996)
MADR2 is a substrate of the TGFbeta receptor and its phosphorylation is required for nuclear accumulation and signaling.
Cell 87**:** 1215-24

68. Magee PNaB, J.M. (1967)
Carcinogenic Nitroso Compounds, Advances in Cancer Research.
10**:** 163-247

69. March J (1968)
Advanced Organic Chemistry: Reactions, Mechanisms, and Structure, Pages
In: Editor (Hrsg): Book Advanced Organic Chemistry: Reactions, Mechanisms, and Structure
Aufl. McGrawHill Book Company, New York,

70. Massague J (1998)
TGF-beta signal transduction.
Annu Rev Biochem 67**:** 753-91

71. Massague J, Chen YG (2000)
Controlling TGF-beta signaling.
Genes Dev 14**:** 627-44

72. Massague J, Wotton D (2000)
Transcriptional control by the TGF-beta/Smad signaling system.
Embo J 19**:** 1745-54.

73. Masuda Y, Nakamura Y (1990)
Effects of oxygen deficiency and calcium omission on carbon tetrachloride hepatotoxicity in isolated perfused livers from phenobarbital-pretreated rats.
Biochem Pharmacol 40**:** 1865-76

74. Mayer AM, Spitzer JA (1993)
Modulation of superoxide anion generation by manoalide, arachidonic acid and staurosporine in liver infiltrated neutrophils in a rat model of endotoxemia.
J Pharmacol Exp Ther 267**:** 400-9

75. McMahon JB, Richards WL, Campo del AA, Song MKH, Thorgeirsson SS (1986)
Differential effects of transforming growth factor-beta on proliferation of normal and malignant rat liver epithelial cells in culture.
46**:** 4665-4671

76. Michie HR, Spriggs DR, Manogue KR, Sherman ML, Revhaug A, O'Dwyer ST, Arthur K, Dinarello CA, Cerami A, Wolff SM, et al. (1988)
Tumor necrosis factor and endotoxin induce similar metabolic responses in human beings.
Surgery 104**:** 280-6

77. Morrison SJ, White PM, Zock C, Anderson DJ (1999)
Prospective identification, isolation by flow cytometry, and in vivo self-renewal of multipotent mammalian neural crest stem cells.
Cell 96**:** 737-49

78. Mortensen RF (2001)
C-reactive protein, inflammation, and innate immunity.
Immunol Res 24**:** 163-76

79. Murphy-Ullrich JE, Poczatek M (2000)
Activation of latent TGF-beta by thrombospondin-1: mechanisms and physiology.
Cytokine Growth Factor Rev 11**:** 59-69

80.   Nakamura T, Sakata R, Ueno T, Sata M, Ueno H (2000)
        Inhibition of transforming growth factor beta prevents progression of liver fibrosis and enhances hepatocyte regeneration in
        dimethylnitrosamine-treated rats.
        Hepatology 32: 247-55

81.   Nakao A, Afrakhte M, Moren A, Nakayama T, Christian JL, Heuchel R, Itoh S, Kawabata N, Heldin NE, Heldin CH, Tendijke P
        (1997)
        Identification of Smad7, a TGF beta-inducible antagonist of TGF-beta signalling.
        Nature 389: 631-635

82.   Nakao A, Fujii M, Matsumura R, Kumano K, Saito Y, Miyazono K, Iwamoto I (1999)
        Transient gene transfer and expression of Smad7 prevents bleomycin-induced lung fibrosis in mice.
        J Clin Invest 104: 5-11

83.   Nakao A, Fujii M, Matsumura R, Kumano K, Saito Y, Miyazono K, Iwamoto T (1999)
        Transient gene transfer and expression of Smad7 prevents bleomycin-induced lung fibrosis in mice.
        J Clin Invest 104: 5-11

84.   Ng YY, Hou CC, Wang W, Huang XR, Lan HY (2005)
        Blockade of NFkappaB activation and renal inflammation by ultrasound-mediated gene transfer of Smad7 in rat remnant kidney.
        Kidney Int Suppl S83-91

85.   Niki T, Pekny M, Hellemans K, DeBleser P, Vandenberg K, Vaeyens F, Quartier E, Schuit F, Geerts A (1999)
        Class VI intermediate filament protein nestin is induced during activation of rat hepatic stellate cells.
        Hepatology 29: 520-527

86.   Okuno M, Akita K, Moriwaki H, Kawada N, Ikeda K, Kaneda K, Suzuki Y, Kojima S (2001)
        Prevention of rat hepatic fibrosis by the protease inhibitor, camostat mesilate, via reduced generation of active TGF-beta.
        Gastroenterology 120: 1784-800.

87.   Packer JE, Slater TF, Willson RL (1978)
        Reactions of the carbon tetrachloride-related peroxy free radical (CC13O.2) with amino acids: pulse radiolysis evidence.
        Life Sci 23: 2617-20

88.   Pearson JM, Schultze AE, Schwartz KA, Scott MA, Davis JM, Roth RA (1996)
        The thrombin inhibitor, hirudin, attenuates lipopolysaccharide-induced liver injury in the rat.
        J Pharmacol Exp Ther 278: 378-83

89.   Pepper MS, Belin D, Montesano R, Orci L, Vassalli JD (1990)
        Transforming growth factor-beta 1 modulates basic fibroblast growth factor-induced proteolytic and angiogenic properties of
        endothelial cells in vitro.
        J Cell Biol 111: 743-55

90.   Pepys MB, Baltz ML (1983)
        Acute phase proteins with special reference to C-reactive protein and related proteins (pentaxins) and serum amyloid A protein.
        Adv Immunol 34: 141-212

91.   Piek E, Heldin CH, Ten Dijke P (1999)
        Specificity, diversity, and regulation in TGF-beta superfamily signaling.
        Faseb J 13: 2105-24

92.   Pitts JN, Grosjean, P., Cauwenberght, K.V., Schmid, J.P., and Fitz, D.R. (1978)
        Photooxidation of Aliphatic Amines under simulated Atmospheric Conditions: Formation of Nitrosamines, Nitramines, Amides and
        Photochemical Oxidant,.
        Environmental Science and Technology 12: 946-953

93.   Postlethwaite AE, Keski-Oja J, Moses HL, Kang AH (1987)
        Stimulation of the chemotactic migration of human fibroblasts by transforming growth factor-beta.
        165**:** 251-256

94.   Qi Z, Atsuchi N, Ooshima A, Takeshita A, Ueno H (1999)
        Blockade of type beta transforming growth factor signaling prevents liver fibrosis and dysfunction in the rat.
        Proc Nat Acad Sci USA 96**:** 2345-2349

95.   Recknagel RO HA, Glende EA Jr. (1976)
        Absolute dependence of CCL4 induced loss of glucose-6-phosphatase and cytochrome P-450 on lipid peroxidation.
        Panminerva Med 18**:** 375-80

96.   Reed MJ, Iruela-Arispe L, O'Brien ER, Truong T, LaBell T, Bornstein P, Sage EH (1995)
        Expression of thrombospondins by endothelial cells. Injury is correlated with TSP-1.
        Am J Pathol 147**:** 1068-80

97.   Roberts AB, Baker JR (1986)
        Serum fructosamine: a screening test for diabetes in pregnancy.
        Am J Obstet Gynecol 154**:** 1027-30

98.   Roberts AB, Baker JR, Metcalf P, Mullard C (1990)
        Fructosamine compared with a glucose load as a screening test for gestational diabetes.
        Obstet Gynecol 76**:** 773-5

99.   Roberts AB, Sporn MB (1990)
        The transforming growth factor-beta, 419-472
        In: Sporn M.B. and Roberts A.B. (Hrsg.): Peptide growth factors and their receptors. Handbook of experimental pharmacology
        Aufl. Springer Verlag, Heidelberg

100.   Rodriguez C, Chen F, Weinberg RA, Lodish HF (1995)
        Cooperative binding of transforming growth factor (TGF)-beta 2 to the types I and II TGF-beta receptors.
        J Biol Chem 270**:** 15919-22

101.   Roth J, Storr B, Martin D, Voigt K, Zeisberger E (2000)
        The role of local induction of tumor necrosis factor by LPS within a subcutaneous air pouch in the development of a febrile response in guinea pigs.
        Neuroimmunomodulation 7**:** 169-76

102.   Ruoslahti E, Yamaguchi Y (1991)
        Proteoglycans as modulators of growth factor activities.
        Cell 64**:** 867-869

103.   Sanderson N, Factor V, Nagy P, Kopp J, Kondaiah P, Wakefield L, Roberts AB, Sporn MB, Thorgeirsson SS (1995)
        Hepatic expression of mature transforming growth factor beta 1 in transgenic mice results in multiple tissue lesions.
        92**:** 2572-2576

104.   Savagner P (2001)
        Leaving the neighborhood: molecular mechanisms involved during epithelial-mesenchymal transition.
        Bioessays 23**:** 912-23

105.   Savolainen ER, Brocks D, Ala-Kokko L, Kivirikko KI (1988)
        Serum concentrations of the N-terminal propeptide of type III procollagen and two type IV collagen fragments and gene expression of the respective collagen types in liver in rats with dimethylnitrosamine-induced hepatic fibrosis.
        Biochem J 249**:** 753-7

106.   Shi Y, Hata A, Lo RS, Massague J, Pavletich NP (1997)
        A structural basis for mutational inactivation of the tumour suppressor Smad4 [see comments].

Nature 388**:** 87-93

107. Shi Y, Wang YF, Jayaraman L, Yang H, Massague J, Pavletich NP (1998)
     Crystal structure of a Smad MH1 domain bound to DNA: insights on DNA binding in TGF-beta signaling.
     Cell 94**:** 585-94

108. Shull MM, Ormsby I, Kier AB, Pawlowski S, Diebold RJ, Yin M, Allen R, Sidman C, Proetzel G, Calvin D, Annunziata N, Doetschman T (1992)
     Targeted disruption of the mouse transforming growth factor beta-1 gene results in multifocal inflammatory disease.
     Nature 359**:** 693-699

109. Slater TF (1981)
     Free radicals as reactive intermediates in tissue injury.
     Adv Exp Med Biol 136 Pt A**:** 575-89

110. Smith JD, Bryant SR, Couper LL, Vary CP, Gotwals PJ, Koteliansky VE, Lindner V (1999)
     Soluble transforming growth factor-beta type II receptor inhibits negative remodeling, fibroblast transdifferentiation, and intimal lesion formation but not endothelial growth.
     Circ Res 84**:** 1212-22

111. Sporn MB, Roberts AB (1992)
     Transforming growth factor-beta: recent progress and new challenges.
     J Cell Biol 119**:** 1017-21

112. Sun H, Koike T, Ichikawa T, Hatakeyama K, Shiomi M, Zhang B, Kitajima S, Morimoto M, Watanabe T, Asada Y, Chen YE, Fan J (2005)
     C-reactive protein in atherosclerotic lesions: its origin and pathophysiological significance.
     Am J Pathol 167**:** 1139-48

113. Terada Y, Hanada S, Nakao A, Kuwahara M, Sasaki S, Marumo F (2002)
     Gene transfer of Smad7 using electroporation of adenovirus prevents renal fibrosis in post-obstructed kidney.
     Kidney Int 61 Suppl 1**:** 94-8.

114. Terrell TG, Working PK, Chow CP, Green JD (1993)
     Pathology of recombinant human transforming growth factor beta-1 in rats and rabbits.
     34B**:** 43-67

115. Theret N, Lehti K, Musso O, Clement B (1999)
     MMP2 activation by collagen I and concanavalin A in cultured human hepatic stellate cells.
     Hepatology 30**:** 462-8

116. Thompson D, Pepys MB, Wood SP (1999)
     The physiological structure of human C-reactive protein and its complex with phosphocholine.
     Structure 7**:** 169-77

117. Thuring RW, Sanders JP, Borst P (1975)
     A freeze-squeeze method for recovering long DNA from agarose gels.
     Anal Biochem 66**:** 213-20

118. Tomasek JJ, Gabbiani G, Hinz B, Chaponnier C, Brown RA (2002)
     Myofibroblasts and mechano-regulation of connective tissue remodelling.
     Nat Rev Mol Cell Biol 3**:** 349-63

119. Tsukazaki T, Chiang TA, Davison AF, Attisano L, Wrana JL (1998)
     SARA, a FYVE domain protein that recruits Smad2 to the TGFbeta receptor.
     Cell 95**:** 779-91

120. Ueno H, Sakamoto T, Nakamura T, Qi Z, Astuchi N, Takeshita A, Shimizu K, Ohashi H (2000)
A soluble transforming growth factor beta receptor expressed in muscle prevents liver fibrogenesis and dysfunction in rats.
Hum Gene Ther 11**:** 33-42

121. Uhrig A, Banafsche R, Kremer M, Hegenbarth S, Hamann A, Neurath M, Gerken G, Limmer A, Knolle PA (2005)
Development and functional consequences of LPS tolerance in sinusoidal endothelial cells of the liver.
J Leukoc Biol 77**:** 626-33

122. Verrecchia F, Chu ML, Mauviel A (2001)
Identification of novel TGF-beta /Smad gene targets in dermal fibroblasts using a combined cDNA microarray/promoter transactivation approach.
J Biol Chem 276**:** 17058-62.

123. Vodovotz Y, Bogdan C, Paik J, Xie QW, Nathan C (1993)
Mechanisms of suppression of macrophage nitric oxide release by transforming growth factor beta.
J Exp Med 178**:** 605-13

124. Wahl SM, Hunt DA, Wakefield LM, McCartney-Francis N, Wahl LM, Roberts AB, Sporn MB (1987)
Transforming growth factor type-beta induces monocyte chemotaxis and growth factor production.
84**:** 5788-5792

125. Wang F, Wang LY, Wright D, Parmely MJ (1999)
Redox imbalance differentially inhibits lipopolysaccharide-induced macrophage activation in the mouse liver.
Infect Immun 67**:** 5409-16

126. Wang QJ, Wang YJ, Hyde DM, Gotwals PJ, Koteliansky VE, Ryan ST, Giri SN (1999)
Reduction of bleomycin induced lung fibrosis by transforming growth factor beta soluble receptor in hamsters.
Thorax 54**:** 805-812

127. Weinblatt ME, Kremer JM, Bankhurst AD, Bulpitt KJ, Fleischmann RM, Fox RI, Jackson CG, Lange M, Burge DJ (1999)
A trial of etanercept, a recombinant tumor necrosis factor receptor:Fc fusion protein, in patients with rheumatoid arthritis receiving methotrexate.
N Engl J Med 340**:** 253-9

128. Weng HL, Cai WM, Liu RH (2001)
Animal experiment and clinical study of effect of gamma-interferon on hepatic fibrosis.
World J Gastroenterol 7**:** 42-8

129. West MA, Clair L, Kraatz J, Rodriguez JL (2000)
Endotoxin tolerance from lipopolysaccharide pretreatment induces nuclear factor-kappaB alterations not present in C3H/HeJ mice.
J Trauma 49**:** 298-305

130. Whitehead AS, Zahedi K, Rits M, Mortensen RF, Lelias JM (1990)
Mouse C-reactive protein. Generation of cDNA clones, structural analysis, and induction of mRNA during inflammation.
Biochem J 266**:** 283-90

131. Wieser R, Attisano L, Wrana JL, Massague J (1993)
Signaling activity of transforming growth factor beta type II receptors lacking specific domains in the cytoplasmic region.
Mol Cell Biol 13**:** 7239-47

132. Wrana JL, Attisano L, Wieser R, Ventura F, Massague J (1994)
Mechanism of activation of the TGF-beta receptor.
Nature 370**:** 341-347

133. Xiao Z, Liu X, Lodish HF (2000)
Importin beta mediates nuclear translocation of Smad 3.
J Biol Chem 275**:** 23425-8

134.   Yamamoto H, Ueno H, Ooshima A, Takeshita A (1996)
        Adenovirus-mediated transfer of a truncated transforming growth factor-beta (TGF-beta) type II receptor completely and specifically
        abolishes diverse signaling by TGF-beta in vascular wall cells in primary culture.
        J Biol Chem 271: 16253-9

135.   Yang CS, Tu YY, Koop DR, Coon MJ (1985)
        Metabolism of nitrosamines by purified rabbit liver cytochrome P-450 isozymes.
        Cancer Res 45: 1140-5

136.   Yang CS, Yoo JS, Ishizaki H, Hong JY (1990)
        Cytochrome P450IIE1: roles in nitrosamine metabolism and mechanisms of regulation.
        Drug Metab Rev 22: 147-59

137.   Yang J, Liu Y (2001)
        Dissection of key events in tubular epithelial to myofibroblast transition and its implications in renal interstitial fibrosis.
        Am J Pathol 159: 1465-75

138.   Yasojima K, Schwab C, McGeer EG, McGeer PL (2001)
        Generation of C-reactive protein and complement components in atherosclerotic plaques.
        Am J Pathol 158: 1039-51

139.   Yata Y, Gotwals P, Koteliansky V, Rockey DC (2002)
        Dose-dependent inhibition of hepatic fibrosis in mice by a TGF-beta soluble receptor: implications for antifibrotic therapy.
        Hepatology 35: 1022-30.

140.   Yee SB, Copple BL, Ganey PE, Roth RA (2002)
        The temporal relationship between bacterial lipopolysaccharide and monocrotaline exposures influences toxicity: shift in response from
        hepatotoxicity to nitric oxide-dependent lethality.
        J Toxicol Environ Health A 65: 961-76

141.   Yoo JS, Guengerich FP, Yang CS (1988)
        Metabolism of N-nitrosodialkylamines by human liver microsomes.
        Cancer Res 48: 1499-504

142.   Yoshida T, Adachi E, Nigi H, Fujii S, Yanagi M (1999)
        Changes of sinusoidal basement membrane collagens in early hepatic fibrosis induced with CCl4 in cynomolgus monkeys.
        Pathology 31: 29-35

143.   Zawel L, Dai JL, Buckhaults P, Zhou SB, Kinzler KW, Vogelstein B, Kern SE (1998)
        Human Smad3 and Smad4 are sequence-specific transcription activators.
        Mol Cell 1: 611-617

144.   Zhang Y, Musci T, Derynck R (1997)
        The tumor suppressor Smad4/DPC 4 as a central mediator of Smad function.
        Curr Biol 7: 270-6

145.   Zheng H, Wang J, Koteliansky VE, Gotwals PJ, Hauer-Jensen M (2000)
        Recombinant soluble transforming growth factor beta type II receptor ameliorates radiation enteropathy in mice.
        Gastroenterology 119: 1286-96

146.   Zhu HT, Kavsak P, Abdollah S, Wrana JL, Thomsen GH (1999)
        A SMAD ubiquitin ligase targets the BMP pathway and affects embryonic pattern formation.
        Nature 400: 687-693

147.   Zugmaier G, Paik S, Wilding G, Knabbe C, Bano M, Lupu R, Deschauer B, Simpson S, Dickson RB, Lippman M (1991)
        Transforming growth factor beta1 induces cachexia and systemic fibrosis without an antitumor effect in nude mice.

51**:** 3590-3594

Acknowledgment

I would like to thank Mr. Prof. Dr. Steven Dooley and Mrs. Dr. Nadja Meindl-Beinker for their valuable advice and co-operation during preparation of this thesis.

Persönliche Angaben

Name: Jafar Hamzavi Sarkhaei
Geburtsdatum: 18.08.1958
Geburtsort: Abadan / Iran
Familienstand: ledig

Schulbildung

09.1965 – 06.1971	Grundschule in Abadan / Iran
09.1971 – 06.1977	Gymnasium in Abadan / Iran
Abschluss:	Abitur

Berufsbildung

03.2000 – 06.2001	Wissenschaftlicher Mitarbeiter am Institut für Mikrobiologie der Universität Hannover

Studienvorbreitung und Studium

04.1989 – 10.1989	Sprachkurs an der Volkshochschule Göttingen
04.1990 – 04.1991	Studienkolleg in Hannover
10.1991	Immatrikulation an der Universität Hannover für das Fach Biologie, Diplomstudiengang
10.1993	Diplom-Vorprüfung (bestanden, Note: gut)
10.1997	Diplom-Prüfung (bestanden, Note: gut)
06.1999 – 03.2000	Diplomarbeit am Institut für Mikrobiologie in Hannover Thema: In situ Identifizierung von Ammoniak-oxidierenden Bakterien durch 16S rDNA Hybridisierungstechnik

Promotion

07. 2001-30.08.2006	Durchführung der experimentellen Arbeiten zur vorliegenden Promotion